



**INTERFERENCE SUPPRESSION IN MULTIPLE ACCESS  
COMMUNICATIONS USING M-ARY PHASE SHIFT KEYING  
GENERATED VIA SPECTRAL ENCODING**

THESIS

Abel Sanchez Nunez, Captain, USAF

AFIT/GE/ENG/04-20

DEPARTMENT OF THE AIR FORCE

AIR UNIVERSITY

***AIR FORCE INSTITUTE OF TECHNOLOGY***

Wright-Patterson Air Force Base, Ohio

APPROVED FOR PUBLIC RELEASE; DISTRIBUTION UNLIMITED

The views expressed in this thesis are those of the author and do not reflect the official policy or position of the United States Air Force, Department of Defense, or the United States Government.

AFIT/GE/ENG/04-20

INTERFERENCE SUPPRESSION IN MULTIPLE ACCESS  
COMMUNICATIONS USING M-ARY PHASE SHIFT KEYING  
GENERATED VIA SPECTRAL ENCODING

THESIS

Presented to the Faculty  
of the Department of Electrical and Computer Engineering  
of the Graduate School of Engineering and Management  
of the Air Force Institute of Technology

Air University

In Partial Fulfillment of the  
Requirements for the Degree of  
Master of Science in Electrical Engineering

Abel Sanchez Nunez, BSE  
Captain, USAF

March 2004

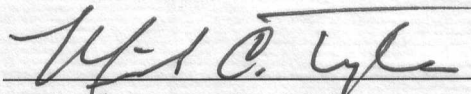
APPROVED FOR PUBLIC RELEASE; DISTRIBUTION UNLIMITED

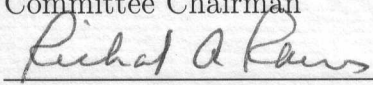
INTERFERENCE SUPPRESSION IN MULTIPLE ACCESS  
COMMUNICATIONS USING M-ARY PHASE SHIFT KEYING  
GENERATED VIA SPECTRAL ENCODING

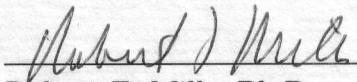
Abel Sanchez Nunez, BSE

Captain, USAF

Approved:

 10 Mar 04  
Michael A. Temple, Ph.D. Date  
Committee Chairman

 10 Mar 04  
Richard A. Raines, Ph.D. Date  
Committee Member

 10 Mar 2004  
Robert F. Mills, Ph.D. Date  
Committee Member

# Table of Contents

	Page
List of Figures . . . . .	viii
List of Tables . . . . .	xiii
Abstract . . . . .	xiv
1. Introduction . . . . .	1-1
1.1 Introduction . . . . .	1-1
1.2 Problem Statement . . . . .	1-5
1.3 Research Assumptions . . . . .	1-5
1.4 Research Scope . . . . .	1-6
1.5 Research Approach . . . . .	1-6
1.6 Materials and Equipment . . . . .	1-7
1.7 Thesis Organization . . . . .	1-7
2. Literature Review . . . . .	2-1
2.1 Introduction . . . . .	2-1
2.2 Phase Shift Keying . . . . .	2-1
2.2.1 Binary Phase Shift Keying . . . . .	2-1
2.2.2 M-Ary Phase Shift Keying . . . . .	2-3
2.3 Transform Domain Communication System (TDCS) . . . . .	2-6
2.3.1 TDCS Transmitter . . . . .	2-7
2.3.2 TDCS Receiver Processor . . . . .	2-10
2.4 Code Division Multiple Access . . . . .	2-10
2.5 Summary . . . . .	2-11

	Page
3. Modeling and Simulation Techniques . . . . .	3-1
3.1 Introduction . . . . .	3-1
3.2 Transform Domain Symbol Definition . . . . .	3-1
3.3 Symbol Cross-Correlation For Synchronous Users . . .	3-3
3.3.1 Mean and Variance of Symbol Cross-Correlation	3-3
3.3.2 Mean and Variance of Symbol Cross-Correlation: Orthogonal Code Selection . . . . .	3-4
3.4 Symbol Cross-Correlation and Bandlimited Noise . . .	3-5
3.5 Symbol Cross-Correlation for Asynchronous Users . . .	3-6
3.6 Cross-Correlation Between Two Symbols of Single Syn- chronous User . . . . .	3-8
3.7 Interference Model . . . . .	3-9
3.8 Monte Carlo Verification . . . . .	3-10
3.9 Modeling and Simulation Assumptions . . . . .	3-10
3.10 Summary . . . . .	3-10
4. Modeling and Simulation: Random Code Selection . . . . .	4-1
4.1 Introduction . . . . .	4-1
4.2 Modeling Parameters . . . . .	4-1
4.2.1 Spectral Response of Communication Symbol	4-1
4.2.2 Spectral Response of Jamming . . . . .	4-2
4.2.3 Spectrum of Notched User . . . . .	4-3
4.2.4 Number of Users . . . . .	4-4
4.3 No Interference Present . . . . .	4-5
4.4 Spectral Notching Effects . . . . .	4-6
4.5 Jamming Present With <i>No Spectral Notching</i> . . . . .	4-8
4.6 Jamming Present <i>With Spectral Notching</i> . . . . .	4-8
4.7 Multiple Access Interference: $N_U = 3$ Users With <i>No</i> <i>Spectral Notching</i> . . . . .	4-9

	Page
4.8 Multiple Access Interference: $N_U = 2$ to 32 Users With <i>No Spectral Notching</i> . . . . .	4-11
4.9 Asynchronous vs. Synchronous Multiple Access Perfor- mance . . . . .	4-12
4.10 Multiple Access Interference: $N_U = 3$ Users <i>With Spec-</i> <i>tral Notching</i> . . . . .	4-14
4.11 Multiple Access Interference: $N_U = 2$ to 32 Users <i>With</i> <i>Spectral Notching</i> . . . . .	4-15
4.12 Jamming and $N_U = 3$ Users Present With <i>No Spectral</i> <i>Notching</i> . . . . .	4-17
4.13 Jamming and $N_U$ 2 to 32 Users Present With <i>No Spectral</i> <i>Notching</i> . . . . .	4-20
4.14 Jamming and $N_U = 3$ Users Present <i>With Spectral Notch-</i> <i>ing</i> . . . . .	4-20
4.15 Jamming and $N_U = 2$ to 32 Users Present With <i>With</i> <i>Spectral Notching</i> . . . . .	4-21
4.16 Summary . . . . .	4-22
5. Modeling and Simulation: Orthogonal Code Selection . . . . .	5-1
5.1 Introduction . . . . .	5-1
5.2 Modeling Parameters . . . . .	5-1
5.2.1 Spectral Response of Communication Symbol . . . . .	5-1
5.2.2 Spectral Response of Jamming . . . . .	5-2
5.2.3 Spectrum of Notched User . . . . .	5-2
5.3 Synchronous Multiple Access Interference: Orthogonal Users With <i>No Spectral Notching</i> . . . . .	5-2
5.4 Asynchronous Multiple Access Interference: Orthogonal Users With <i>No Spectral Notching</i> . . . . .	5-3
5.5 Multiple Access Interference: $N_U = 2$ to 32 Users <i>With</i> <i>Spectral Notching</i> . . . . .	5-4

	Page
5.6 Jamming and Orthogonal Users Present With <i>No Spectral Notching</i> . . . . .	5-6
5.7 Jamming and Orthogonal Users Present <i>With Spectral Notching</i> . . . . .	5-8
5.8 Special Case: Reassigning Phase Codes to Maintain Orthogonality . . . . .	5-9
5.9 Summary . . . . .	5-12
6. Conclusions and Recommendations . . . . .	6-1
6.1 Summary . . . . .	6-1
6.2 Conclusions . . . . .	6-2
6.2.1 Performance in the Presence of Interference . . . . .	6-2
6.2.2 Multiple Access Performance (Randomly Coded Users) . . . . .	6-2
6.2.3 Multiple Access Performance (Orthogonally Coded Users) . . . . .	6-2
6.3 Recommendations for Future Research . . . . .	6-3
6.3.1 Quadrature Amplitude Modulation . . . . .	6-3
6.3.2 Synchronization . . . . .	6-3
6.3.3 Orthogonal Jammers . . . . .	6-3
6.3.4 Propagation Effects . . . . .	6-3
6.3.5 Optimal Multiple Access Codes . . . . .	6-3
Appendix A. Matlab Simulation Code . . . . .	A-1
Appendix B. Cross-Correlation Between PSK Symbols . . . . .	B-1
B.1 Cross Correlation Between Symbol 1 and Symbol 2 . . . . .	B-1
B.2 Cross Correlation Between Symbols of a Single user . . . . .	B-3
B.3 Autocorrelation of symbol . . . . .	B-3



	Page
B.4 Expected Value of the Variance for the BPSK Case with Random Data Phase Modulation . . . . .	B-13
B.5 Expected Value of the Variance for the MPSK Case with Random Data Phase Modulation . . . . .	B-15
B.6 Expected Value of the Variance for the BPSK and MPSK Case with Random Multiple Access Phase Coding . . .	B-16
B.7 Orthogonal Users for PSK Symbols . . . . .	B-17
Bibliography . . . . .	BIB-1

## List of Figures

Figure		Page
2.1.	Single Channel BPSK Correlation Receiver . . . . .	2-2
2.2.	Two Channel Correlation Receiver for MPSK Signaling . . .	2-4
2.3.	Conceptual TDCS Transmitter . . . . .	2-6
4.1.	Spectral Response (Magnitude of DFT) of Modeled Communi- cation Symbols . . . . .	4-2
4.2.	Time Domain Response of Modeled Communication Symbol .	4-3
4.3.	Spectral Response of Narrow Band Jammer ( $P = 31$ Sinusoids)	4-3
4.4.	Spectral Response (Magnitude of DFT) of Modeled Communi- cation Symbol with Narrow Band Notched Spectrum ( $P = 31$ Sinusoids) . . . . .	4-5
4.5.	No Interference Present: $P_E$ vs $E_b/N_0$ for TD-MPSK Signaling with $P = 31$ Sinusoids . . . . .	4-6
4.6.	No Interference Present: $P_B$ vs $E_b/N_0$ for TD-MPSK Signaling with $P = 31$ Sinusoids . . . . .	4-6
4.7.	Spectral Notching: $P_E$ vs $E_b/N_0$ for TD-MPSK Signaling with $P = 31$ Sinusoids . . . . .	4-7
4.8.	Spectral Notching: $P_B$ vs $E_b/N_0$ for TD-MPSK Signaling with $P = 31$ Sinusoids . . . . .	4-7
4.9.	Jamming Present with <i>No Spectral Notching</i> : $P_E$ vs $E_b/N_0$ for TD-MPSK Signaling with $J/S = 3.14$ dB and $P = 31$ Sinusoids	4-8
4.10.	Jamming Present with <i>No Spectral Notching</i> : $P_B$ vs $E_b/N_0$ for TD-MPSK Signaling with $J/S = 3.14$ dB and $P = 31$ Sinusoids	4-9
4.11.	Jamming Present <i>With Spectral Notching</i> : $P_E$ vs $E_b/N_0$ for TD- MPSK Signaling with $J/S = 3.14$ dB and $P = 31$ Sinusoids .	4-10
4.12.	Jamming Present <i>With Spectral Notching</i> : $P_B$ vs $E_b/N_0$ for TD- MPSK Signaling with $J/S = 3.14$ dB and $P = 31$ Sinusoids .	4-10

Figure		Page
4.13.	Multiple Access Interference for $N_U = 3$ Users With <i>No Spectral Notching</i> : $P_E$ vs $E_b/N_0$ for TD-MPSK Signaling with $P = 31$ Sinusoids . . . . .	4-11
4.14.	Multiple Access Interference for $N_U = 3$ Users With <i>No Spectral Notching</i> : $P_B$ vs $E_b/N_0$ for TD-MPSK Signaling with $P = 31$ Sinusoids . . . . .	4-12
4.15.	Multiple Access Interference for $N_U = 2$ to 32 Users With <i>No Spectral Notching</i> : $P_E$ vs $N_U$ for TD-QPSK Signaling with $P = 31$ Sinusoids . . . . .	4-13
4.16.	Multiple Access Interference for $N_U = 2$ to 32 Users With <i>No Spectral Notching</i> : $P_B$ vs $N_U$ for TD-QPSK Signaling with $P = 31$ Sinusoids . . . . .	4-13
4.17.	Multiple Access Interference with $N_U = 2$ to 32 <i>Asynchronous</i> Users: $P_E$ vs $N_U$ for TD-QPSK Signaling with $P = 31$ Sinusoids	4-14
4.18.	Multiple Access Interference with $N_U = 2$ to 32 <i>Asynchronous</i> Users: $P_B$ vs $N_U$ for TD-QPSK Signaling with $P = 31$ Sinusoids	4-14
4.19.	Multiple Access Interference for $N_U = 3$ Users <i>With Spectral Notching</i> : $P_E$ vs $E_b/N_0$ for TD-MPSK Signaling with $P = 31$ Sinusoids . . . . .	4-15
4.20.	Multiple Access Interference for $N_U = 3$ Users <i>With Spectral Notching</i> : $P_B$ vs $E_b/N_0$ for TD-MPSK Signaling with $P = 31$ Sinusoids . . . . .	4-16
4.21.	Multiple Access Interference for $N_U = 2$ to 32 Users <i>With Spectral Notching</i> : <i>Synchronous</i> Users: $P_E$ vs $N_U$ for TD-QPSK Signaling with $P = 31$ Sinusoids . . . . .	4-17
4.22.	Multiple Access Interference for $N_U = 2$ to 32 Users <i>With Spectral Notching</i> : <i>Synchronous</i> Users: $P_B$ vs $N_U$ for TD-QPSK Signaling with $P = 31$ Sinusoids . . . . .	4-17
4.23.	Multiple Access Interference for $N_U = 6$ Users <i>With Spectral Notching</i> : $P_E$ vs Notch Width $N_s$ for TD-QPSK Signaling . .	4-18
4.24.	Multiple Access Interference for $N_U = 6$ Users <i>With Spectral Notching</i> : $P_B$ vs Notch Width $N_s$ for TD-QPSK Signaling . .	4-18

Figure		Page
4.25.	Jamming and $N_U = 3$ Users Present With <i>No Spectral Notching</i> : $P_E$ vs $E_b/N_0$ for TD-MPSK Signaling with $J/S = 3.14$ dB and $P = 31$ Sinusoids . . . . .	4-19
4.26.	Jamming and $N_U = 3$ Users Present With <i>No Spectral Notching</i> : $P_B$ vs $E_b/N_0$ for TD-MPSK Signaling with $J/S = 3.14$ dB and $P = 31$ Sinusoids . . . . .	4-19
4.27.	Jamming and Multiple Access Interference for $N_U = 2$ to 32 Users <i>No Spectral Notching: Synchronous</i> Users: $P_E$ vs $N_U$ for TD-QPSK Signaling with $P = 31$ Sinusoids . . . . .	4-20
4.28.	Jamming and Multiple Access Interference for $N_U = 2$ to 32 Users <i>No Spectral Notching: Synchronous</i> Users: $P_B$ vs $N_U$ for TD-QPSK Signaling with $P = 31$ Sinusoids . . . . .	4-21
4.29.	Jamming and $N_U = 3$ Users Present With <i>With Spectral Notching</i> : $P_B$ vs $E_b/N_0$ for TD-MPSK Signaling with $J/S = 3.14$ dB and $P = 31$ Sinusoids . . . . .	4-22
4.30.	Jamming and $N_U = 3$ Users Present With <i>With Spectral Notching</i> : $P_B$ vs $E_b/N_0$ for TD-MPSK Signaling with $J/S = 3.14$ dB and $P = 31$ Sinusoids . . . . .	4-22
4.31.	Jamming and Multiple Access Interference for $N_U = 2$ to 32 Users <i>With Spectral Notching: Synchronous</i> Users: $P_E$ vs $N_U$ for TD-QPSK Signaling with $P = 31$ Sinusoids . . . . .	4-23
4.32.	Jamming and Multiple Access Interference for $N_U = 2$ to 32 Users <i>With Spectral Notching: Synchronous</i> Users: $P_B$ vs $N_U$ for TD-QPSK Signaling with $P = 31$ Sinusoids . . . . .	4-23
4.33.	Jamming and Multiple Access Interference for $N_U = 2$ to 32 Users <i>With and without Spectral Notching</i> : $P_B$ vs $N_U$ for TD-MPSK Signaling with $P = 31$ Sinusoids . . . . .	4-24
4.34.	Jamming and Multiple Access Interference for $N_U = 2$ to 3 Users <i>With and without Spectral Notching</i> : $P_B$ vs $E_b/N_0$ for TD-QPSK Signaling with $P = 31$ Sinusoids . . . . .	4-25

Figure		Page
5.1.	Multiple Access Interference for $N_U = 2$ to 32 Orthogonal Users With <i>No Spectral Notching</i> : $P_E$ vs $N_U$ for TD-QPSK Signaling with $P = 31$ Sinusoids . . . . .	5-3
5.2.	Multiple Access Interference for $N_U = 2$ to 32 Orthogonal Users With <i>No Spectral Notching</i> : $P_B$ vs $N_U$ for TD-QPSK Signaling with $P = 31$ Sinusoids . . . . .	5-4
5.3.	Multiple Access Interference with $N_U = 2$ to 32 <i>Asynchronous</i> Users: $P_E$ vs $N_U$ for TD-QPSK Signaling with $P = 31$ Sinusoids . . . . .	5-4
5.4.	Multiple Access Interference with $N_U = 2$ to 32 <i>Asynchronous</i> Users: $P_B$ vs $N_U$ for TD-QPSK Signaling with $P = 31$ Sinusoids . . . . .	5-5
5.5.	Multiple Access Interference for $N_U = 2$ to 32 Orthogonal Users With <i>Spectral Notching</i> : $P_E$ vs $N_U$ for TD-QPSK Signaling with $P = 31$ Sinusoids . . . . .	5-5
5.6.	Multiple Access Interference for $N_U = 2$ to 32 Orthogonal Users With <i>Spectral Notching</i> : $P_B$ vs $N_U$ for TD-QPSK Signaling with $P = 31$ Sinusoids . . . . .	5-6
5.7.	Multiple Access Interference for $N_U = 6$ Orthogonal Users With <i>Spectral Notching</i> : $P_E$ vs Spectral Notch Width $N_s$ for TD-QPSK Signaling . . . . .	5-7
5.8.	Multiple Access Interference for $N_U = 6$ Orthogonal Users With <i>Spectral Notching</i> : $P_B$ vs Spectral Notch Width $N_s$ for TD-QPSK Signaling . . . . .	5-7
5.9.	Jamming and Multiple Access Interference for $N_U = 2$ to 32 Orthogonal Users <i>No Spectral Notching</i> : $P_E$ vs $N_U$ for TD-QPSK Signaling with $P = 31$ Sinusoids . . . . .	5-8
5.10.	Jamming and Multiple Access Interference for $N_U = 2$ to 32 Orthogonal Users <i>No Spectral Notching</i> : $P_B$ vs $N_U$ for TD-QPSK Signaling with $P = 31$ Sinusoids . . . . .	5-8
5.11.	Jamming and Multiple Access Interference for $N_U = 2$ to 32 Orthogonal Users With <i>Spectral Notching</i> : $P_E$ vs $N_U$ for TD-QPSK Signaling with $P = 31$ Sinusoids . . . . .	5-10

Figure		Page
5.12.	Jamming and Multiple Access Interference for $N_U = 2$ to 32 Orthogonal Users <i>With Spectral Notching: <math>P_B</math> vs <math>N_U</math></i> for TD-QPSK Signaling with $P = 31$ Sinusoids . . . . .	5-10
5.13.	Multiple Access Interference for $N_U = 2$ to 24 Orthogonal Users <i>With Spectral Notching, Orthogonality is Restored: <math>P_E</math> vs <math>N_U</math></i> for TD-QPSK Signaling with $P = 31$ Sinusoids . . . . .	5-11
5.14.	Multiple Access Interference for $N_U = 2$ to 24 Orthogonal Users <i>With Spectral Notching, Orthogonality is Restored: <math>P_B</math> vs <math>N_U</math></i> for TD-QPSK Signaling with $P = 31$ Sinusoids . . . . .	5-11
5.15.	Jamming and Multiple Access Interference for $N_U = 2$ to 24 Orthogonal Users <i>With Spectral Notching, Orthogonality Restored: <math>P_E</math> vs <math>N_U</math></i> for TD-QPSK Signaling with $P = 31$ Sinusoids . . . . .	5-12
5.16.	Jamming and Multiple Access Interference for $N_U = 2$ to 24 Orthogonal Users <i>With Spectral Notching, Orthogonality Restored: <math>P_B</math> vs <math>N_U</math></i> for TD-QPSK Signaling with $P = 31$ Sinusoids . . . . .	5-13
5.17.	Jamming and Multiple Access Interference for $N_U = 2$ to 32 Orthogonal Users <i>With and without Spectral Notching: <math>P_B</math> vs <math>N_U</math></i> for TD-QPSK Signaling with $P = 31$ Sinusoids . . . . .	5-14

## List of Tables

Table		Page
2.1.	Mapping Weights for Theoretical $P_B$ Calculations per (2.8) .	2-5
3.1.	TD-MSPK Symbol Parameters . . . . .	3-2
4.1.	Amplitude Coefficients for Jammer of Fig. 4.3 . . . . .	4-4

## Abstract

A conceptual transform domain communication system (TDCS) is shown capable of operating successfully using  $M$ -Ary phase shift keying (MPSK) data modulation in a multiple access environment. Using spectral encoding, the conceptual TDCS provides an effective means for mitigating interference affects while achieving multiple access communications. The use of transform domain processing with MPSK data modulation (TD-MPSK) provides higher spectral efficiency relative to other modulation techniques (antipodal signaling and cyclic shift keying) considered previously for TDCS applications. The proposed TD-MPSK technique uses spectral encoding for both data and multiple access phase modulations. Demodulation of the spectrally encoded TD-MPSK communication symbols is accomplished using conventional, multi-channel time domain correlation techniques.

Analytic expressions for TD-MPSK probability of symbol error ( $P_E$ ) and probability of bit error ( $P_B$ ) are derived and validated using simulated results over the range of signal-to-noise ratios typically considered for communications. This validation includes scenarios with: 1) multiple access interference, 2) spectral notching, 3) jamming present and 4) combinations of all three. For a  $J/S$  of 3.14 dB and a  $E_b/N_0$  of 6 dB,  $P_B$  dropped by up to a factor of 3 for TD-QPSK in a MA environment for the case when spectral notching was present versus the case when spectral notching wasn't present. The cross-correlation between communication symbols of different synchronous users can be made identically zero through proper selection of multiple access phase codes (orthogonal signaling). For a synchronous network containing orthogonal users,  $P_E$  and  $P_B$  are unaffected as the number of orthogonal network users increases. For a  $J/S$  of 3.14 dB and a  $E_b/N_0$  of 6 dB,  $P_B$  dropped by a factor of 12 for TD-QPSK in a MA environment for the case when spectral notching was present versus the case when spectral notching wasn't present.



# INTERFERENCE SUPPRESSION IN MULTIPLE ACCESS COMMUNICATIONS USING M-ARY PHASE SHIFT KEYING GENERATED VIA SPECTRAL ENCODING

## 1. Introduction

### 1.1 Introduction

Digital communication systems have become an integral part of commercial day-to-day operations and are extensively employed across today's modern battlefield. Military applications include airborne, seaborne, and ground-based communications, navigation such as the Global Positioning System (GPS), and unmanned aerial vehicle (UAV) communications and control. However, because of the nature of war itself, military applications often require special capabilities not commonly associated with commercial applications communications, e.g., secure operation, hostile (intentional) radio frequency (RF) interference, and transmission of large amounts of data between systems (platforms) which often times were designed and built without any need or forethought of integration.

There are two aspects to providing secure communications. The first aspect involves preventing the enemy from intercepting the transmitted signal (detecting that communication is occurring). The second aspect involves preventing the enemy from deciphering the transmitted signal if it is intercepted (extracting the information from the communications).

There are several types of RF interference that occur on the battlefield. The first type of interference is the result of thermal noise and is inherent in all communication systems, including commercial ones. The random electron motion which

occurs in all electronic devices induces thermal noise [1]. The second type of battlefield interference comes from additional communication transmitters operating in the environment, including radio stations, television stations, and cell phone systems. The third type of battlefield interference is intentional, i.e., communication and radar jammers which are introduced solely for the purpose of disrupting effective communications.

The transmission of large amounts of data allows accurate instructions to be transmitted on the battlefield. One example is the control of a UAV which requires precise instructions from its home base. Another example is a smart bomb which requires precise targeting instructions from an aircraft. A reduction in transmission rate from the communication system could hinder the ability of these weapon systems to effectively accomplish their mission.

In communication systems, a transmitter sends a signal over a channel. By the time the signal reaches the receiver, the received signal consists of the transmitted signal plus interference. Traditional communication systems deal with channel interference in one of two ways. First, the receiver may notch out frequencies where it senses interference is occurring. Although this receiver notching effectively removes the source of interference, it also removes some of the desired signal energy which was transmitted in the signal. Second, the receiver can estimate the interference and subtract the estimate from the received signal. The main problem with this interference estimation method is that portions of the transmitted signal could be confused with interference and be subtracted from the received signal as well [2]. In both of these receiver processing techniques, desired signal energy is removed prior to detection and estimation.

Communication systems can provide secure communications by encrypting information. One problem with encrypting information is that system bandwidth typically increases (assuming the desired data rate of the information remains the same). Another problem is that the signal may still be non-cooperatively intercepted even

though it may be undecipherable. Although the information content of messages are not discernable, the detection of a signal betrays the presence of the communication system and could still lead to system geolocation.

Traditional communication systems provide high data transmission rates by efficiently using bandwidth [3]. Different data modulation techniques permit different transmission rates and provide different probability of bit error. Choosing the appropriate data modulation technique generally requires a trading-off analysis of data transmission rate and bit error probability.

Spread spectrum systems were primarily developed by the military as a method for providing secure communications in environments containing significant amounts of RF interference. Two widely used spread spectrum modulation schemes are direct sequence spread spectrum (DSSS) and frequency hopping spread spectrum (FHSS) [4]. FHSS systems mitigate interference effects by spectrally hopping from one frequency band to another. If interference is present during operations, it only affects the received signal for the portion of time when the hop frequency is in the same frequency band as the interference. Frequency hopping systems provide secure communications since the receiver needs to know the frequency hopping sequence to demodulate the received signal [4].

In DSSS communications, interference is suppressed by having the transmitter spread the desired signal over a bandwidth which is much wider than otherwise required. The receiver then despreads the received signal. Any interference present during despreading has less of an effect on received signal-to-noise ratio since it spans a smaller fraction of the received signal versus a traditional communication system. The DSSS technique also provides security since the intended receiver needs to know the despreading code to effectively demodulate the received signal [4].

The transform domain communication system (TDCS) uses a form of spectral coding to take interference suppression (avoidance) one step beyond traditional spread spectrum techniques. The TDCS spreads the transmitted signal over a large

bandwidth while excluding spectral regions containing significant amounts of interference. The receiver then receives the transmitted TDCS signal energy without significant amounts of interference [5]. Because of the spectral coding method used by the TDCS to spread the signal, the time domain signal appears noise-like and unintended receivers have a more difficult time intercepting it. If the TDCS signal is non-cooperatively intercepted, the signal remains nearly impossible to demodulate without prior knowledge of the spreading code used to modulate the signal.

The origin of the TDCS concept can be traced back to work by German and Andren. German proposed designing a direct sequence system which avoided jammed frequencies. This was done by having the transmitter generate a spreading code which did not have any frequency components in areas containing spectral interference. Andren subsequently designed a system where the transmitter generated a signal which avoided frequency components in spectral regions containing interference. The receiver only extracts energy from spectral regions containing no interference (i.e., using only spectral components where the transmitter placed energy) and then processes the signal [5].

Radcliffe combined the ideas of German and Andren to generate the conceptual TDCS considered here. In Radcliffe's TDCS design, time domain "basis functions" (called fundamental signaling waveforms in this work) are generated which don't contain energy in spectral regions containing interference. The TDCS technique then data modulates these basis functions to produce the digitally encoded waveform. The types of data modulation considered by Radcliffe were cyclic shift keying (CSK) and binary phase shift keying modulation (antipodal signaling) [5].

Swackhammer expanded Radcliffe's work by investigating a multiple access version of the TDCS. Multiple access capability allows multiple transmitter/receiver pairs to simultaneously communicate using the same portion of the RF spectrum. Swackhammer implemented a multiple access design using spreading codes (multiple access codes) generated from linear feedback shift registers. The spreading codes

were used in a phase-mapping process to generate a set of unique phase values to spectrally encode multiple access users. The types of data modulation considered for his design were CSK and BPSK modulation [6].

## 1.2 Problem Statement

Previous research has shown that the TDCS technique can be used to provide reliable communications in hostile RF environments while generating a low probability of intercept signal. Previous research has also shown that multiple access capability is achievable through properly phase coding (spectrally encoding) the spectrally notched, interference avoiding waveforms. Previous TDCS research predominantly focused on CSK and BPSK data modulation for communicating. This work introduces a form of spectral encoding which provides  $M$ -Ary phase shift keying data modulation and orthogonal signaling for multiple access capability. As with traditional MPSK signaling, the spectrally encoded waveforms generated here can carry more information than BPSK waveforms using the same bandwidth. Performance of the proposed TD-MPSK technique will be first characterized for a single transmitter-receiver pair operating in an environment containing multiple access and intentional interference (jamming).

## 1.3 Research Assumptions

The following assumptions were used when modeling the communication system and are consistent with previous TDCS work [7, 5, 2]

1. Communication channel noise is additive white Gaussian noise.
2. Perfect synchronization between each transmitter/receiver pair.
3. Perfect code synchronization between each transmitter/receiver pair.
4. There are no multi-path signals present in the network. Transmitted signals only propagate along one line-of-sight path to the receiver of interest.
5. There is no Doppler shift on the received signals. The receiver of interest and all

transmitters are stationary relative to each other.

## 1.4 Research Scope

The scope of this research was limited by assumptions contained in Section 1.3. Spectrally encoded TDCS techniques were analyzed and simulations conducted for communication performance and multiple access capability using  $M = 2, 4, 8$  and 16 communication symbols, i.e., TD-BPSK, TD-QPSK, TD-8PSK, and TD-16PSK systems, respectively. The first research goal was to establish the probability of symbol error ( $P_E$ ) and probability of bit error ( $P_B$ ) versus normalized signal-to-noise ratio ( $E_b/N_0$ ) performance for the TD-MPSK systems considered. The error was determined for different multiple access and jamming environments. The second research goal was to determine  $P_B$  performance versus the number of multiple access users in a jamming environment. The third research goal involved an investigation for optimizing the spectral encoding (phase code selection and/or assignment) such that multiple access interference is minimized.

## 1.5 Research Approach

The first part of the research involved establishing communication performance of a single TD-MPSK transmitter-receiver pair. Performance for this part of the research was characterized using probability of bit error ( $P_B$ ) versus the normalized signal-to-noise ratio. A Matlab<sup>®</sup> model of the TD-MPSK communication system was developed. This model generated a random data modulated signal, added AWGN to the signal and then demodulated the signal. After demodulating the signal, communication symbol estimates were compared to originally modulated symbols to determine if there was an error. A Monte Carlo analysis was then conducted using this modulation-demodulation process which was repeated at different normalized signal-to-noise ratios. The  $P_B$  for different normalized signal-to-noise ratios was then

observed. The observed  $P_B$  was then compared with that obtained from expressions for analytic  $P_B$  performance. Different scenarios were tested for multiple access interference, jamming, and notching of frequency components with interference. The second part of the research involved determining communication performance of a single transmitter-receiver pair using a fixed, normalized signal-to-noise ratio while varying the number of network users. Using the same Matlab® model used for communication performance characterization, random symbols were again generated, the fundamental signaling waveform was modulated, AWGN was added, and multiple access signals from the different users were added. The demodulated symbols at the receiver were then compared to modulated symbols and errors determined. A Monte Carlo analysis was again conducted using the modulation-demodulation process using a different numbers of additional users. The  $P_B$  for the different number of users was observed and once again compared to analytic  $P_B$  performance. The different scenarios included jamming, notching, and a combination of jamming and notching.

## 1.6 Materials and Equipment

The proposed, spectrally encoded TDCS system was simulated using Matlab®, Version 6.1. Mathworks, Inc., developed by Matlab® as a computer language for technical computing[8]. The simulations were run on a 1.0 GHz Pentium III personal computer.

## 1.7 Thesis Organization

Chapter 2 of the thesis provides background information on the conceptual TDCS system, phase shift keying modulation, CSK modulation, and linear phase shift registers. Chapter 3 provides an overview of how the communication signals and the RF environment are modeled. It also provides a discussion on Monte Carlo analysis as used in computer simulation of the proposed TDCS technique. Chapter 4 provides a comparison of theoretical and simulated results for different scenarios

considered under the research. Chapter 5 discusses conclusions that can be drawn from the research and provides recommendations for future research. Appendix A contains the Matlab® simulation code developed and used for the communication system. Appendix B contains mathematical derivations for some of the key results obtained as part of the research and dispersed throughout the document.



## 2. Literature Review

### 2.1 Introduction

This chapter introduces MPSK as a modulation technique obtained via spectral encoding, with specific application to a multiple access transform domain communication system (MA-TDCS). Section 2.2 describes MPSK. Section 2.3 describes a conceptual transform domain communication system (TDCS) which uses spectral encoding to achieve multiple access capability and interference suppression. Section 2.4 describes code division multiple access (CDMA) and Section 2.5 summarizes the chapter.

### 2.2 Phase Shift Keying

Phase shift keying (PSK) is a method of modulation where each communication symbol has equal energy and can be represented as the sum of two amplitude modulated orthonormal signals (a pair of unit energy, orthogonal basis functions). The orthonormal signals are represented by the functions  $\psi_1(t)$  and  $\psi_2(t)$ . The sum of the two amplitude modulated orthonormal signals making up the  $i^{th}$  symbol (one of  $M$ ) is given by (2.1) [3]. The symbol phase values  $\phi_i$  can be assigned per (2.2) which ensures equal angular spacing between phase values.

$$s_i(t) = \sqrt{E} \cos(\phi_i) \psi_1(t) + \sqrt{E} \sin(\phi_i) \psi_2(t) \quad 0 \leq t \leq T \quad (2.1)$$

$$\phi_i = \frac{2\pi i}{M} \quad i = 1, \dots, M \quad (2.2)$$

**2.2.1 Binary Phase Shift Keying.** For Binary phase shift keying (BPSK) there are two communication symbols with each representing one of two bit values. Given  $M = 2$  for binary signaling, (2.1) reduces to (2.3).

$$s_i(t) = \sqrt{E} \cos(\phi_i) \psi_1(t) \quad 0 \leq t \leq T \quad i = 1, 2 \quad (2.3)$$

$$\phi_i = \pi i \quad i = 1, 2 \quad (2.4)$$

For optimal maximum likelihood detection and estimation of BPSK signals, only one correlator is needed to obtain matched filter performance. Assuming the transmitted bit values are equally probable, and signaling is being conducted over an AWGN channel, the single correlator can be “matched” to the basis function used to create the communication symbols and achieve optimal performance (minimum bit error rate). In this case, the optimum detection threshold is zero and the correlator output “sign” determines the symbol estimate, e.g., a positive output dictates estimating the bit as a 1 and a negative output dictates estimating the bit as a 0. Figure 2.1 shows a block diagram of a single channel BPSK correlation receiver [3] where the correlation reference signal is the  $\psi_1(t)$  basis function. Received signal  $r(t)$  is the sum of the modulated communication signal, environmental interference (other signals) and channel noise. Received signal  $r(t)$  and the correlator reference signal  $\psi_1(t)$  are multiplied and integrated over one symbol interval  $T_s$ . The sign of the integration result forms the basis for making a decision (estimating) as to which of the two symbols are present in  $r(t)$ .

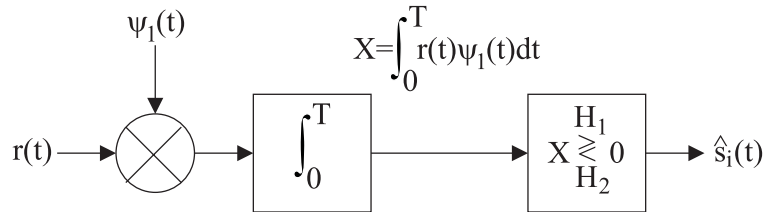


Figure 2.1 Single Channel BPSK Correlation Receiver

Given there are only two symbols in binary signaling, and assuming equal energy signaling, the average symbol energy ( $E_s$ ) equals average bit energy ( $E_b$ ).

Once the normalized signal-to-noise ratio ( $E_b/N_0$ ) is calculated, probability of bit error  $P_B$  can be determined using (2.5) [3] where  $N_0/2$  is the two-sided noise power spectral density.

$$P_B = Q \left[ \sqrt{2 \left( \frac{E_b}{N_0} \right)} \right] \quad (2.5)$$

**2.2.2 M-Ary Phase Shift Keying.** For  $M$ -Ary Phase Shift Keying (MPSK), there are  $M$  communication symbols where  $M = 2^k$  and  $k > 1$ ; each MPSK symbol represents  $k$  bits. Figure 2.2 shows a two channel correlation receiver that can be used for all MPSK systems [3]. Received signal  $r(t)$  is split and passed to two correlation paths. In each correlation path,  $r(t)$  is multiplied by one of the two basis functions originally used to represent the communication symbols. Following integration over each symbol interval, a ratio ( $Y/X$ ) is formed between the two correlator channel outputs. Estimated phase value  $\hat{\phi}$  is established by taking the arctangent of  $Y/X$  and compared with each possible phase value of the  $M$  communications symbols. The symbol phase value which is closest to the estimated phase value is estimated as being received. Under equally probable conditions (all symbols transmitted with equal apriori probability) and signaling over an AWGN channel, this two channel correlation process is equivalent to maximum likelihood detection and provides minimum probability of symbol error ( $P_E$ ) and bit error ( $P_B$ ) [9]

For MPSK signaling, average symbol energy ( $E_s$ ) is  $k$  times average bit energy ( $E_b$ ) where  $k$  is the number of bits represented by each symbol. Equation (2.6) and (2.7) provide good estimates of  $P_E$  and  $P_B$  under high signal-to-noise conditions and are based on Gray code bit-to-symbol assignment [3]. These equations are primarily based on accounting for adjacent symbol errors only, i.e., they only take into account the most probable (dominant) symbol error conditions which are adjacent symbol

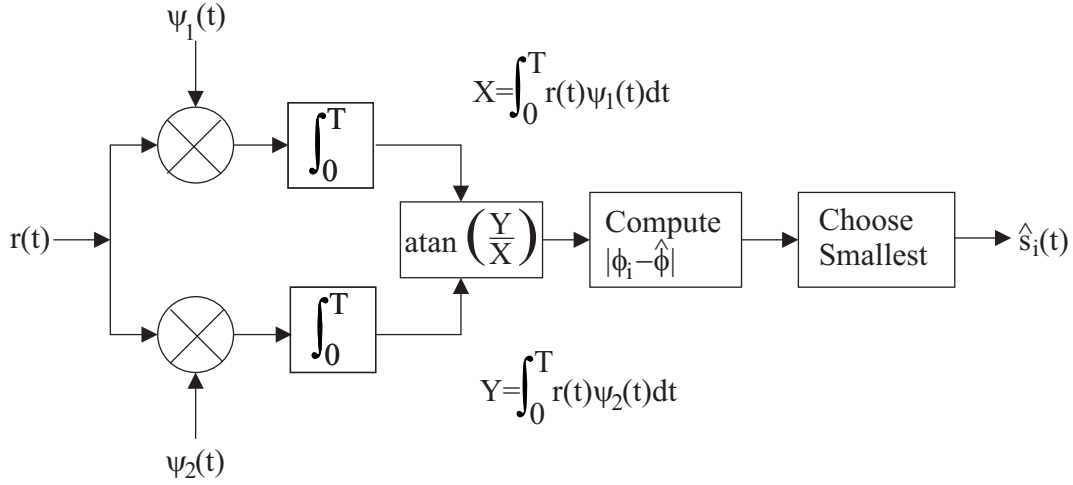


Figure 2.2 Two Channel Correlation Receiver for MPSK Signaling

estimation errors. As the signal-to-noise ratio decreases, adjacent symbol errors become less dominant and these equations become less accurate.

$$P_E \approx 2Q \left[ \sqrt{2k \left( \frac{E_b}{N_0} \right) \sin \left( \frac{\pi}{M} \right)} \right] \quad (2.6)$$

$$P_B \approx \frac{2}{k} Q \left[ \sqrt{2k \left( \frac{E_b}{N_0} \right) \sin \left( \frac{\pi}{M} \right)} \right] \quad (2.7)$$

Under lower signal-to-noise conditions, (2.8) provides a more accurate means for calculating a theoretical  $P_B$  estimate [10].

$$P_B = \frac{1}{k} \sum_{m=1}^{M-1} W_m D_m \left( \frac{E_b}{N_0} \right) \quad (2.8)$$

The  $D_m$  term in (2.8) is calculated using (2.9) where  $Q[x]$  is the complementary error function. The  $W_m$  terms in (2.8) are given in Table 2.1 for the three  $M$  values shown.

Table 2.1 Mapping Weights for Theoretical  $P_B$  Calculations per (2.8)

	$M = 4$			$M = 8$			$M = 16$
m	$W_m$		m	$W_m$		m	$W_m$
0	0		0	0		0	0
1	1		1	1		1	1
2	2		2	2		2	2
3	1		3	2		3	2
			4	2		4	2
			5	2		5	2.5
			6	2		6	3
			7	1		7	2.5
						8	2
						9	2.5
						10	3
						11	2.5
						12	2
						13	2
						14	2
						15	1

$$D_m = \begin{cases} \int_0^\infty f\left(z - \sqrt{2k \frac{E_b}{N_0}}\right) \{Q[z \tan((2m-1)\frac{\pi}{2^k})] - Q[z \tan((2m+1)\frac{\pi}{2^k})]\} dz \\ m = 0, 1, \dots, \frac{M}{4} - 1 \\ \int_0^\infty f\left(z + \sqrt{2k \frac{E_b}{N_0}}\right) \{Q[z \tan((M-2m-1)\frac{\pi}{2^k})] - Q[z \tan((M-2m+1)\frac{\pi}{2^k})]\} dz \\ m = \frac{M}{4} + 1, \dots, \frac{M}{2} \end{cases} \quad (2.9)$$

$$f(t) = e^{\frac{-t^2}{2}}$$

It should be noted that (2.9) in and of itself does not provide all the required values of  $D_m$  for all  $m$ . However, the relationships provided in (2.10) and (2.11) can be used to permit complete generation of required  $D_m$  values.

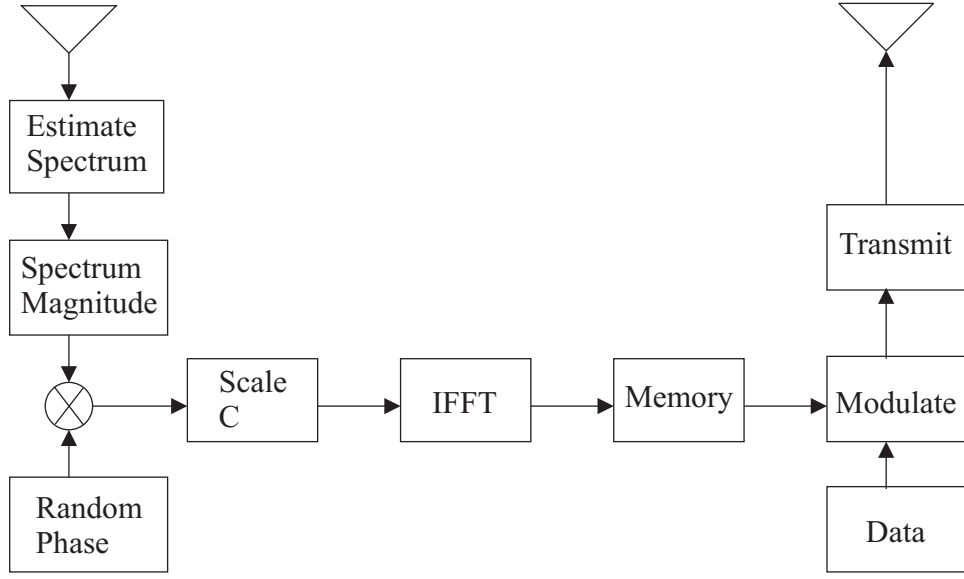


Figure 2.3 Conceptual TDCS Transmitter

$$D_{M-m} = D_m \quad (2.10)$$

$$\sum_{m=0}^{M-1} D_m = 1 \quad (2.11)$$

### 2.3 Transform Domain Communication System (TDCS)

The purpose of a TDCS system is to communicate in a radio frequency (RF) environment containing extensive interference. Normally, communication systems attempt to mitigate interference effects by employing sophisticated filtering techniques in the time and/or frequency domains. A TDCS effectively samples the RF environment and generates “smart” waveforms at the transmitter; “smart” here simply implies the transmitted waveforms contain no (minimal) energy in spectral areas containing interference [5]. Figure 2.3 shows a block diagram of a conceptual TDCS transmitter.

**2.3.1 TDCS Transmitter.** The TDCS transmitter of Fig. 2.3 uses several processing steps for signal generation prior to transmission. First, the RF environment is sampled and a spectral estimate of the energy obtained. Second, the spectral estimate is analyzed to determine which region(s) of the RF environment contain interference (interference here includes all sources of radiation not generated by the TDCS itself). Third, a fundamental signaling waveform is generated containing frequency components in the region(s) containing interference. Fourth, the fundamental waveform is stored for subsequent replication and modulation. Finally, the fundamental waveform is data modulated to create the final signal for transmission [5]. The following paragraphs describe the functionality of each block in Fig. 2.3 in greater detail.

**2.3.1.1 Spectral Estimation.** The first step in TDCS processing involves estimating / locating where in frequency spectral interference is occurring. In fourier-based spectral estimation, the RF environment is sampled at uniform intervals and a discrete Fourier transform (DFT) performed. The DFT is a computational tool for performing frequency analysis of a sampled time domain signal. The DFT effectively describes the spectral content of the RF environment using a discrete number of equally spaced frequency components. The number of frequency components equals the number of samples taken. Each frequency component is described by frequency, amplitude, and phase parameters [11]. The TDCS processing extracts frequency and amplitude information from the DFT and determines which spectral region(s) (actual frequency components) is clear of interference.

**2.3.1.2 Spectral Thresholding.** Given the spectral magnitude response provided by the DFT processing, the TDCS establishes a threshold such that all frequency components (samples) exceeding the threshold (those containing interference) are assigned a value of zero. Frequency components whose magnitudes are below the threshold are deemed interference free and assigned a value of one [12].

**2.3.1.3 Spectral Phase Coding.** Given the TDCS thresholding process has established which frequency components are available for fundamental waveform generation (dictated by the DFT sample values that have been set to one), selection of phase values to be assigned to those components provides the degree of freedom required to enable interference avoiding, multiple access capability; the selection of phase values and their subsequent assignment to frequency components is the form of *spectral encoding* employed here. The Random Phase Generator generates a phase for each of these frequency components. In previous TDCS work, a Pseudo-Random Phase Generator has been employed to generate the required sets of phase values [6]. In this case, linear feedback shift registers were used to generate periodic pseudo-random sequences [4] which were subsequently used in a “phase mapping” process which pseudorandomly assigned a unique sequence of phase values to each user in the network. If both the transmitter and receiver use the same initial register contents for their linear shift register, and the receiver can autonomously synchronize to the transmitter, reliable detection and estimation takes place [6].

**2.3.1.4 Magnitude Scaling for Equal Energy Signaling.** After spectral estimation, thresholding and spectral encoding, the frequency components are scaled to ensure that equal energy symbols are transmitted independent of the number frequency components being used. For example, if only a third of the frequency components remain after thresholding due to interference, the amount of required power contained in each remaining component is tripled relative to the case when no interference is present.

**2.3.1.5 Inverse Discrete Fourier Transform.** The fundamental signaling waveform is obtained by taking the inverse discrete Fourier transform (IDFT) of the scaled, spectrally encoded frequency components. The energy in the resultant time domain waveform is contained entirely in frequency components (spectral locations) where no interference is present [12]. The final set of  $M$  commu-



nication symbols is then created from the fundamental signaling waveform. Perhaps the easiest form of data modulation that can be employed is binary antipodal signaling. For binary antipodal signaling, one symbol is the fundamental waveform itself and the other symbol is the negative of the fundamental waveform. If only one frequency component remains after thresholding, the fundamental waveform is a simple sinusoid and antipodal signaling produces results identical to BPSK [3]; multiplying a simple sinusoid by negative one is equivalent to shifting its phase by  $\pi$ . Using the TDCS process described above, it can be shown that antipodal signaling can be achieved by either 1) negating the fundamental waveform after generation, or, 2) by shifting the spectrally encoded phases of all frequency components by  $\pi$ . An alternate form of data modulation that has been explored extensively in previous TDCS applications is CSK [5, 2, 6]. In CSK symbols are generated by cyclically shifting (in the time domain) the fundamental signaling waveform in proportional amounts determined by the number of desired communication symbols. For example, in binary CSK the first symbol would be the fundamental signaling waveform itself and the second symbol would be generated by extracting the second half of the fundamental waveform and concatenating it onto the first half of the waveform.

**2.3.1.6 Waveform Storage in Memory.** After the fundamental signaling waveform is generated, it is stored in memory and made available to the modulator for subsequent data modulation. As changes in the RF environment are sensed, or at scheduled intervals, the fundamental waveform generation process is repeated and memory updated [12].

**2.3.1.7 Data Modulation.** Data (information) is modulated onto the fundamental waveform prior to transmission. Data modulation is the process whereby baseband information is impressed onto a bandpass signal [1]. In the TDCS case, the baseband information (data bits) is received by the modulator and the modulator decides/determines which of the  $M$  communication symbols to output

in accordance with a predefined bit-to-symbol assignment process. For the binary antipodal signaling described earlier, the modulator would simply take in one bit at a time and output either  $s_1(t)$  (for a binary 1) or  $s_2(t) = -s_1(t)$  (for a binary 0).

**2.3.1.8 Signal Transmission.** Following data modulation, the continuous digitally encoded waveform is ready for transmission. The transmitter may do several things to the waveform prior to actual transmission, including, 1) apply amplification/gain, 2) apply shaping/filtering, 3) apply frequency translation for radiation efficiency, 4) apply frequency translation to ensure operation in assigned spectral region, etc.

**2.3.2 TDCS Receiver Processor.** Functionally, the TDCS receiver contains the same fundamental waveform generator as the transmitter and employs a conventional  $M$ -channel correlation receiver for symbol detection and estimation. Overall system performance is primarily driven by how “similar” the fundamental waveform generated in the receiver “looks like” the one generated at the transmitter. Under ideal conditions, the receiver and transmitter “see” the same interference and generate identical fundamental waveforms; the transmitter puts no energy in the frequency components that were notched out and the receiver extracts no energy (interference) from these same components. In this case, the only remaining error is attributable to the AWGN channel itself. Assuming each of the TDCS receiver channels is “matched” to one of  $M$  possible communication symbols, maximum likelihood detection and estimation is accomplished by simply estimating the received symbol based on the maximum correlator output [3].

## 2.4 Code Division Multiple Access

In code division multiple access (CDMA), multiple users share communication resources (e.g., spectrum) without significantly affecting each other’s performance. In general, multiple users in a CDMA systems do not need to be synchronized to ef-

fectively operate. Coding of the multiple users is usually done in the time domain [4]. As demonstrated in previous TDCS research, it is possible to apply phase coding in the frequency domain (spectrally encode) and achieve multiple access performance; by selecting a set of codes with desirable properties and uniquely assigning them to users CDMA capability can be achieved with TDCS techniques [6].

Frequency Division Multiple Access (FDMA) and Time Division Multiple Access (TDMA) are limited in their multiple access capacity by bandwidth. The mechanism(s) involved in implementing CDMA is different from these and multiple access capability is limited by interference [13]. The capacity is limited only by the level of interference the communication system can tolerate.

## **2.5 Summary**

The conceptual TDCS employing spectral encoding, as introduced in this chapter, provides one method for mitigating interference affects while achieving multiple access communications. By creating “smart” waveforms at the transmitter that effectively “avoid” spectral regions containing interference, the receiver’s task is greatly simplified in that sophisticated filtering techniques are not required to remove interference. The use of MPSK with TDCS process promises to provide more efficient use of bandwidth relative to other modulation techniques (antipodal signaling and CSK modulation) considered previously for TDCS applications.

### 3. Modeling and Simulation Techniques

#### 3.1 Introduction

This chapter provides an overview on how TDCS symbols interact with each other and with interference. It also describes how the TDCS can be used in a MPSK system. Simulation assumptions and a description of the Monte Carlo simulation process are also discussed.

#### 3.2 Transform Domain Symbol Definition

Symbol development for the proposed TD-MPSK technique begins in the frequency domain where phase modulation, both data and coded multiple access, are applied directly to sinusoidal components; this is the spectral encoding referenced throughout this document. Although the spectral encoding process used here is similar to orthogonal frequency division multiplexing (OFDM) [14], i.e., in the OFDM technique data phase modulation is applied in the frequency domain, the TD-MPSK spectral encoding process differs in that data phase modulation applied here is *constant* across all spectral components for a given user. The  $k^{th}$  TD-MPSK communication symbol for user  $v$  is generated from (3.1) where the frequency, time and phase parameters are defined in Table 3.1. The time domain representation of a TD-MPSK symbols is generated by taking the inverse Fourier transform of (3.1), as shown in (3.2), and selecting a portion of this result to represent the actual communication symbols as shown in (3.3).

$$S_k^{(v)}(f) = \sum_{p=1}^P A_p^{(v)} \left[ \delta(f - pf_{sb})e^{+j(\phi_p^{(v)} + \theta_k^{(v)})} + \delta(f + pf_{sb})e^{-j(\phi_p^{(v)} + \theta_k^{(v)})} \right] \quad (3.1)$$

$$s_k^{(v)}(t) = F^{-1} \left\{ S_k^{(v)}(f) \right\} \quad -\infty \leq t \leq \infty \quad (3.2)$$

Table 3.1 TD-MSPK Symbol Parameters

$t$	Time
$P$	Number of Sinusoidal Components
$T_{sb}$	Symbol Duration
$f_{sb}$	Spectral Sample Spacing
$\theta_k^{(v)}$	Data Phase Modulation
$\phi_n^{(v)}$	Multiple Access Phase Coding

$$s_k^{(v)}(t) = 2 \sum_{p=1}^P A_p \cos \left( 2\pi f_{sb} p t + \phi_p^{(v)} + \theta_k^{(v)} \right) \quad t_o \leq t \leq t_o + T_{sb} \quad (3.3)$$

The time domain symbol sampling rate is chosen as an integer multiple of  $f_{sb}$  where sampling starts at  $t = t_o$ ; sampling can start at  $t_o = 0$  without loss of generality. The important information in the symbol is amplitude, frequency and phase for each sinusoid in the symbol. To ensure all the information from the continuous waveform is in the sampled waveform, the sampling needs to be greater than twice the frequency of the highest frequency sinusoid. The equation for time sampled TD-MSPK symbols is given in (3.4).

$$s_k^{(v)}(n) = \frac{2}{N} \sum_{p=1}^P A_p \cos \left( 2\pi p \frac{n}{N} + \phi_p^{(v)} + \theta_k^{(v)} \right) \quad (3.4)$$

The discrete fourier transform (frequency index =  $m$ ) of the symbol is shown in equation (3.5)

$$S_k^{(v)}(m) = \begin{cases} A_p e^{j(\phi_p^{(v)} + \theta_k^{(v)})} & \text{if } m = p \\ A_p e^{-j(\phi_p^{(v)} + \theta_k^{(v)})} & \text{if } m = N - p \\ 0 & \text{otherwise} \end{cases} \quad (3.5)$$

Since each TD-MPSK symbol is sampled at a frequency which is more than twice that of the highest frequency sinusoid,  $N - p$  is always greater than  $p$  and

there is no aliasing. Analysis of (3.5) provides the key as to how time domain phase modulation is achieved through spectral encoding in the frequency domain.

The energy in a symbol is determined from its autocorrelation. The energy in any TD-MPSK symbol is shown in (3.6). This equation is derived from Section B.3.

$$E_s = \frac{2}{N} \sum_{p=1}^P A_p^2 \quad (3.6)$$

### 3.3 Symbol Cross-Correlation For Synchronous Users

Modifying (3.4), a symbol from another user is shown in equation (3.7).

$$s_l^{(w)}(n) = \frac{2}{N} \sum_{p=1}^P B_p \cos \left( 2\pi p \frac{n}{N} + \phi_p^{(w)} + \theta_l^{(w)} \right) \quad (3.7)$$

The cross-correlation between symbols of synchronous users is shown in (3.8). This equation is derived from Section B.1.

$$\sigma_{s_k^{(v)} s_l^{(w)}} = \frac{2}{N} \sum_{p=1}^P A_p B_p \cos \left( \phi_p^{(v)} - \phi_p^{(w)} + \theta_k^{(v)} - \theta_l^{(w)} \right) \quad (3.8)$$

**3.3.1 Mean and Variance of Symbol Cross-Correlation.** If the data modulation is completely random, the mean value of the cross-correlation between symbols of synchronous users is zero. In this case, the variance of the cross-correlation between symbols of synchronous users for the TD-BPSK version is given by (3.9). This equation is derived from Section B.4. For TD-MPSK ( $M = 2^k$  where  $k > 1$ ), the variance of the cross correlation is given by (3.10). This equation is derived from Section B.5.

$$\mathcal{E}_\theta \left\{ \left( \sigma_{s_k^{(v)} s_l^{(w)}} \right)^2 \right\} = \frac{4}{N^2} \sum_{p=1}^P \sum_{q=1}^P A_p B_p A_q B_q \cos(\phi_p^{(v)} - \phi_p^{(w)}) \cos(\phi_q^{(v)} - \phi_q^{(w)}) \quad (3.9)$$

$$\mathcal{E}_\theta \left\{ \left( \sigma_{s_k^{(v)} s_l^{(w)}} \right)^2 \right\} = \frac{2}{N^2} \sum_{p=1}^P \sum_{q=1}^P A_p B_p A_q B_q \cos(\phi_p^{(v)} - \phi_p^{(w)} - \phi_q^{(v)} + \phi_q^{(w)}) \quad (3.10)$$

If the data phase modulation and multiple access phase coding are completely random, the mean value of the cross-correlation between symbols of synchronous users is zero. The variance of the cross-correlation between symbols of synchronous users for this case is given by (3.11). This equation is derived from Section B.6.

$$\mathcal{E}_{\theta\phi} \left\{ \left( \sigma_{s_k^{(v)} s_l^{(w)}} \right)^2 \right\} = \frac{2}{N^2} \sum_{p=1}^P A_p^2 B_p^2 \quad (3.11)$$

**3.3.2 Mean and Variance of Symbol Cross-Correlation: Orthogonal Code Selection.** The cross-correlation between communication symbols of different synchronous users can be made zero through proper multiple access phase code selection (the orthogonal code case). Section B.7 provides a derivation of how the phase codes are selected. Orthogonal symbols are defined using (3.12).  $P$  is the number of sinusoids that make up a symbol.  $N$  is the number of samples in a symbol where  $N > 2P$ .  $v$  is the number of the user where  $v$  can equal 0 to  $G - 1$  where  $G$  is defined in (3.12). A symbol for another user can be defined with (3.13) where  $w$  is the number of users which can also equal 0 to  $G - 1$ . As long as  $v \neq w$  the correlation between the symbols of the two different users is 0.

$$s_k^{(v)}(n) = \frac{2}{N} \sum_{p=1}^P A_p \cos \left( 2\pi p \frac{n}{N} + \phi_p^{(v)} + \theta_k^{(v)} \right) \quad v = 0, \dots, G - 1 \quad (3.12)$$

$$\phi_p^{(v)} = \phi_p + \sum_{q=1}^p \text{sgn}(A_q) \frac{q2\pi v}{G}$$

$$G = \sum_{r=1}^P \text{sgn}(A_r)$$

$$\text{sgn}(t) = \begin{cases} 1 & t > 0 \\ 0 & t = 0 \\ -1 & t < 0 \end{cases}$$

$$s_l^{(w)}(n) = \frac{2}{N} \sum_{p=1}^P A_p \cos \left( 2\pi p \frac{n}{N} + \phi_p^{(w)} + \theta_l^{(w)} \right) \quad w = 0, \dots, G-1 \quad (3.13)$$

$$\phi_p^{(w)} = \phi_p + \sum_{q=1}^p \text{sgn}(A_q) \frac{q2\pi w}{\sum_{r=1}^P \text{sgn}(A_r)}$$

### 3.4 Symbol Cross-Correlation and Bandlimited Noise

Equation (3.14) provides a definition for narrowband interference ( $I_{NB}$ ) considered for this work. The interference is modeled similar to a symbol in the sense that it is the sum of sinusoids, each with a specific amplitude. However, the phases of the sinusoidal components making up the narrow band interference change each time the interference is generated.

$$I_{NB}(n) = \frac{2}{N} \sum_{p=1}^P B_p \cos \left( 2\pi p \frac{n}{N} + \phi_p \right) \quad (3.14)$$

If the amplitude of each sinusoidal component,  $B_p$ , is known, the noise can be treated as a synchronous symbol with random spreading phases. This gives the cross-correlation mean and variance results obtained when cross-correlating synchronous



symbols with random multiple access phase coding. The final cross-correlation result is shown in (3.15).

$$\mathcal{E}_{\theta\phi} \left\{ \left( \sigma_{s_k^{(v)} I} \right)^2 \right\} = \frac{2}{N^2} \sum_{r=1}^P A_r^2 B_r^2 \quad (3.15)$$

### 3.5 Symbol Cross-Correlation for Asynchronous Users

For the asynchronous case three symbols need to be defined. The first symbol comes from user  $v$  and is defined by (3.16). The second and third symbols come from user  $w$  and are defined by (3.17) and (3.18) respectively. The first symbol is correlated with the concatenation of the last part of the second symbol and the first part of the third symbol. The end part of the second symbol has a length of a symbol interval minus a delay defined as  $\tau$ . The beginning part of the third symbol has a length of  $\tau$ .

$$s_i^{(v)}(t) = 2 \sum_{p=1}^P A_p \cos \left( 2\pi f_{sb} p t + \phi_p^{(v)} + \theta_i^{(v)} \right) \quad (3.16)$$

$$s_j^{(w)}(t) = 2 \sum_{p=1}^P B_p \cos \left( 2\pi f_{sb} p t + \phi_p^{(w)} + \theta_j^{(w)} \right) \quad (3.17)$$

$$s_k^{(w)}(t) = 2 \sum_{p=1}^P B_p \cos \left( 2\pi f_{sb} p t + \phi_p^{(w)} + \theta_k^{(w)} \right) \quad (3.18)$$

Using the definitions of (3.16), (3.17) and (3.18), the cross-correlation between Symbol  $i$  of User  $v$  and the symbol transition boundary of Symbol  $j$  and Symbol  $k$  for User  $w$ , can be expressed as

$$\begin{aligned}
R_{i,j,k}^{(u,v)} &= \int_0^{T_{sb}-\tau} s_i^{(v)}(t) s_j^{(w)}(t+\tau) dt \\
&+ \int_{T_{sb}-\tau}^{T_{sb}} s_i^{(v)}(t) s_k^{(w)}(t+\tau-T_{sb}) dt
\end{aligned} \tag{3.19}$$

For the case of the sampled symbol where multiple access phase coding is random and uniformly distributed between  $[0, 2\pi]$ , the variance of the cross-correlation can be estimated with (3.20).

$$\begin{aligned}
&\frac{1}{6f_{sb}^2\pi^2} \sum_{p=1}^P A_p^2 B_p^2 \frac{(8p^2\pi^2 + 3)}{p^2} \\
&+ \frac{4}{f_{sb}^2\pi^2} \sum_{p=1}^P \sum_{q=1, q \neq p}^P A_p^2 B_q^2 \frac{(p^2 + q^2)}{(p-q)^2 (p+q)^2}
\end{aligned} \tag{3.20}$$

When the waveforms are sampled at a rate of  $N$  samples per symbol where  $P < 2N$ , the correlation can be estimated by substituting  $N$  for  $f_{sb}$ . The estimate of the correlation of the sampled waveforms is given by 3.21.

$$\begin{aligned}
&\frac{1}{6N^2\pi^2} \sum_{p=1}^P A_p^2 B_p^2 \frac{(8p^2\pi^2 + 3)}{p^2} \\
&+ \frac{4}{N^2\pi^2} \sum_{p=1}^P \sum_{q=1, q \neq p}^P A_p^2 B_q^2 \frac{(p^2 + q^2)}{(p-q)^2 (p+q)^2}
\end{aligned} \tag{3.21}$$

### 3.6 Cross-Correlation Between Two Symbols of Single Synchronous User

As derived in Appendix B, the cross-correlation between two symbols of a single synchronous user is shown in (3.22). Using the symbol energy expression of (3.6), (3.22) can be rewritten as shown in (3.23). As indicated in (3.23), the symbol cross-correlation is simply the symbol energy multiplied by the cosine of the difference between data phase modulation values for the two symbol intervals under consideration.

$$R_{i,j}^{(u,u)} = \frac{2}{N} \sum_{p=1}^P A_p^2 \cos \left( \theta_i^{(v)} - \theta_j^{(v)} \right) \quad (3.22)$$

$$R_{i,j}^{(u,u)} = E_s \cos \left( \theta_i^{(v)} - \theta_j^{(v)} \right) \quad (3.23)$$

The cross-correlation results of (3.23) lead directly into the MPSK data modulation technique proposed for the TDCS. The first step in developing a MPSK system is determining two orthogonal symbols. Equation (3.24) shows the equation for the first orthogonal symbol. Equation (3.25) shows the equation for the second orthogonal symbol. These two equations are the reference symbols used in the demodulator of the MPSK system.

$$\psi_1^{(v)} = \frac{2}{N} \sum_{p=1}^P A_p \cos \left( 2\pi p \frac{n}{N} + \phi_p^{(v)} \right) \quad (3.24)$$

$$\psi_2^{(v)} = \frac{2}{N} \sum_{p=1}^P A_p \sin \left( 2\pi p \frac{n}{N} + \phi_p^{(v)} \right) \quad (3.25)$$

The correlation with the first symbol is the symbol energy multiplied by the cosine of the angle modulation. The correlation with the second symbol is the symbol

energy multiplied by the sine of the angle modulation. The arctangent of the second correlation divided by the first correlation is the phase modulation.

### 3.7 Interference Model

If the normalized signal-to-noise ratio is known, the probability of symbol error ( $P_E$ ) and probability of bit error ( $P_B$ ) can be calculated in the presence of interference. When multiple access interferers are present, the normalized signal-to-noise ratio can be modified to account for the additional interference effects. In this case, the  $E_b/N_0$  term in analytic  $P_E$  and  $P_B$  expressions of section 2.2.1 and section 2.2.2 are commonly replaced with  $E_b/(N_0 + N_i)$  to incorporate interference effects; this  $E_b/(N_0 + N_i)$  can be rewritten as shown in (3.26) [6].

$$\frac{E_b}{N_0 + N_i} = \left[ \left( \frac{E_b}{N_0} \right)^{-1} + \left( \frac{E_b}{N_i} \right)^{-1} \right]^{-1} \quad (3.26)$$

For the proposed TD-MPSK technique, the  $E_b/N_i$  term of (3.26) can be estimated using (3.27) where  $R$  is the number of bits per communication symbol.  $\mathcal{E}_{\theta\phi} \left\{ \left( \sigma_{s_c^{(v)} s_d^{(w)}} \right)^2 \right\}$  is calculated using (3.11).  $E_s$  is calculated using (3.6).

$$\frac{E_b}{N_i} = \frac{1}{2R} \frac{E_s}{\mathcal{E}_{\theta\phi} \left\{ \left( \sigma_{s_c^{(v)} s_d^{(w)}} \right)^2 \right\}} \quad (3.27)$$

If the multiple access phase coding ( $\phi_p$ ) is known for both users the  $E_b/N_i$  term of (3.26) can be estimated using (3.28).  $\mathcal{E}_{\theta} \left\{ \left( \sigma_{s_c^{(v)} s_d^{(w)}} \right)^2 \right\}$  is calculated using (3.9) for the TDCS-BPSK case and (3.10) for the TD-MPSK case.  $E_s$  is once again calculated using (3.6).

$$\frac{E_b}{N_i} = \frac{1}{2R} \frac{E_s}{\mathcal{E}_{\theta} \left\{ \left( \sigma_{s_c^{(v)} s_d^{(w)}} \right)^2 \right\}} \quad (3.28)$$

### 3.8 Monte Carlo Verification

To verify correctness of the analytical results obtained thus far, Monte Carlo simulations were conducted with Matlab<sup>®</sup> generating the AWGN channel response. The AWGN was simply summed with the transmitted signal upon reception by the receiver. The total received signal was demodulated and the estimated communication symbol compared with the modulated symbol. Multiple Bernoulli trials were conducted and probability of error determined [7].

### 3.9 Modeling and Simulation Assumptions

Several limitations are placed on communication system simulations. First, spectral estimation was deemed outside the scope of this research. Therefore, a predetermined interference envelope was established such that the spectral notch removes most of the jamming power. Second, phase mapping development and characterization was also deemed outside the scope of this thesis. Extensive research has been conducted on the phase mapping process used with the conceptual TDCS technique [6]; these previous results are believed to be directly extendable into the proposed TD-MPSK process. The random multiple access phase codes used here are generated based on Matlab<sup>®</sup>'s "*RAND*" function. Third, transmitter/receiver pairs are synchronous. Finally, data phase modulation values are equally likely and uniformly distributed for all  $M$  values considered.

### 3.10 Summary

This chapter provided the definition and development of proposed a TDCS technique using spectral encoding for both data phase and multiple access phase modulations. This chapter described how phase values were selected and MPSK was achieved in a multiple access environment; the resultant technique is termed TD-MPSK. Communication symbol cross-correlation was characterized in both synchronous and asynchronous networks. The correlation of communication symbols

with interference was also discussed. Next the chapter discussed how MPSK signaling can be implemented using conventional, multichannel correlation techniques. Finally, the assumptions used for modeling and simulation were presented.

## 4. Modeling and Simulation: Random Code Selection

### 4.1 Introduction

This chapter provides an overview of the modeling parameters and the scenarios used for testing the proposed TD-MPSK system. The parameters described include the communication symbol spectral response, the jammer spectral response and the notched symbol spectral response. The modeled scenarios include: 1) no interference present (AWGN only), 2) multiple access interference, 3) jamming interference and 4) multiple access and jamming interference without spectral notching and 5) multiple access and jamming interference with spectral notching. The scenarios considered help characterize the TD-MPSK system's ability to communicate in the presence of noise and interference. All scenarios were tested with and without notching.

### 4.2 Modeling Parameters

**4.2.1 Spectral Response of Communication Symbol.** For modeling and simulation purposes, each TD-MPSK communication symbol is made up of  $P = 31$  equal amplitude sinusoids. The sinusoid frequencies range from the symbol rate ( $f_{sb}$ ) to 31 times the symbol rate. The communication symbols are sampled at a rate of 64 samples per symbol. By sampling the symbols at this rate, there is no aliasing. Equation (4.1) is a discrete form of the analytic representation of communication symbols. The magnitude of the discrete Fourier transform of each frequency component of the sampled signal equals one except for the DC and Nyquist components which equal zero. Each communication symbol is made up of 64 samples. Since the number of samples is a power of two, processing is potentially faster. Figure 4.1 is a stem plot showing the spectral response of communication symbols obtained by taking the magnitude of the DFT of a communication symbol. Figure 4.2 is a corresponding time domain representation which was obtained using random

spectral encoding, i.e., a random data phase modulation and a random set of multiple access phase coding.

$$s_k^{(v)}(n) = \frac{1}{32} \sum_{p=1}^{31} \cos \left( 2\pi p \frac{n}{64} + \phi_p^{(v)} + \theta_k^{(v)} \right) \quad (4.1)$$

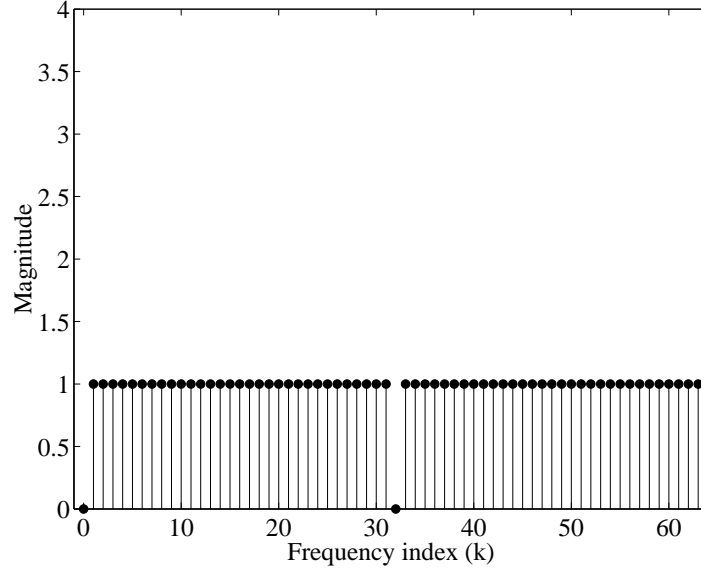


Figure 4.1 Spectral Response (Magnitude of DFT) of Modeled Communication Symbols

**4.2.2 Spectral Response of Jamming.** Narrow band jamming interference can be represented using  $P = 31$  sinusoids with amplitudes and random phase values assigned to provide desired spectral characteristics. Figure 4.3 is a stem plot of the magnitude of the spectrum. Equation (4.2) analytically describes the jamming considered using the values of  $A_p$  listed in Table 4.1. The phase values assigned to spectral components of the jammer are randomly changed for every iteration of the simulation.

$$J(n) = \frac{1}{32} \sum_{p=31}^P A_p \cos \left( 2\pi p \frac{n}{64} + \phi_p \right) \quad (4.2)$$



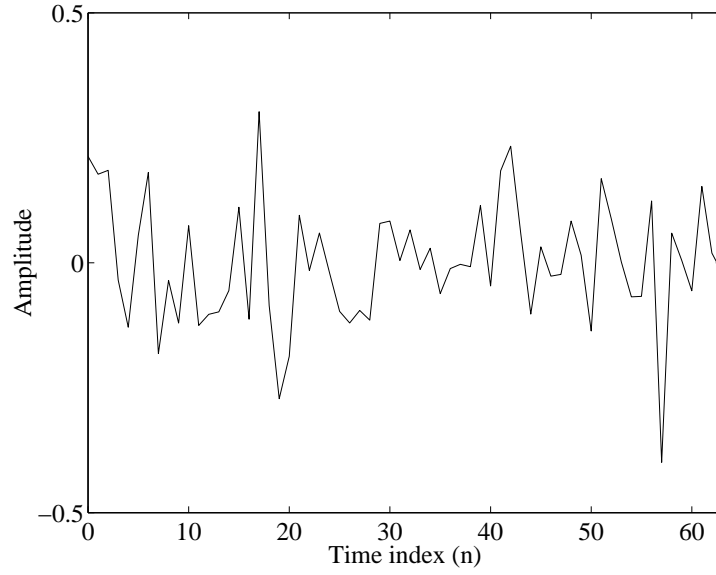


Figure 4.2 Time Domain Response of Modeled Communication Symbol

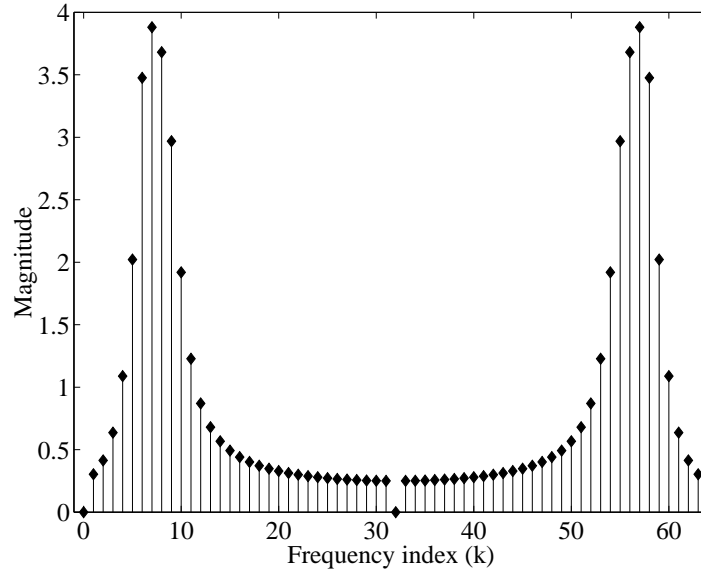


Figure 4.3 Spectral Response of Narrow Band Jammer ( $P = 31$  Sinusoids)

**4.2.3 Spectrum of Notched User.** As stated previously, spectral estimation was not within the scope of this research. However, when modeling the spectrally notched cases, frequency components of the communication symbols in regions containing the highest jamming were selectively notched out (manually set

Table 4.1 Amplitude Coefficients for Jammer of Fig. 4.3

Amplitude	Value		Amplitude	Value		Amplitude	Value
$A_0$	0.0000		$A_1$	0.3034		$A_2$	0.4142
$A_3$	0.6362		$A_4$	1.0888		$A_5$	2.0215
$A_6$	3.4755		$A_7$	3.8799		$A_8$	3.6811
$A_9$	2.9683		$A_{10}$	1.9194		$A_{11}$	1.2279
$A_{12}$	0.8696		$A_{13}$	0.6794		$A_{14}$	0.5667
$A_{15}$	0.4928		$A_{16}$	0.4406		$A_{17}$	0.4017
$A_{18}$	0.3716		$A_{19}$	0.3477		$A_{20}$	0.3284
$A_{21}$	0.3125		$A_{22}$	0.2994		$A_{23}$	0.2884
$A_{24}$	0.2793		$A_{25}$	0.2718		$A_{26}$	0.2656
$A_{27}$	0.2605		$A_{28}$	0.2566		$A_{29}$	0.2535
$A_{30}$	0.2514		$A_{31}$	0.2502		$A_{32}$	0.0000

to zero after applying a manual threshold level). For narrow band simulation, 8 of 31 ( $\approx 25\%$ ) sinusoidal components were notched out. The only criteria used for notching out a frequency component was that the jamming amplitude for that particular component exceeded one. Notching out these frequency components significantly reduces the effects of the jamming interference (12 dB reduction in jamming power). After spectral notching, the amplitude of remaining frequency components is scaled such that the energy of notched symbols equals that of the original symbols. For this 25% narrow band case, the amplitude of remaining frequency components was raised to approximately 1.16. Figure 4.4 is a stem plot of the notched symbol.

**4.2.4 Number of Users.** One variable used throughout this document is  $N_U$ , the number of users in a network. For these simulations, the first user in the network is defined as the receiver in the transmitter/receiver pair whose communication performance is being analyzed. The second user in the network is the transmitter in the transmitter/receiver pair being analyzed. Users 3 through 32 are additional transmitters in the network, i.e., the multiple access interferers. When  $N_U = 2$ , there is no multiple access interference. When  $N_U = 3$  the number of trans-

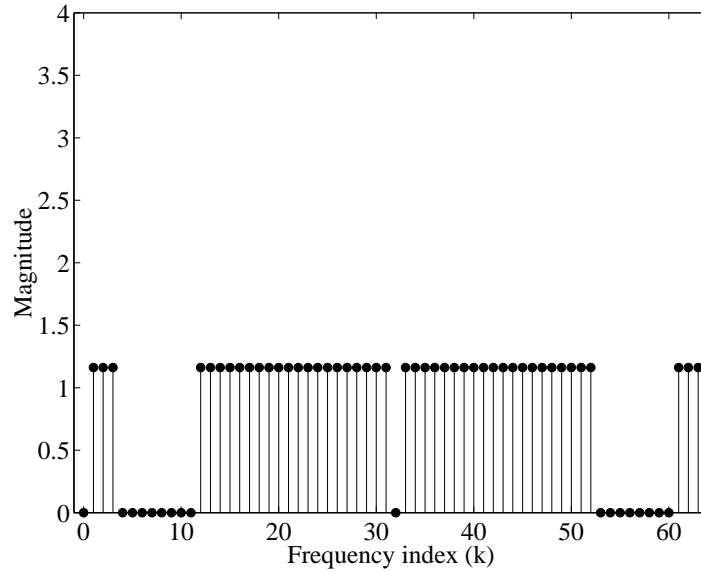


Figure 4.4 Spectral Response (Magnitude of DFT) of Modeled Communication Symbol with Narrow Band Notched Spectrum ( $P = 31$  Sinusoids)

mitters causing multiple access interference is equal to one. In general, the number of multiple access interferers is  $(N_U - 2)$ .

### 4.3 No Interference Present

Figure 4.5 and Fig. 4.6 show probability of symbol error ( $P_E$ ) and probability of bit error ( $P_B$ ) versus normalized signal-to-noise ratio respectively. The Monte Carlo results matched the analytic results for coherent detection of TD-MPSK. One thing that should be noted is that  $P_B$  and  $P_E$  are the same for TD-BPSK; one bit is represented by one symbol in TD-BPSK. It is also interesting to note that the  $P_B$  versus the normalized signal to noise ratio ( $E_b/N_0$ ) is the same for TD-BPSK and TD-QPSK [3]. Another interesting feature of TD-MPSK is that as the level of modulation ( $M$ ) increases, the probability of error increases for fixed  $E_b/N_0$ . This means that there is a trade-off between probability of error and bandwidth efficiency.

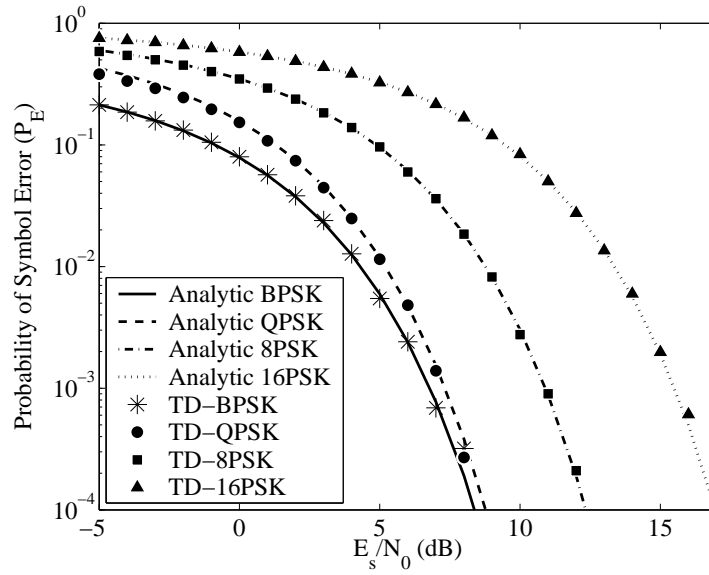


Figure 4.5 No Interference Present:  $P_E$  vs  $E_b/N_0$  for TD-MPSK Signaling with  $P = 31$  Sinusoids

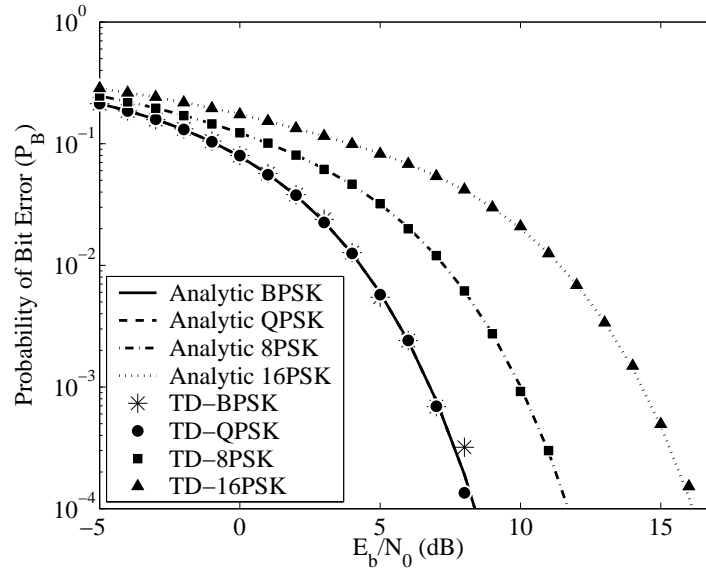


Figure 4.6 No Interference Present:  $P_B$  vs  $E_b/N_0$  for TD-MPSK Signaling with  $P = 31$  Sinusoids

#### 4.4 Spectral Notching Effects

When arbitrary frequency components are spectrally notched and there is no interference present, the  $P_E$  and  $P_B$  performance of the TD-MPSK system are unaf-

affected. Although this is an obvious result, given that scaling is applied after spectral notching, simulations were conducted to ensure proper model operation. Figure 4.7 and Fig 4.8 show  $P_E$  and  $P_B$ , respectively, versus normalized signal-to-noise ratio.

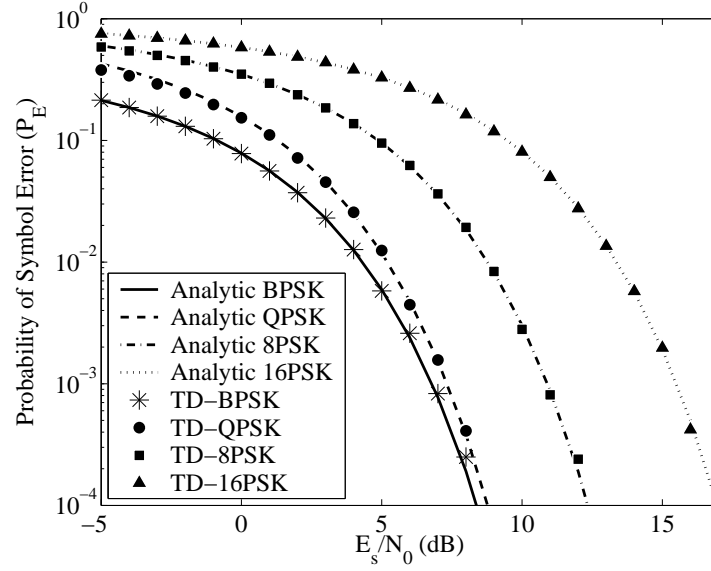


Figure 4.7 Spectral Notching:  $P_E$  vs  $E_b/N_0$  for TD-MPSK Signaling with  $P = 31$  Sinusoids

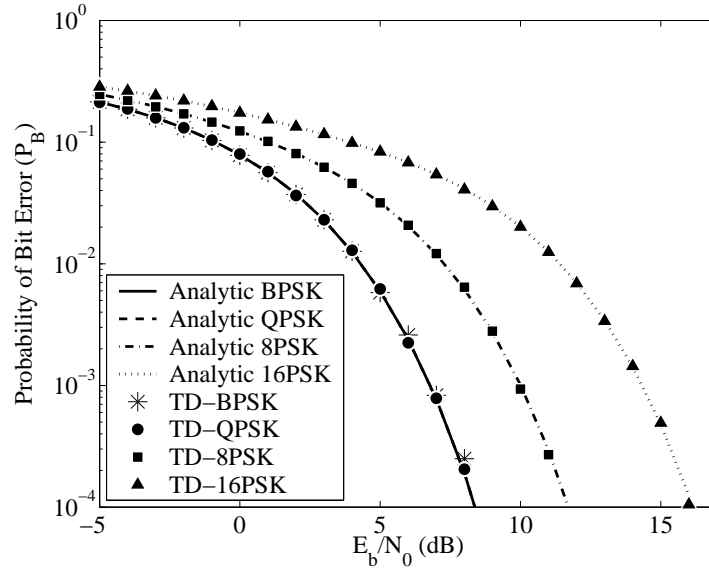


Figure 4.8 Spectral Notching:  $P_B$  vs  $E_b/N_0$  for TD-MPSK Signaling with  $P = 31$  Sinusoids

## 4.5 Jamming Present With *No Spectral Notching*

For the following simulations, the signal-to-interference (average symbol energy-to-average jamming power) ratio ( $J/S$ ) is maintained at 3.14 dB. Figure 4.9 and Fig. 4.10 show  $P_E$  and  $P_B$  versus normalized signal-to-noise ratio, respectively, for the case where the jammer is present. Both figures show how error performance degrades when interference is present. Because the normalized signal-to-noise ratio is maintained, interference effects the higher levels of modulation more than the lower levels of modulation. This can be seen by comparing  $P_E$  for a TD-BPSK system with that of the TD-16PSK system.

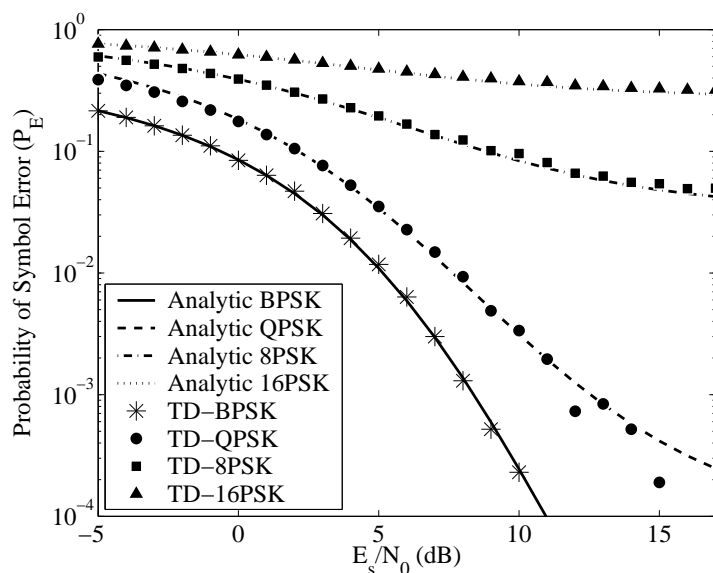


Figure 4.9 Jamming Present with *No Spectral Notching*:  $P_E$  vs  $E_b/N_0$  for TD-MPSK Signaling with  $J/S = 3.14$  dB and  $P = 31$  Sinusoids

## 4.6 Jamming Present *With Spectral Notching*

When spectral notching is added during generation of the communication symbols, there is a dramatic improvement in  $P_E$  and  $P_B$  performance. Figure 4.11 and Fig. 4.12 show  $P_E$  and  $P_B$  versus normalized signal-to-noise ratio, respectively, for this scenario. System performance when spectral notching is employed nearly

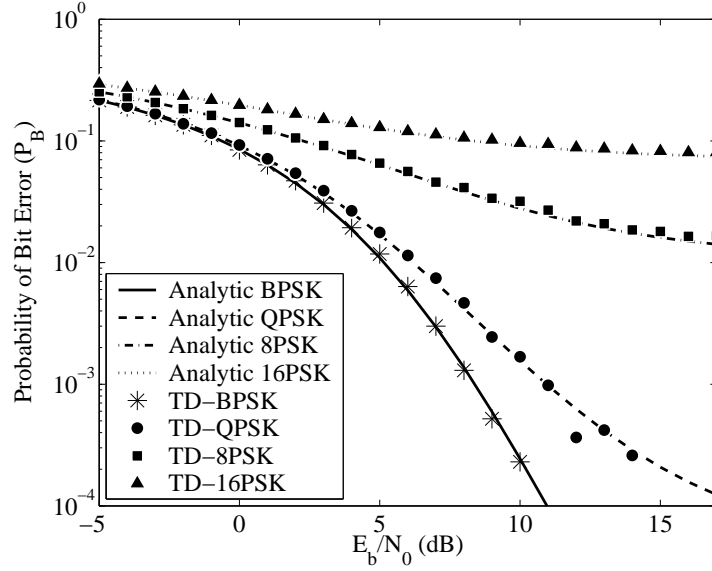


Figure 4.10 Jamming Present with *No Spectral Notching*:  $P_B$  vs  $E_b/N_0$  for TD-MPSK Signaling with  $J/S = 3.14$  dB and  $P = 31$  Sinusoids

matches system performance when no jamming is present (compare these two figures with Fig. 4.5 and Fig. 4.6). However, because the jamming power is not entirely removed, there is a slight increase in error by comparison with scenarios containing no jamming (see TD-BPSK and TD-QPSK performance at higher normalized signal-to-noise ratios). At higher normalized signal-to-noise ratios there is a separation in the error between the two modulation types. If no jamming had been present,  $P_B$  for the two modulation types would have been identical. However, since the signal-to-interference ratio is held constant, the interference affects higher modulation levels, such as TD-QPSK, more than lower levels of modulation, such as TD-BPSK.

#### 4.7 Multiple Access Interference: $N_U = 3$ Users With *No Spectral Notching*

The next scenario involved multiple access interference given only one additional user (transmitter) is present. This additional transmitter uses the same magnitude frequency spectrum as the transmitter/receiver pair (link) of interest. The multiple access phase coding of the additional transmitter is random relative to the

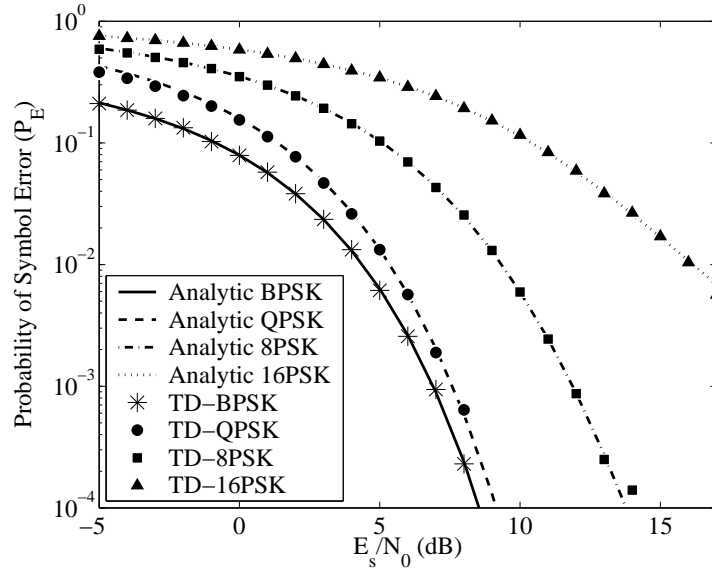


Figure 4.11 Jamming Present *With Spectral Notching*:  $P_E$  vs  $E_b/N_0$  for TD-MPSK Signaling with  $J/S = 3.14$  dB and  $P = 31$  Sinusoids

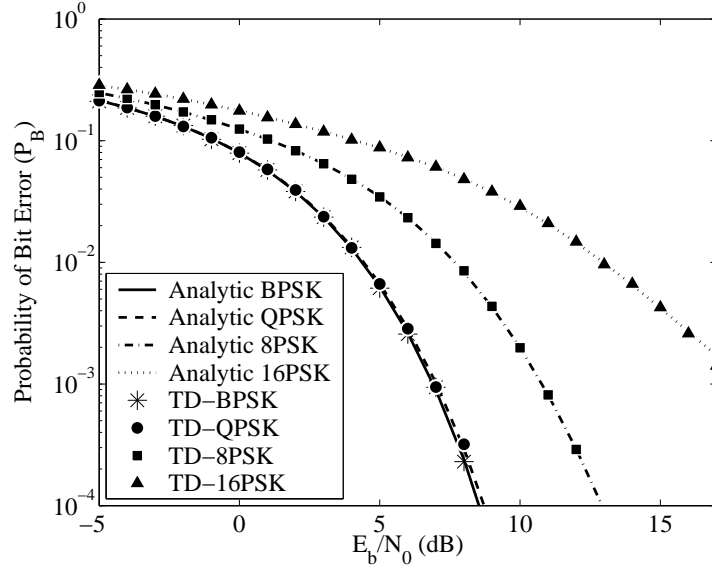


Figure 4.12 Jamming Present *With Spectral Notching*:  $P_B$  vs  $E_b/N_0$  for TD-MPSK Signaling with  $J/S = 3.14$  dB and  $P = 31$  Sinusoids

multiple access phase coding used for the link of interest. Figure 4.13 and Fig. 4.14 show  $P_E$  and  $P_B$  versus normalized signal-to-noise ratio, respectively, for this scenario. In this case, interference from the additional transmitter can be modeled



as being broad band and has the same power as the link of interest. The signal-to-interference ratio remains constant for different levels of modulation. As in the narrow band jamming scenario, the interference affects the higher modulation levels more than the lower modulation levels. Once again this is most obvious by comparing  $P_B$  curves for the TD-QPSK and TD-BPSK data modulations where the multiple access interference affects TD-QPSK more than TD-BPSK.

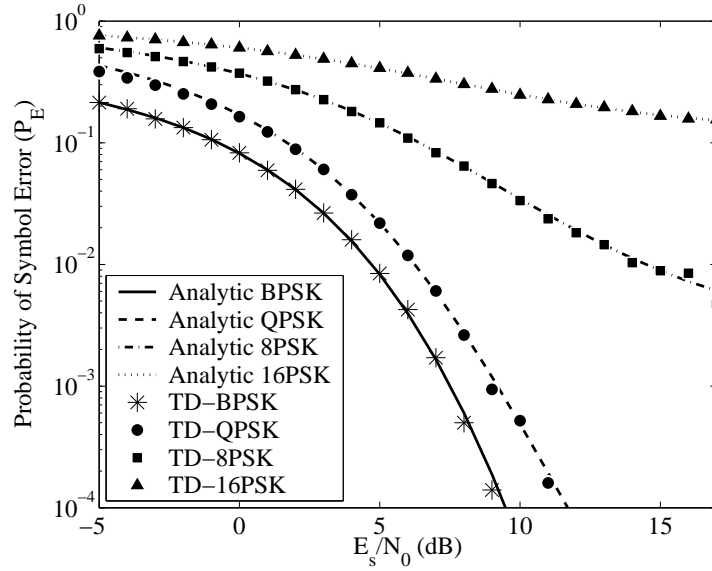


Figure 4.13 Multiple Access Interference for  $N_U = 3$  Users With *No Spectral Notching*:  $P_E$  vs  $E_b/N_0$  for TD-MPSK Signaling with  $P = 31$  Sinusoids

#### 4.8 Multiple Access Interference: $N_U = 2$ to 32 Users With *No Spectral Notching*

As the number of users ( $N_U$ ) increases the probability of error increases. Interference by  $N_U$  users at a particular  $E_b/N_i$  is calculated using (4.3), where  $(N_U - 2)$  is the number of additional users, and it is assumed that the spectrum magnitudes of all users are identical. Equation (4.3) is a modified version of (3.27 which only took into consideration the effect of one additional user.

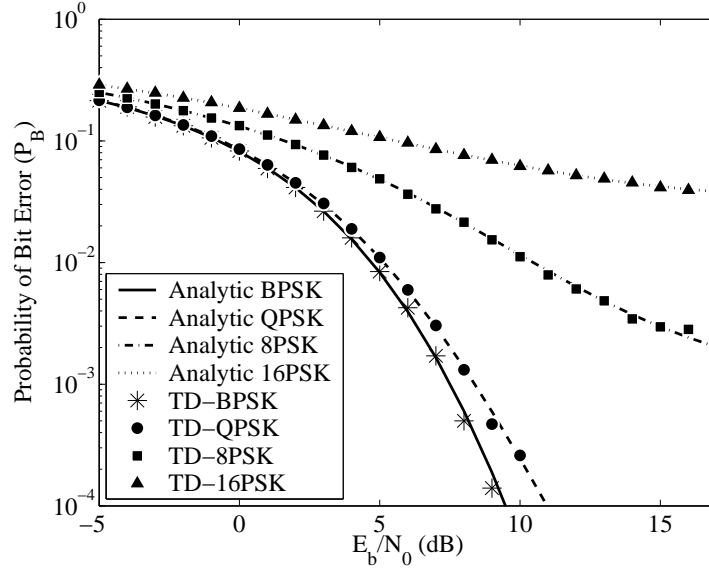


Figure 4.14 Multiple Access Interference for  $N_U = 3$  Users With *No Spectral Notching*:  $P_B$  vs  $E_b/N_0$  for TD-MPSK Signaling with  $P = 31$  Sinusoids

$$\frac{E_b}{N_i} = \frac{1}{2R} \frac{E_s}{(N_U - 2)\mathcal{E}_{\theta\phi} \left\{ \left( \sigma_{s_c^{(v)} s_d^{(w)}} \right)^2 \right\}} \quad (4.3)$$

The result of (4.3) is substituted into the equation for calculating  $E_b/(N_0 + N_i)$  which in turn is used in the analytic  $P_B$  and  $P_E$  equations. As  $N_U$  increases the probability of error increases. Figure 4.15 and Fig. 4.16 show  $P_E$  and  $P_B$  versus  $N_U$ , respectively, for  $N_U = 2$  to 32 users and TD-QPSK data modulation. For these simulations, the normalized signal-to-noise ratio was maintained constant at  $E_b/N_0 = 6.0$  dB. The interference caused by the additional users is proportional to the number of additional users present in the network.

#### 4.9 Asynchronous vs. Synchronous Multiple Access Performance

For equal amplitude sinusoids, asynchronous cross-correlation is approximately the same as synchronous cross-correlation. Figure 4.17 and Fig. 4.18 show  $P_E$  and  $P_B$  versus  $N_U$  respectively for asynchronous networks. A comparison with Fig. 4.15

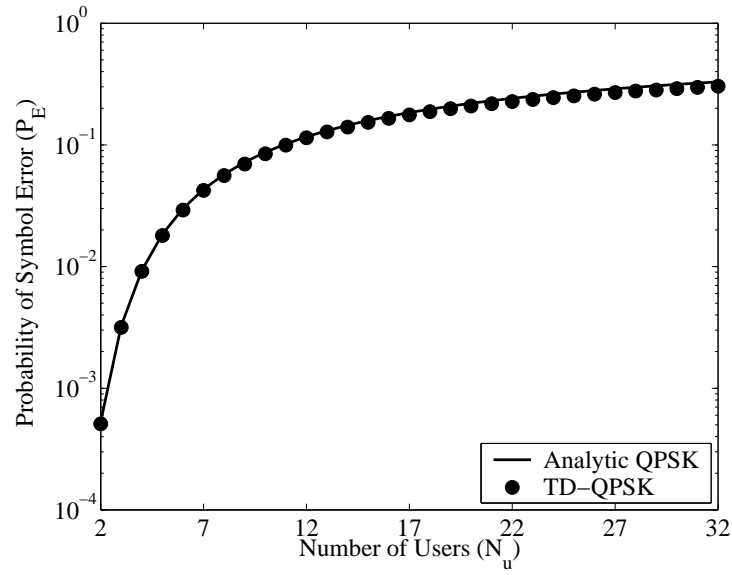


Figure 4.15 Multiple Access Interference for  $N_U = 2$  to 32 Users With *No Spectral Notching*:  $P_E$  vs  $N_U$  for TD-QPSK Signaling with  $P = 31$  Sinusoids

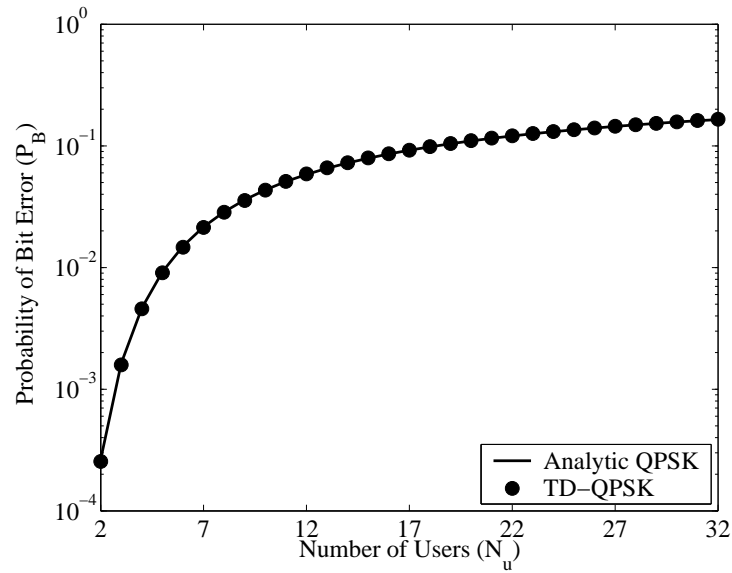


Figure 4.16 Multiple Access Interference for  $N_U = 2$  to 32 Users With *No Spectral Notching*:  $P_B$  vs  $N_U$  for TD-QPSK Signaling with  $P = 31$  Sinusoids

and Fig. 4.16 shows bit error performance is nearly identical under multiple access conditions in synchronous and asynchronous networks.

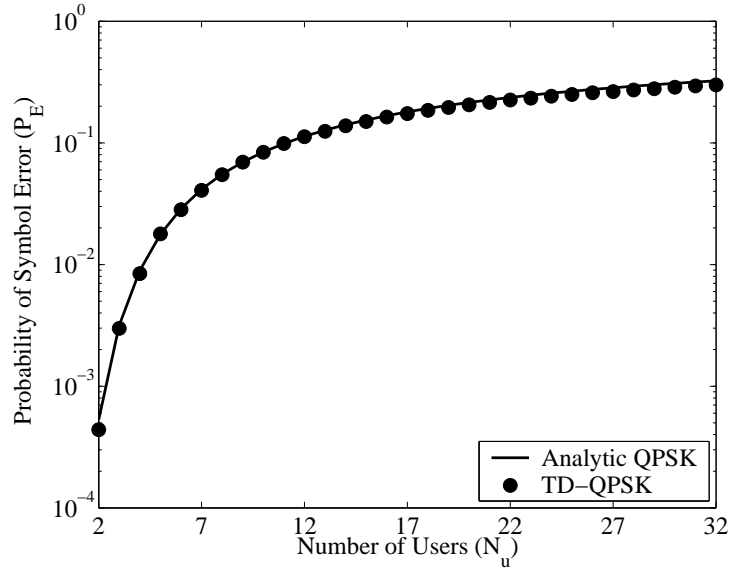


Figure 4.17 Multiple Access Interference with  $N_U = 2$  to 32 *Asynchronous* Users:  $P_E$  vs  $N_U$  for TD-QPSK Signaling with  $P = 31$  Sinusoids

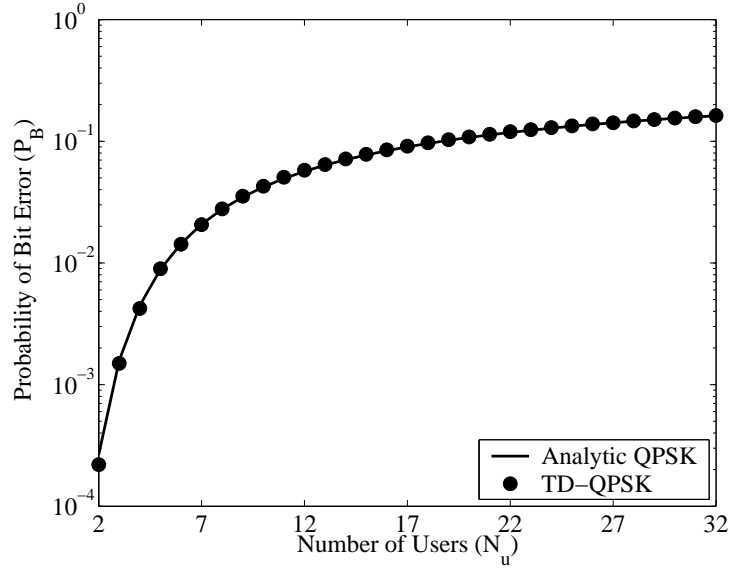


Figure 4.18 Multiple Access Interference with  $N_U = 2$  to 32 *Asynchronous* Users:  $P_B$  vs  $N_U$  for TD-QPSK Signaling with  $P = 31$  Sinusoids

#### 4.10 Multiple Access Interference: $N_U = 3$ Users *With Spectral Notching*

When an additional multiple access user is added to a network employing spectral notching, performance is degraded. As simulated here, additional multiple

access users are assumed to be experiencing the same electromagnetic interference (spectral location and power) as the link of interest. Therefore, all network users generate identical spectral notches as the link of interest. Figure 4.19 and Fig. 4.20 show  $P_B$  and  $P_E$  versus normalized signal-to-noise ratio, respectively, for the  $N_U = 3$  user case. As indicated, the performance of a network using notching is degraded when an additional user is added. Furthermore, the degradation indicated is greater than observed in a system without notching (see Fig. 4.13 and Fig. 4.14 for comparison). This occurs because the notched signal power is spread over fewer frequency components than the signal without notching; fewer frequency components yields higher cross-correlation with additional users and produces higher bit error rates.

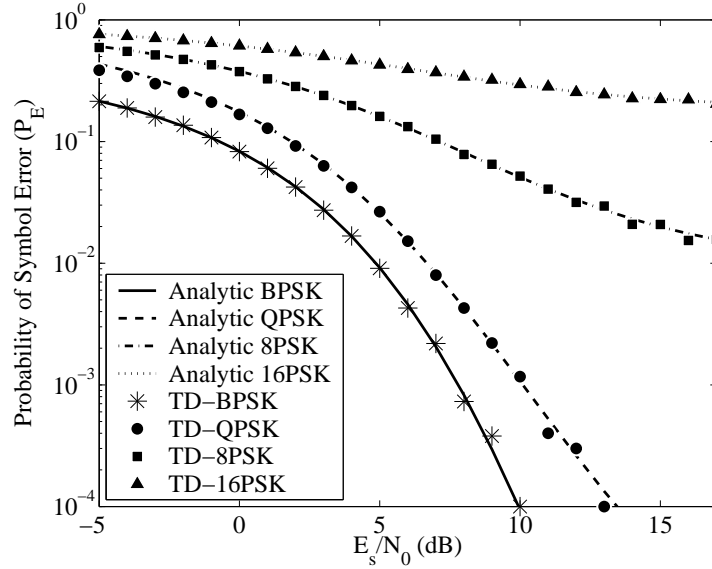


Figure 4.19 Multiple Access Interference for  $N_U = 3$  Users *With Spectral Notching*:  $P_E$  vs  $E_b/N_0$  for TD-MPSK Signaling with  $P = 31$  Sinusoids

#### 4.11 Multiple Access Interference: $N_U = 2$ to 32 Users *With Spectral Notching*

As in the multiple access case with no spectral notching, the amount of multiple access interference is proportional to the number of additional users. However, the amount of interference caused by each user is greater than experienced in the case

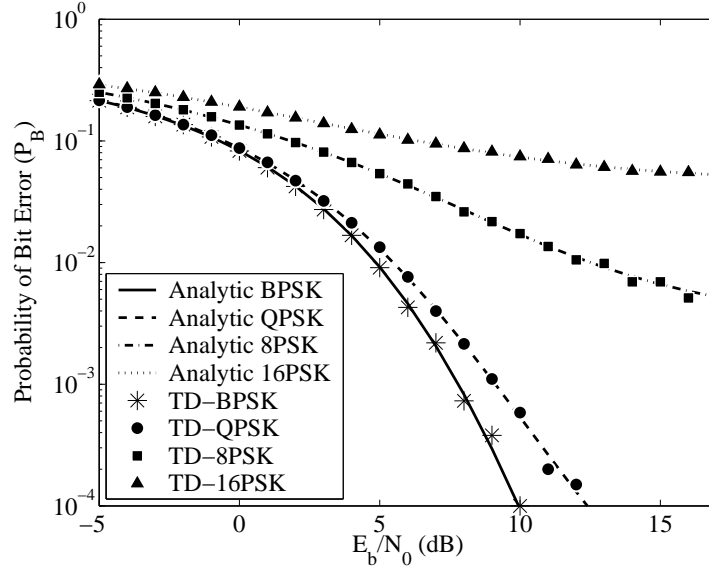


Figure 4.20 Multiple Access Interference for  $N_U = 3$  Users *With Spectral Notching*:  $P_B$  vs  $E_b/N_0$  for TD-MPSK Signaling with  $P = 31$  Sinusoids

with no spectral notching. Figure 4.21 and Fig. 4.22 show  $P_B$  and  $P_E$  versus  $N_U$ , respectively, for  $N_U = 2$  to 32 users with spectral notching. A comparison with results presented in Fig. 4.15 and Fig. 4.16 show how probability of error increases at a greater rate for increasing  $N_U$  when notching is present.

As the spectral notch width increases, multiple access interference increases. Figure 4.23 and Fig. 4.24 show  $P_E$  and  $P_B$  versus notch width  $N_s$  (the number of sinusoidal components zeroed), respectively, for  $N_U = 6$  users and TD-QPSK data modulation. The multiple access interference for these simulations is from 4 additional users having identical magnitude spectra at the transmitters. The simulation process started by modeling all transmitters as using  $P = 31$  sinusoids;  $P_E$  and  $P_B$  performance were then established with the multiple access interference present. The highest frequency sinusoid was then removed and  $P_E$  and  $P_B$  again determined with the multiple access interference present. The process was repeated until only the lowest frequency sinusoid remained. Clearly, as the notch width increases both  $P_E$  and  $P_B$  increase.

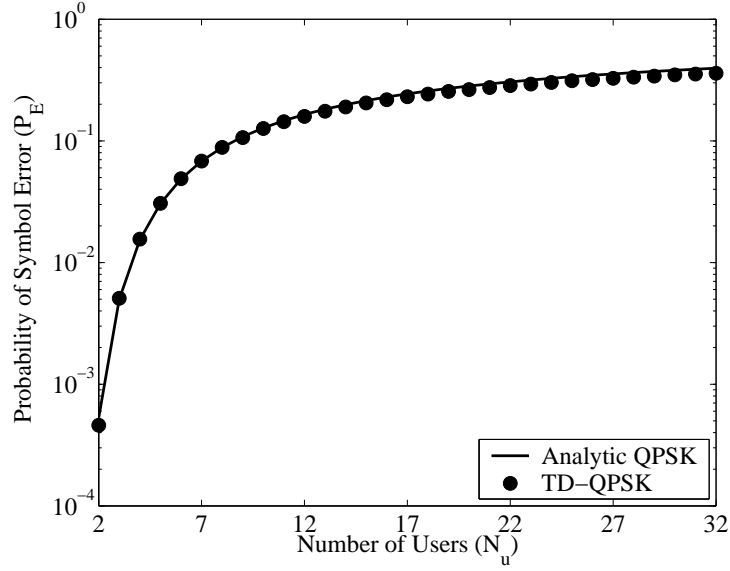


Figure 4.21 Multiple Access Interference for  $N_U = 2$  to 32 Users *With Spectral Notching: Synchronous* Users:  $P_E$  vs  $N_U$  for TD-QPSK Signaling with  $P = 31$  Sinusoids

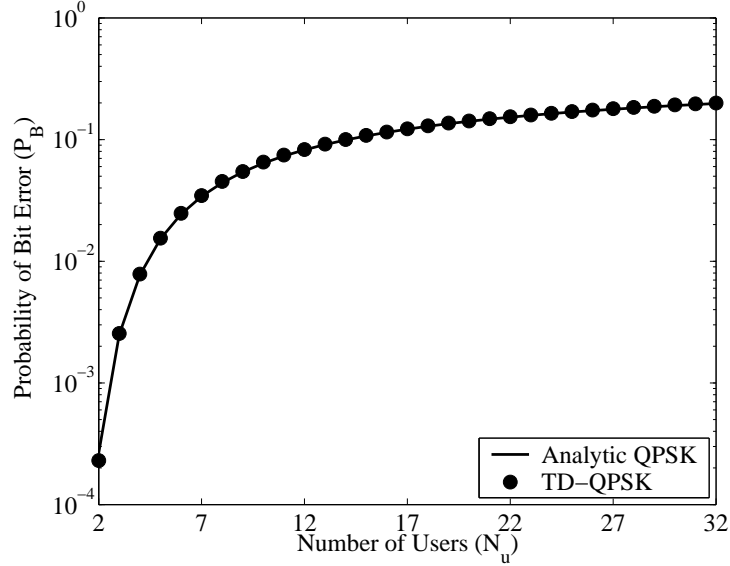


Figure 4.22 Multiple Access Interference for  $N_U = 2$  to 32 Users *With Spectral Notching: Synchronous* Users:  $P_B$  vs  $N_U$  for TD-QPSK Signaling with  $P = 31$  Sinusoids

#### 4.12 Jamming and $N_U = 3$ Users Present With *No Spectral Notching*

When jamming and  $N_U = 3$  Users are present, the interference introduced into the system effectively compounds. Figure 4.25 and Fig. 4.26 show  $P_E$  and

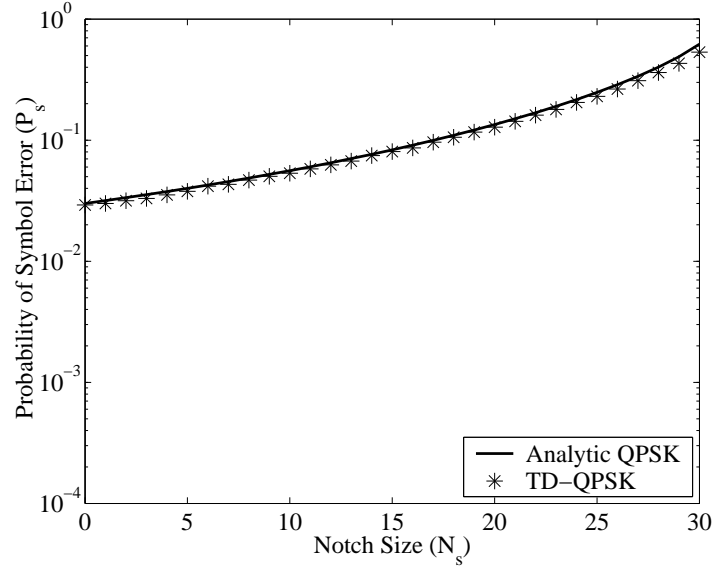


Figure 4.23 Multiple Access Interference for  $N_U = 6$  Users *With Spectral Notching*:  $P_E$  vs Notch Width  $N_s$  for TD-QPSK Signaling

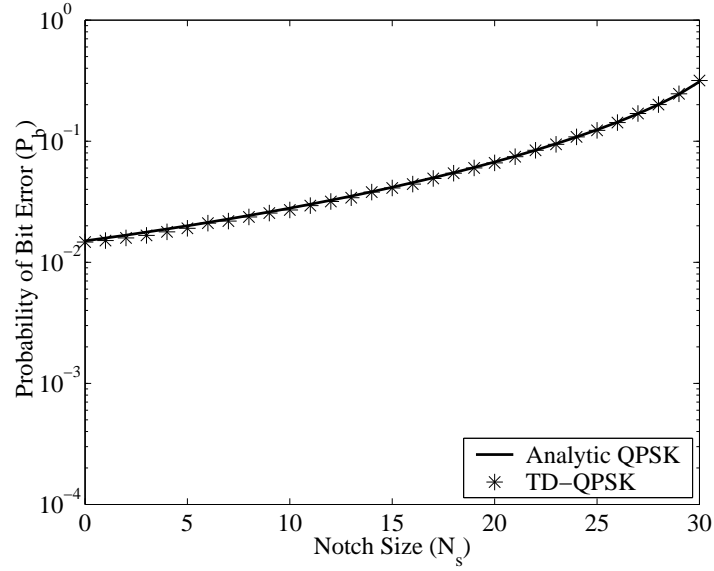


Figure 4.24 Multiple Access Interference for  $N_U = 6$  Users *With Spectral Notching*:  $P_B$  vs Notch Width  $N_s$  for TD-QPSK Signaling

$P_B$  versus the normalized signal-to-noise ratio, respectively, for the case when both jamming and  $N_U = 3$  users are present. As expected, the degradation induced in



system performance is greater than what occurs when either the additional user or the jammer are independently introduced.

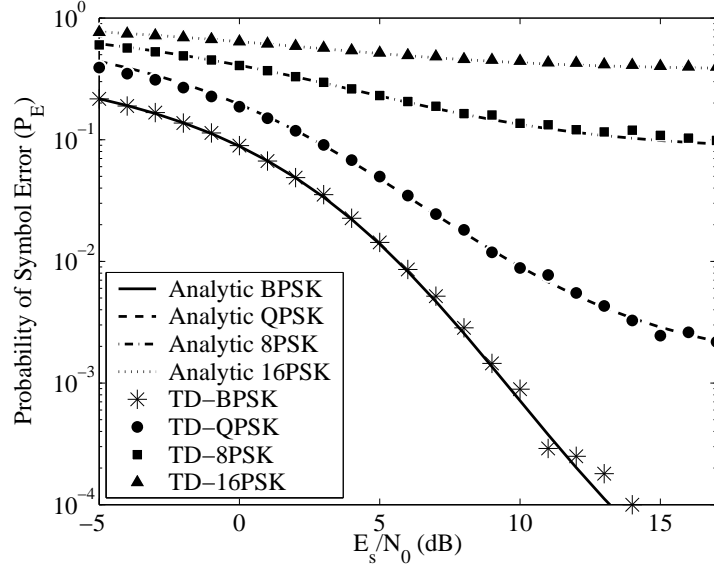


Figure 4.25 Jamming and  $N_U = 3$  Users Present With *No Spectral Notching*:  $P_E$  vs  $E_b/N_0$  for TD-MPSK Signaling with  $J/S = 3.14$  dB and  $P = 31$  Sinusoids

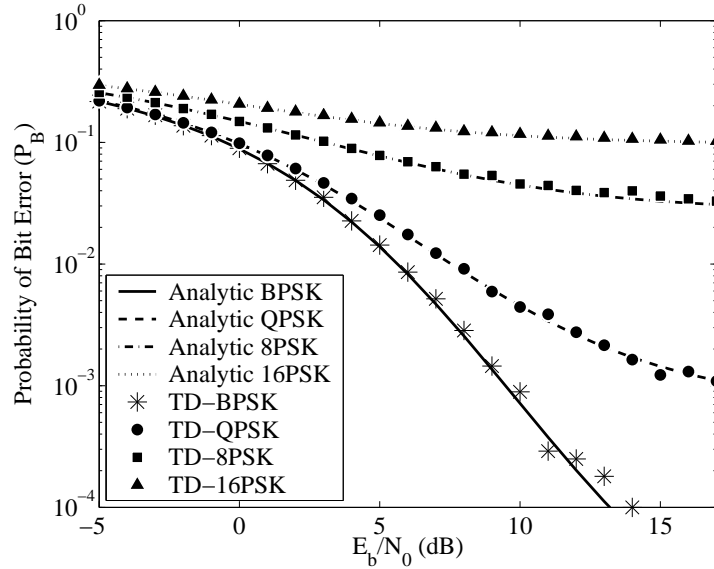


Figure 4.26 Jamming and  $N_U = 3$  Users Present With *No Spectral Notching*:  $P_B$  vs  $E_b/N_0$  for TD-MPSK Signaling with  $J/S = 3.14$  dB and  $P = 31$  Sinusoids

### 4.13 Jamming and $N_U$ 2 to 32 Users Present With *No Spectral Notching*

When jamming is present it has the affect of raising the noise floor in a multiple access environment. Figure 4.27 and Fig. 4.28 show  $P_E$  and  $P_B$  versus  $N_U$ , respectively, for  $J/S = 3.14$  dB and TD-QPSK data modulation. By comparison with Fig. 4.15 and Fig. 4.16,  $P_E$  and  $P_B$  are greater than the  $N_U = 3$  multiple access case with no jamming present.

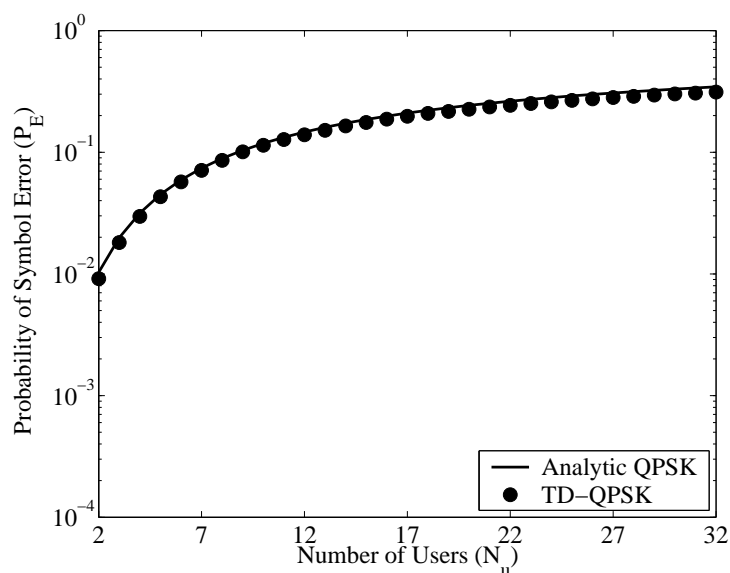


Figure 4.27 Jamming and Multiple Access Interference for  $N_U = 2$  to 32 Users *No Spectral Notching: Synchronous* Users:  $P_E$  vs  $N_U$  for TD-QPSK Signaling with  $P = 31$  Sinusoids

### 4.14 Jamming and $N_U = 3$ Users Present *With Spectral Notching*

When jamming, an additional user, and a notch are all present, the probability of symbol error and probability of bit error performance are almost as good as when an additional user is present and a notch is present. Figure 4.29 and Fig. 4.30 show  $P_E$  and  $P_B$  versus normalized signal to noise ratio ( $E_b/N_0$ ), respectively. As indicated, spectral notching is able to remove most of the jamming, yet there remains some degradation caused by the notch. When adding a notch to remove jamming the multiple access interference should be considered. It is possible to remove most

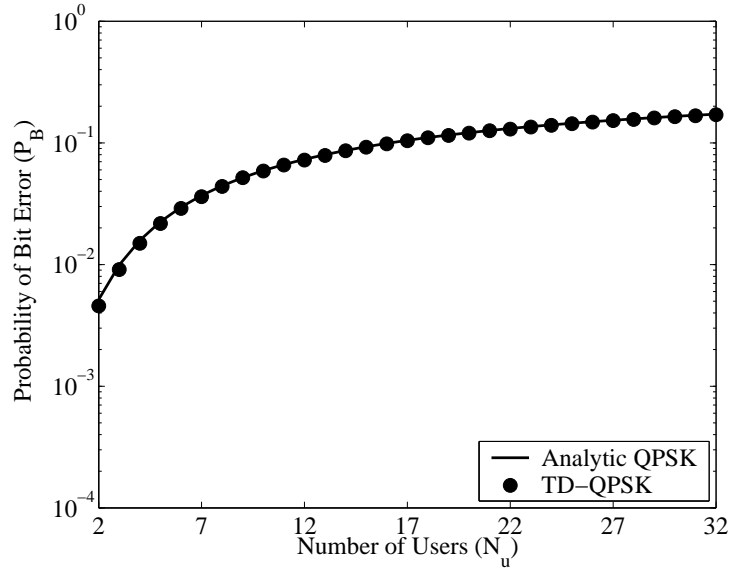


Figure 4.28 Jamming and Multiple Access Interference for  $N_U = 2$  to 32 Users *No Spectral Notching: Synchronous* Users:  $P_B$  vs  $N_U$  for TD-QPSK Signaling with  $P = 31$  Sinusoids

of the effects of jamming but increase the effect of multiple access interference to such a degree that the system is worse off. A notch should be large enough to remove most of the jamming. However, it should not be so large that it increases the multiple access interference to such a degree that the system is worse off.

#### 4.15 Jamming and $N_U = 2$ to 32 Users Present With *With Spectral Notching*

Jamming has the affect of raising the noise floor in a multiple access environment. Figure 4.31 and Fig. 4.32 show  $P_E$  and  $P_B$  versus  $N_U$ , respectively, for the number of users. The performance of this scenario is degraded slightly versus the scenario with a notch but no jamming. This is because there is still some residual jamming that wasn't notched away. It is interesting to compare this scenario versus the scenario with jamming but no notch. Figure 4.33 shows this comparison. After five additional users, probability of bit error is better for the case without the notch.

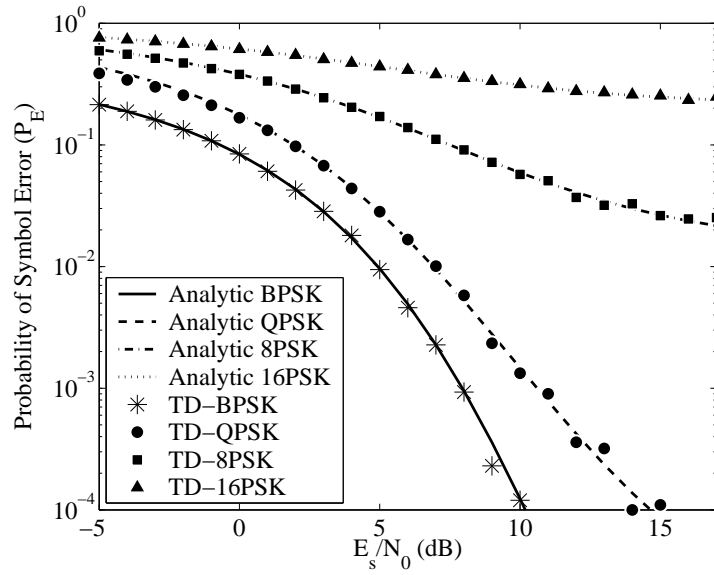


Figure 4.29 Jamming and  $N_U = 3$  Users Present With *With Spectral Notching*:  $P_B$  vs  $E_b/N_0$  for TD-MPSK Signaling with  $J/S = 3.14$  dB and  $P = 31$  Sinusoids

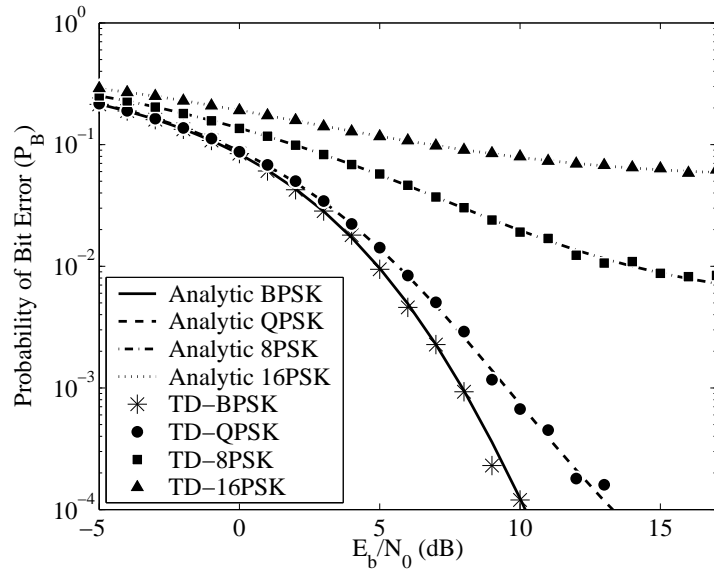


Figure 4.30 Jamming and  $N_U = 3$  Users Present With *With Spectral Notching*:  $P_B$  vs  $E_b/N_0$  for TD-MPSK Signaling with  $J/S = 3.14$  dB and  $P = 31$  Sinusoids

#### 4.16 Summary

Simulated results for probability of symbol error ( $P_E$ ) and probability of bit error ( $P_B$ ) performance versus normalized signal-to-noise ratio ( $E_b/N_0$ ) are shown

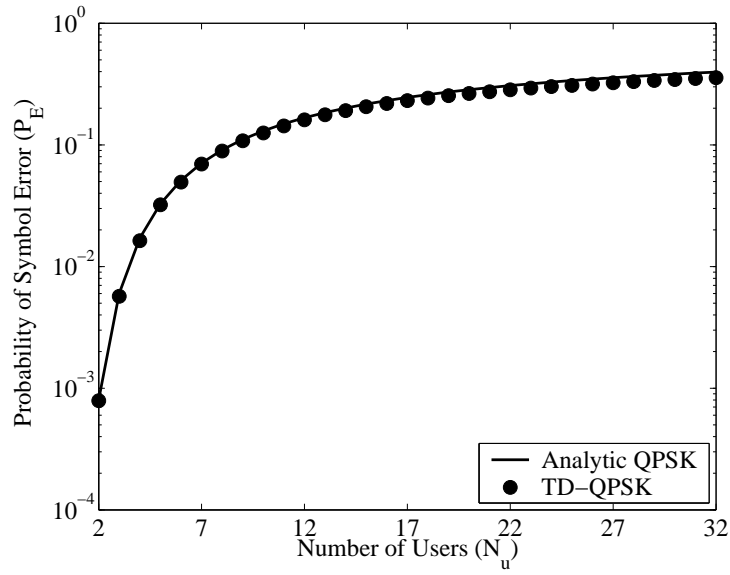


Figure 4.31 Jamming and Multiple Access Interference for  $N_U = 2$  to 32 Users  
*With Spectral Notching: Synchronous Users:  $P_E$  vs  $N_U$  for TD-QPSK*  
 Signaling with  $P = 31$  Sinusoids

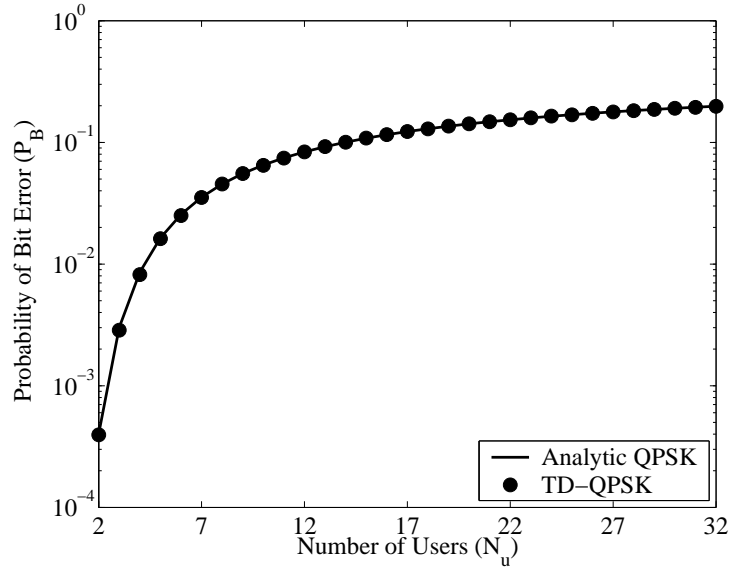


Figure 4.32 Jamming and Multiple Access Interference for  $N_U = 2$  to 32 Users  
*With Spectral Notching: Synchronous Users:  $P_B$  vs  $N_U$  for TD-QPSK*  
 Signaling with  $P = 31$  Sinusoids

consistent (nearly identical) to analytic results obtained from equations provided in Section 2.2.1 and Section 2.2.2. This includes the cases when only spectral notching

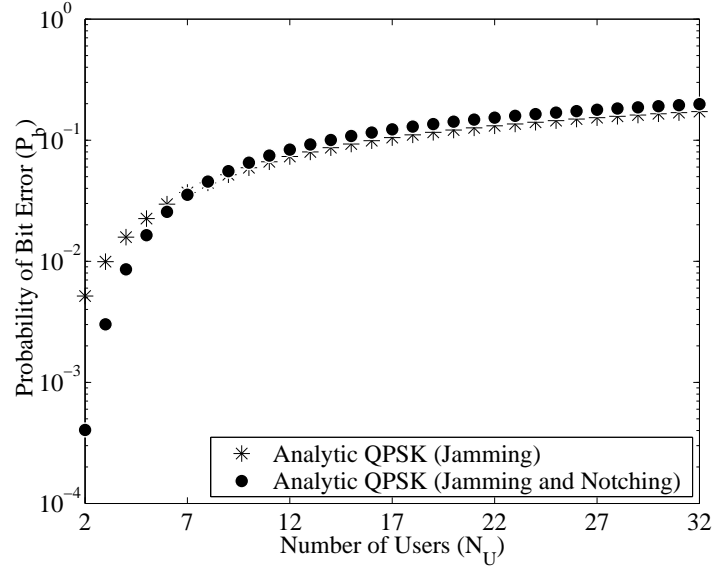


Figure 4.33 Jamming and Multiple Access Interference for  $N_U = 2$  to 32 Users *With and without Spectral Notching*:  $P_B$  vs  $N_U$  for TD-MPSK Signaling with  $P = 31$  Sinusoids

or only jamming are considered, as well as, the case when jamming with spectral notching is considered. Results for scenarios containing multiple access interference are consistent with analytic expressions as well. Again, this includes multiple access interference scenarios where only spectral notching or only jamming are present, as well as, the multiple access case when jamming with spectral notching is considered. Figure 4.34 shows for an  $E_b/N_0$  of 6 dB, an equal power additional user degrades  $P_B$  from  $7.9 \times 10^{-2}$  to  $8.5 \times 10^{-2}$ . If an equal power additional user and jamming are added to the system,  $P_B$  further degrades to  $9.8 \times 10^{-2}$ . If a spectral notch is added to the system when jamming is not present,  $P_B$  degrades to  $8.8 \times 10^{-2}$ . This is because the communication symbols are not spread over as many spectral components, which increases the correlation between different users, which then increases the multiple access interference. If jamming, an additional equal power, user and a spectral notch are present,  $P_B$  is  $8.9 \times 10^{-2}$ .  $P_B$  in the case with an additional user, jamming, and spectral notching is slightly larger than the case with an additional user and notching

because the small amount of jamming (6 %) that was not notched away causes some degradation.

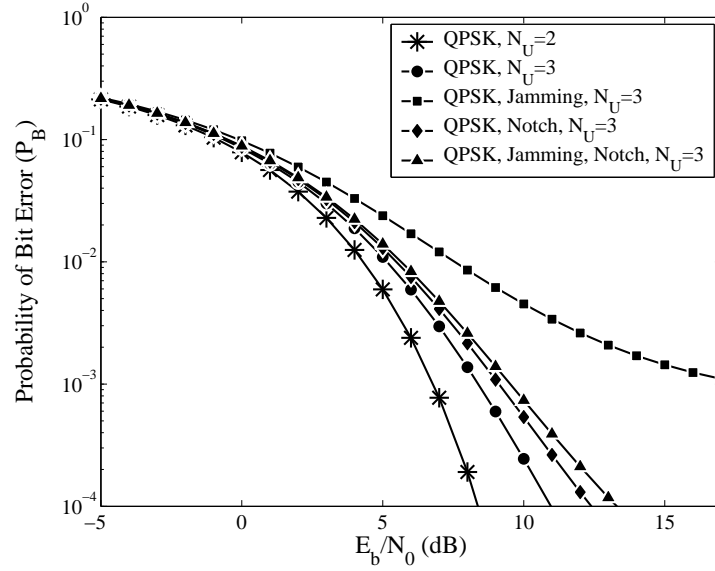


Figure 4.34 Jamming and Multiple Access Interference for  $N_U = 2$  to 3 Users *With and without Spectral Notching*:  $P_B$  vs  $E_b/N_0$  for TD-QPSK Signaling with  $P = 31$  Sinusoids

## 5. Modeling and Simulation: Orthogonal Code Selection

### 5.1 Introduction

This chapter provides an overview of modeling parameters and scenarios used for testing performance of orthogonally coded users in the proposed TD-MPSK system. The parameters described include the communication symbol spectral response, the jammer spectral response and the notched symbol spectral response. The modeled scenarios include: 1) multiple access interference, 2) multiple access interference with spectral notching, 3) multiple access and jamming interference without spectral notching and 4) multiple access and jamming interference with spectral notching. The scenarios considered help characterize the TD-MPSK system's ability to communicate in the presence of noise and interference when the system is using orthogonally coded users.

### 5.2 Modeling Parameters

**5.2.1 Spectral Response of Communication Symbol.** For the orthogonal code selection case, the spectral response is almost the same as presented in the previous chapter in Fig. 4.1. The only difference is the multiple access phase codes of the orthogonal users are interrelated. Equation (5.1) is a discrete form of the analytic representation of communication symbols in an orthogonal network. Equation (5.2) describes the phase codes for the different users in the network. Equations (5.3) and (5.4) describe the variable  $G$  and the number of possible users in the network. Each member in the set of orthogonal users uses the same  $\phi_p$  to adjust the phase of each of the sinusoids. The phase of each sinusoid for each symbol is further adjusted based on user number ( $v_o$ ) where  $v_o = 0$  identifies the *primary user* being modeled. The remaining orthogonal users are identified as *additional users*. The first additional orthogonal user is based on using  $v_o = 1$ , the second is based



on using  $v_o = 2$ , and so on, up to the thirtieth additional user which is based on  $v_o = 30$ .

$$s_k^{(v)}(n) = \frac{2}{64} \sum_{p=1}^P A_p \cos \left( 2\pi p \frac{n}{64} + \phi_p^{(v)} + \theta_k^{(v)} \right) \quad v = 0, \dots, G-1 \quad (5.1)$$

$$\phi_p^{(v)} = \phi_p + \sum_{q=1}^p \text{sgn}(A_q) \frac{q2\pi v}{G} \quad (5.2)$$

$$G = \sum_{r=1}^{31} \text{sgn}(A_r) \quad (5.3)$$

$$\text{sgn}(t) = \begin{cases} 1 & t > 0 \\ 0 & t = 0 \\ -1 & t < 0 \end{cases} \quad (5.4)$$

**5.2.2 Spectral Response of Jamming.** The spectrum of the jamming is the same as that of the previous chapter.

**5.2.3 Spectrum of Notched User.** The magnitude of the spectrum of the notched users is the same as that of the previous chapter.

### 5.3 Synchronous Multiple Access Interference: Orthogonal Users With *No Spectral Notching*

Probability of error ( $P_E$  and  $P_B$ ) generally increases as the number of multiple access users ( $N_U$ ) increases. However, for the case of a synchronous network containing orthogonal users,  $P_E$  and  $P_B$  are unaffected as  $N_U$  increases provided each additional user is mutually orthogonal to all previous users. Figure 5.1 and Fig. 5.2 show  $P_E$  and  $P_B$  versus  $N_U$ , respectively, for  $N_U = 2$  to 32 users and TD-QPSK

data modulation. For these simulations, the normalized signal-to-noise ratio was maintained constant at  $E_b/N_0 = 6.0$  dB. As indicated by the data in these figures, for  $P = 31$  sinusoids as given in (5.1), it is possible to assign multiple access phase coding in accordance with 5.2 through 5.4 such that  $G$  users in the network are mutually orthogonal.

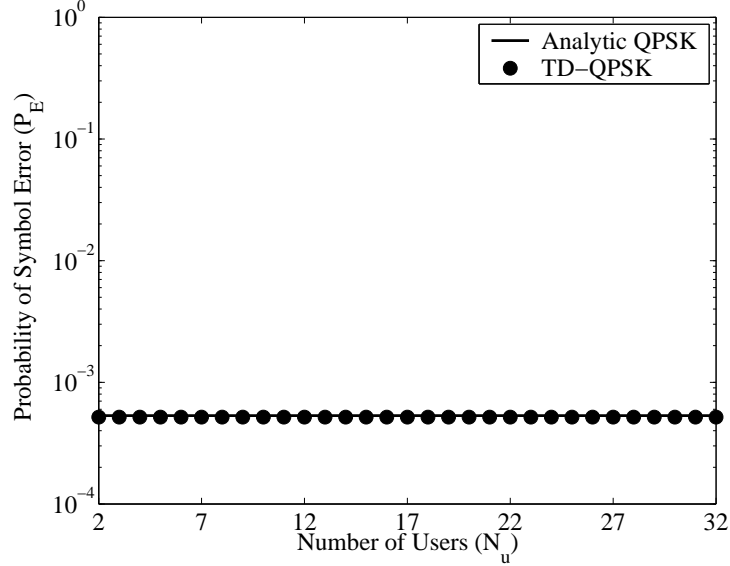


Figure 5.1 Multiple Access Interference for  $N_U = 2$  to 32 Orthogonal Users With *No Spectral Notching*:  $P_E$  vs  $N_U$  for TD-QPSK Signaling with  $P = 31$  Sinusoids

#### 5.4 Asynchronous Multiple Access Interference: Orthogonal Users With *No Spectral Notching*

The cross-correlation of orthogonal users is approximately the same as asynchronous cross-correlation with randomly coded users with the same magnitude spectrum as the orthogonal users. Figure 5.3 and Fig. 5.4 show  $P_E$  and  $P_B$  versus  $N_U$  respectively for asynchronous networks.

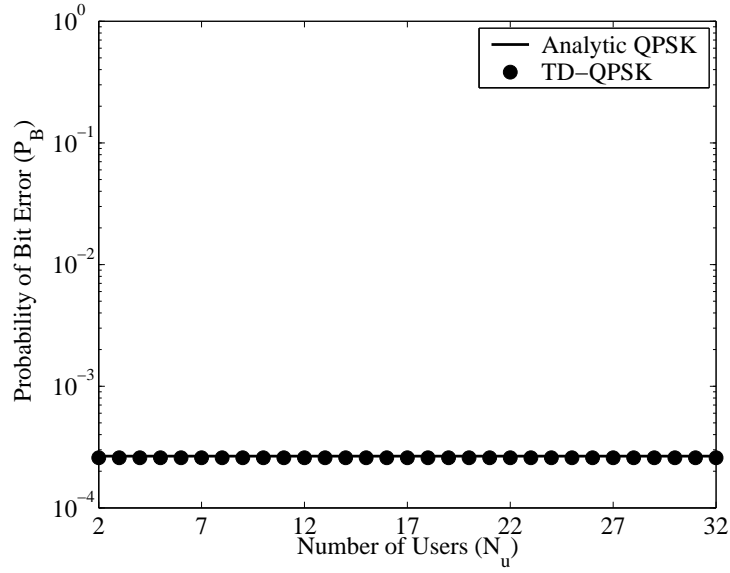


Figure 5.2 Multiple Access Interference for  $N_U = 2$  to 32 Orthogonal Users With *No Spectral Notching*:  $P_B$  vs  $N_U$  for TD-QPSK Signaling with  $P = 31$  Sinusoids

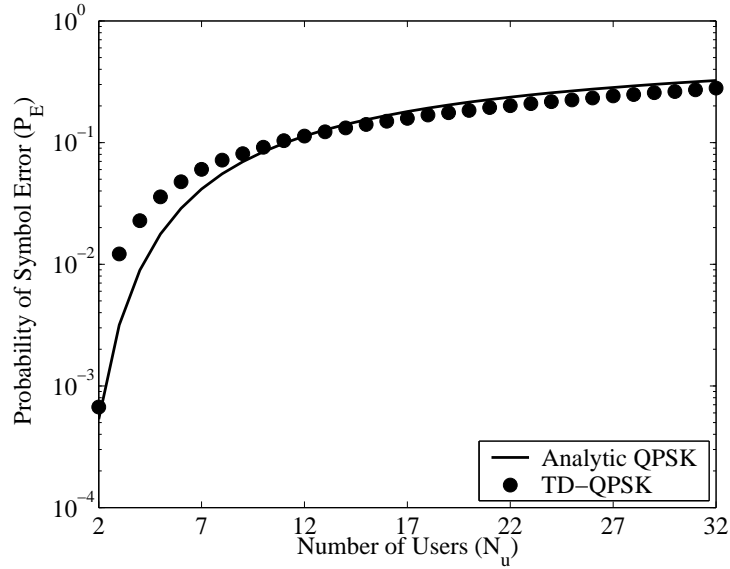


Figure 5.3 Multiple Access Interference with  $N_U = 2$  to 32 *Asynchronous* Users:  $P_E$  vs  $N_U$  for TD-QPSK Signaling with  $P = 31$  Sinusoids

### 5.5 Multiple Access Interference: $N_U = 2$ to 32 Users *With Spectral Notching*

If spectral notching is introduced into a group of orthogonal users, orthogonality is lost. Figure 5.5 and Fig. 5.6 show  $P_E$  and  $P_B$  versus the number of users, respectively, when spectral notching is employed.

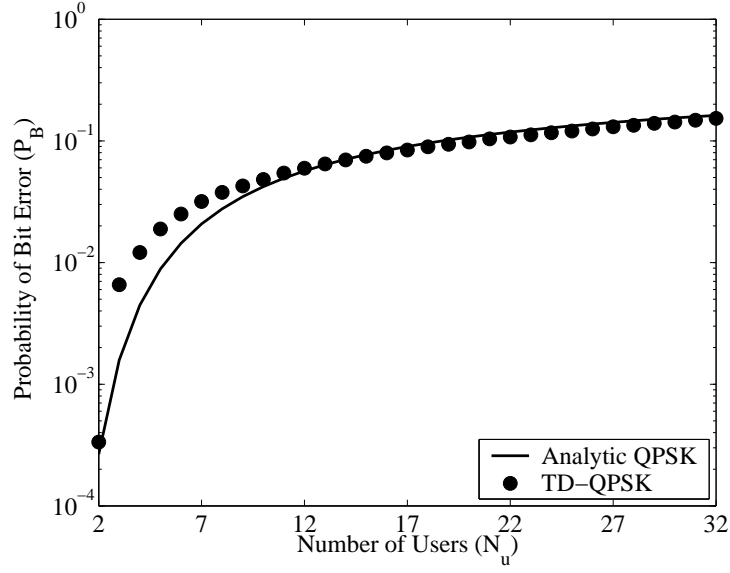


Figure 5.4 Multiple Access Interference with  $N_U = 2$  to 32 *Asynchronous* Users:  $P_B$  vs  $N_U$  for TD-QPSK Signaling with  $P = 31$  Sinusoids

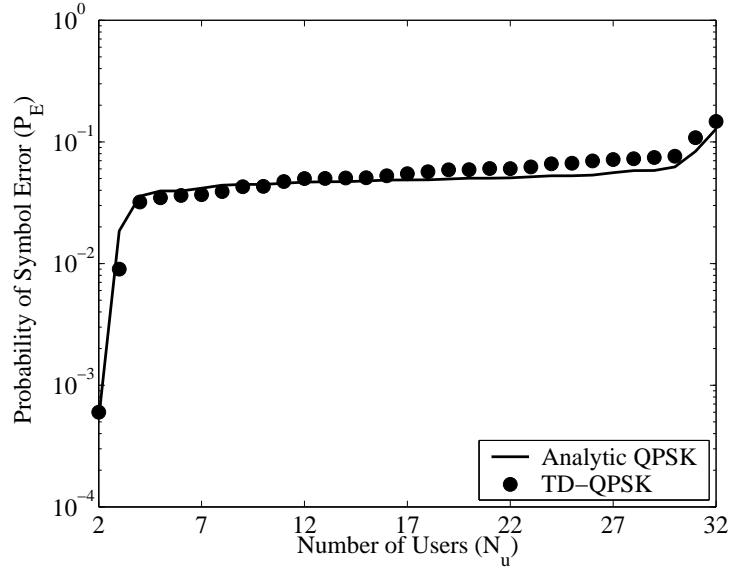


Figure 5.5 Multiple Access Interference for  $N_U = 2$  to 32 Orthogonal Users *With Spectral Notching*:  $P_E$  vs  $N_U$  for TD-QPSK Signaling with  $P = 31$  Sinusoids

As the spectral notch width increases, multiple access interference increases. Figure 5.7 and Fig. 5.8 show  $P_E$  and  $P_B$  the versus spectral notch width, respectively. The multiple access interference for the simulations comes from four additional or-

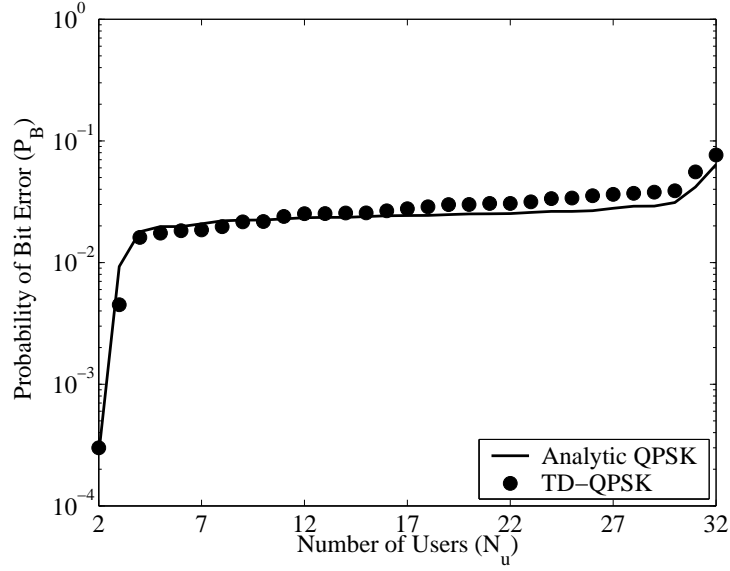


Figure 5.6 Multiple Access Interference for  $N_U = 2$  to 32 Orthogonal Users *With Spectral Notching*:  $P_B$  vs  $N_U$  for TD-QPSK Signaling with  $P = 31$  Sinusoids

thogonal users. Each of these orthogonal users has the same magnitude spectrum as the transmitter/receiver pair. The simulations start by modeling performance when the transmitter uses all 31 sinusoids. At this point, users maintain mutual orthogonality and do not induce any multiple access interference during the correlation process; any resultant symbol and bit errors are due solely to the environmental noise. At the next step, only the highest frequency sinusoid is removed and  $P_E$  and  $P_B$  determined again. At this point the orthogonal users lost their orthogonality. The process is repeated by removing one sinusoid at a time until there is only one sinusoid remaining. As the spectral notch width increases (by progressively removing one sinusoid at a time)  $P_E$  and  $P_B$  increase.

## 5.6 Jamming and Orthogonal Users Present With *No Spectral Notching*

As in the randomly coded user case, jamming has a tendency to raise the noise floor. Figure 5.9 and Fig. 5.10 show  $P_E$  and  $P_B$  versus  $N_U$ , respectively, when jamming and orthogonal users are present and no spectral notching is applied. For

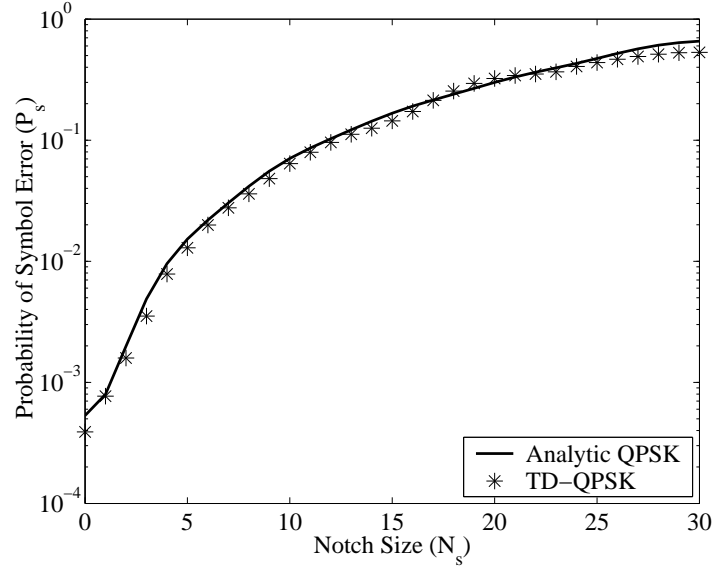


Figure 5.7 Multiple Access Interference for  $N_U = 6$  Orthogonal Users *With Spectral Notching*:  $P_E$  vs Spectral Notch Width  $N_s$  for TD-QPSK Signaling

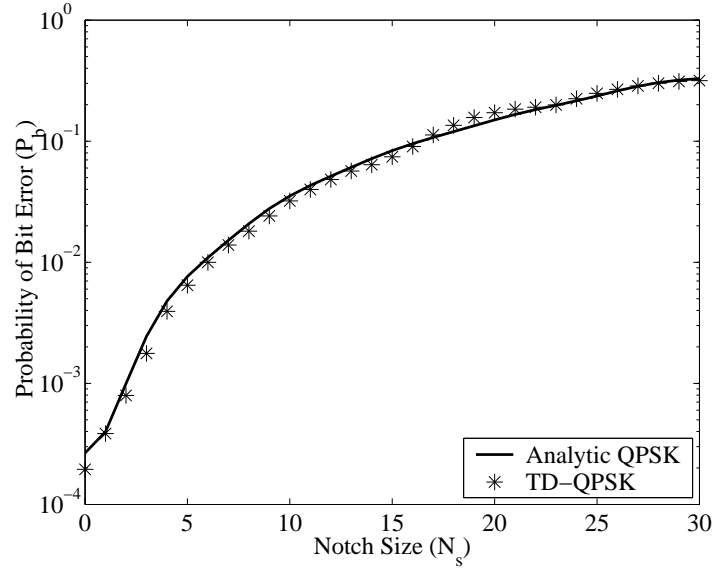


Figure 5.8 Multiple Access Interference for  $N_U = 6$  Orthogonal Users *With Spectral Notching*:  $P_B$  vs Spectral Notch Width  $N_s$  for TD-QPSK Signaling

the  $N_U = 2$  to 32 case,  $P_E$  and  $P_B$  remain constant. As expected, the probability of error is greater here than experienced in the case when no jamming present.

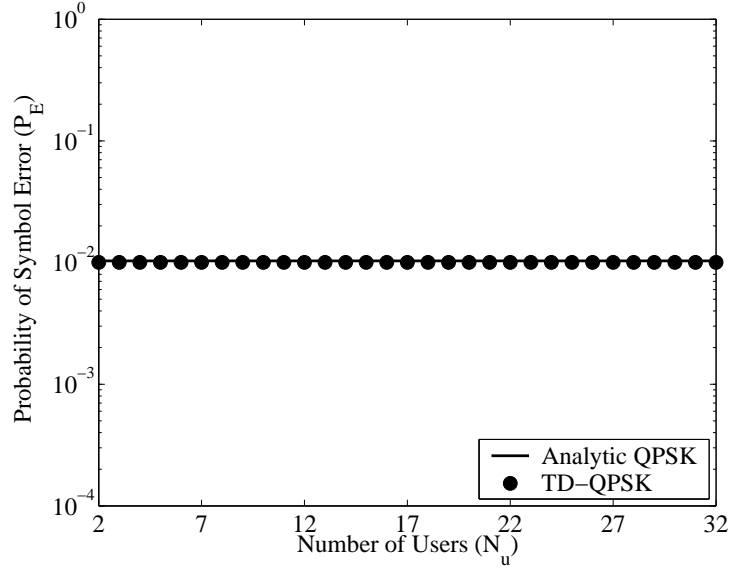


Figure 5.9 Jamming and Multiple Access Interference for  $N_U = 2$  to 32 Orthogonal Users *No Spectral Notching*:  $P_E$  vs  $N_U$  for TD-QPSK Signaling with  $P = 31$  Sinusoids

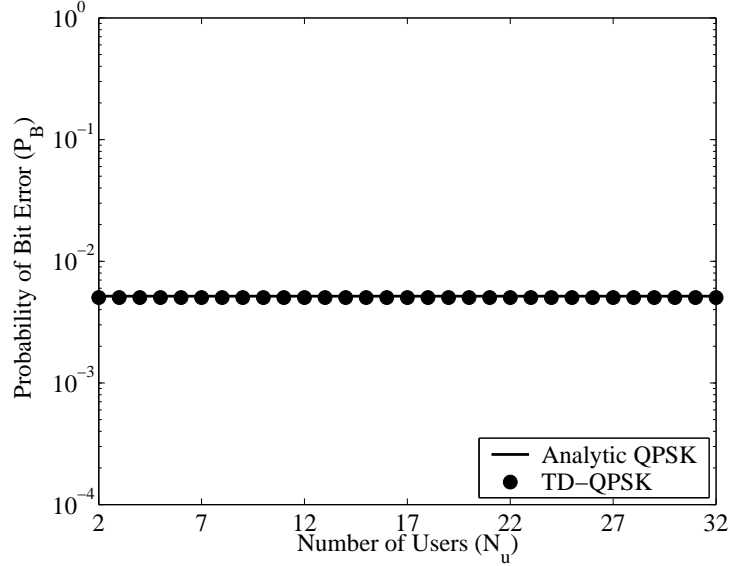


Figure 5.10 Jamming and Multiple Access Interference for  $N_U = 2$  to 32 Orthogonal Users *No Spectral Notching*:  $P_B$  vs  $N_U$  for TD-QPSK Signaling with  $P = 31$  Sinusoids

## 5.7 Jamming and Orthogonal Users Present *With Spectral Notching*

Although adding a spectral notch to the communication system removes most of the jamming, it degrades and possibly destroys the desired mutual orthogonality

between users. Figure 5.11 and Fig. 5.12 show  $P_E$  and  $P_B$  versus the number of users, respectively, when jamming and orthogonal users are present and spectral notching is applied. Results in these figures show slight degradation in performance by comparison with the case where a spectral notch was used without jamming present. This is because there is some residual jamming.

There is a trade-off that needs to be made between spectral notching and maintaining orthogonality. If there are only few additional orthogonal users, spectral notching might be of some benefit. Although orthogonality is lost in this case, the jamming power that is removed as a result of the spectral notch may make this trade-off a viable option. In cases where there are a relatively high number of orthogonal users, multiple access interference that remains after spectral notching becomes greater than the jamming interference that is actually removed by the spectral notch. For the specific scenarios modeled in this chapter, once the number of orthogonal users exceeds two, notching causes more degradation than jamming. The loss of orthogonality caused by the notching causes the multiple access interference to exceed the jamming interference.

## 5.8 Special Case: Reassigning Phase Codes to Maintain Orthogonality

Spectral notching removes some of the sinusoids making up the symbol. However, if the number of users is reduced to the number of available sinusoids, the multiple access code phases can be reassigned to restore orthogonality. The new multiple access code phases are calculated using (5.1) through (5.4). For the case of spectral notching discussed in Section 4.2.3, the value of  $G$  drops from 31 to 23 because of the number of frequency components that were notched away.

Figure 5.13 and Fig. 5.14 show  $P_E$  and  $P_B$  versus the number of users, respectively, when coding phases have been reassigned and spectral notching is applied. The number of remaining sinusoids that make up a symbol is 23 which allows the creation of 23 orthogonal users.



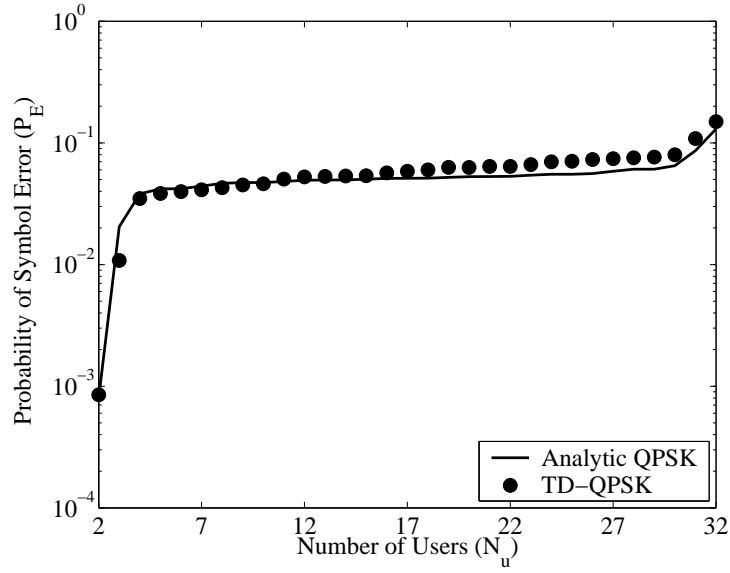


Figure 5.11 Jamming and Multiple Access Interference for  $N_U = 2$  to 32 Orthogonal Users *With Spectral Notching*:  $P_E$  vs  $N_U$  for TD-QPSK Signaling with  $P = 31$  Sinusoids

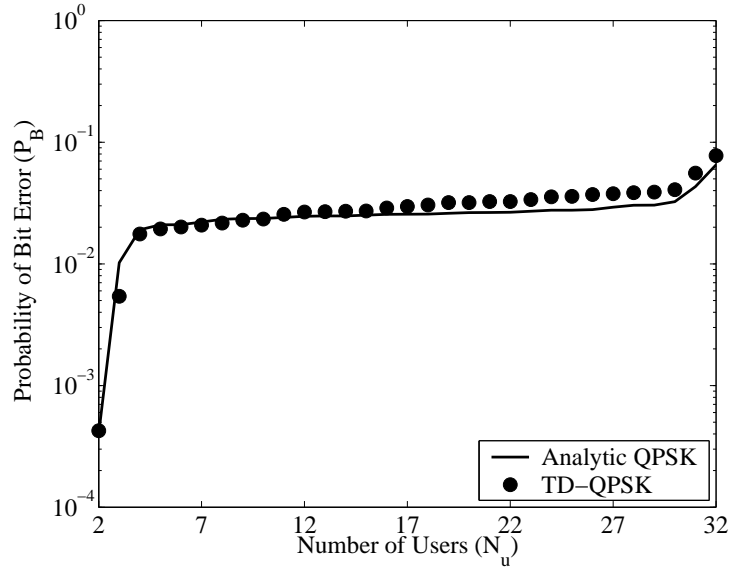


Figure 5.12 Jamming and Multiple Access Interference for  $N_U = 2$  to 32 Orthogonal Users *With Spectral Notching*:  $P_B$  vs  $N_U$  for TD-QPSK Signaling with  $P = 31$  Sinusoids

Figure 5.15 and Fig. 5.16 show  $P_E$  and  $P_B$  versus the number of users, respectively, when coding phases have been reassigned, jamming is present, and spectral

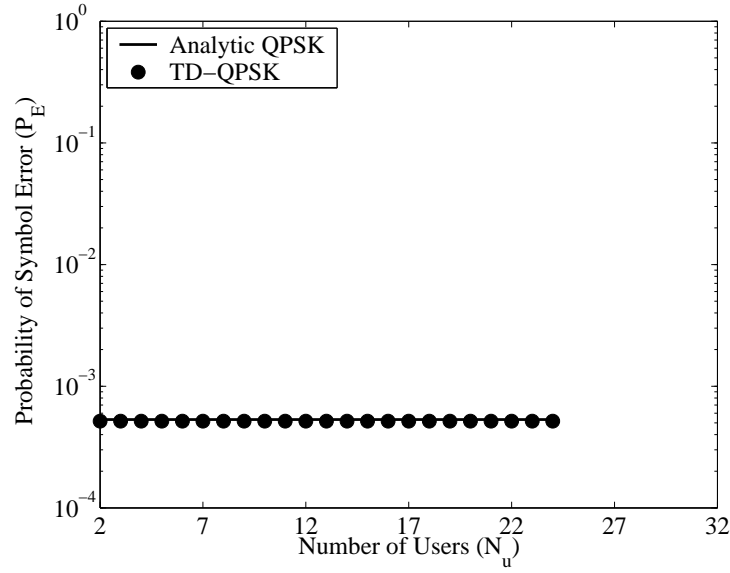


Figure 5.13 Multiple Access Interference for  $N_U = 2$  to 24 Orthogonal Users *With Spectral Notching, Orthogonality is Restored*:  $P_E$  vs  $N_U$  for TD-QPSK Signaling with  $P = 31$  Sinusoids

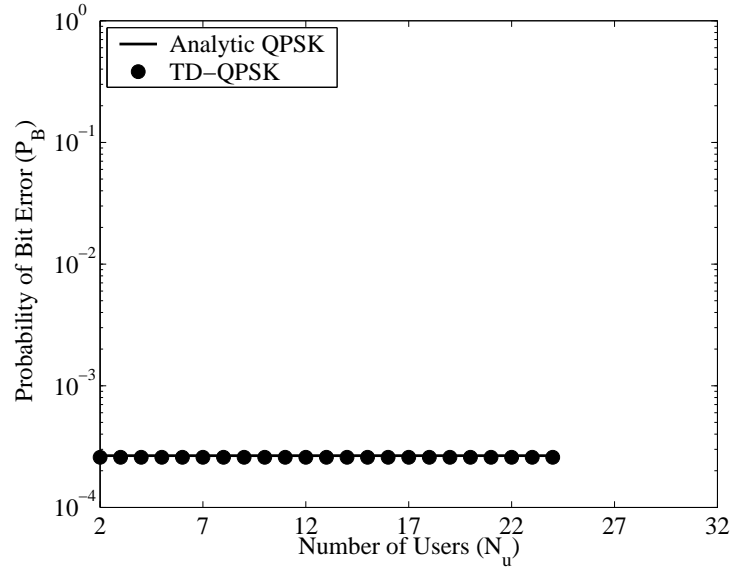


Figure 5.14 Multiple Access Interference for  $N_U = 2$  to 24 Orthogonal Users *With Spectral Notching, Orthogonality is Restored*:  $P_B$  vs  $N_U$  for TD-QPSK Signaling with  $P = 31$  Sinusoids

notching is applied. As in the previous case there are 23 orthogonal users. Performance versus the previous case is degraded since some of the jamming remains in

the frequency components that were not notched. However, this case is only slightly degraded versus the previous case because the majority of the jamming was notched away.

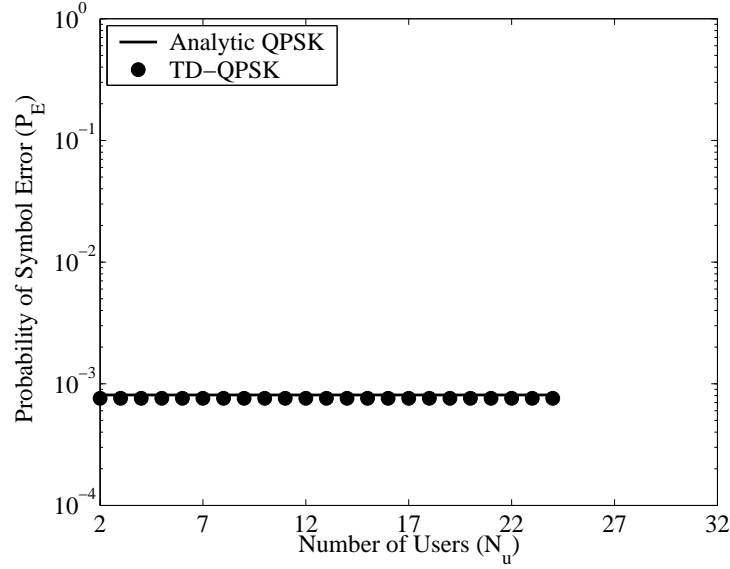


Figure 5.15 Jamming and Multiple Access Interference for  $N_U = 2$  to 24 Orthogonal Users *With Spectral Notching, Orthogonality Restored*:  $P_E$  vs  $N_U$  for TD-QPSK Signaling with  $P = 31$  Sinusoids

## 5.9 Summary

The cross-correlation between communication symbols of different synchronous users can be made identically zero through proper selection of multiple access phase codes (orthogonal signaling). For a synchronous network containing orthogonal users, symbol and bit error probabilities are unaffected as the number of orthogonal network users increases. The addition of jamming does not change the amount of multiple access interference although it does increase the probability of error. The introduction of spectral notching increases the multiple access interference since network users in the network are no longer orthogonal. If the multiple access phase codes are properly reassigned after spectral notching, a reduced number of orthogonal users can be created. Figure 5.17 summarizes the affect of jamming, spectral

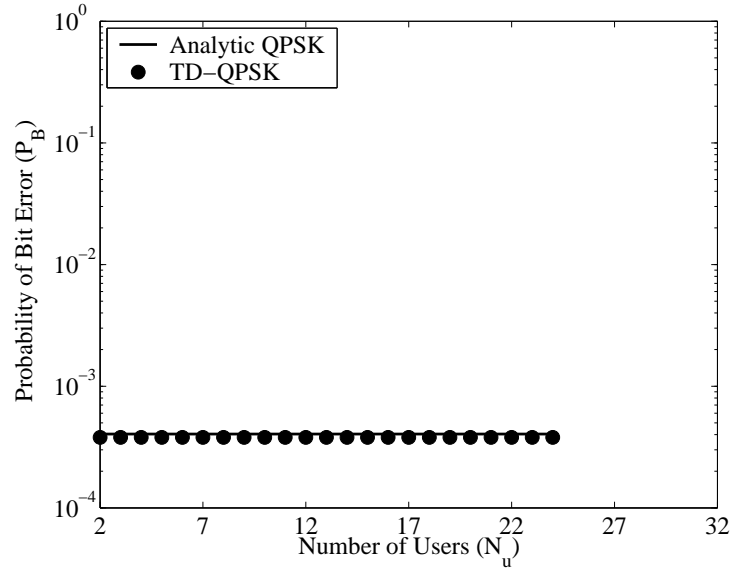


Figure 5.16 Jamming and Multiple Access Interference for  $N_U = 2$  to 24 Orthogonal Users *With Spectral Notching, Orthogonality Restored*:  $P_B$  vs  $N_U$  for TD-QPSK Signaling with  $P = 31$  Sinusoids

notching, and reassigning phase codes to restore orthogonality. When no jamming is present,  $P_B$  is  $2.6 \times 10^{-4}$ . When jamming is added to the system,  $P_B$  error increases sharply to  $5.1 \times 10^{-3}$ . When a spectral notch is added to the system to remove the jamming,  $P_B$  increases to approximately  $2.5 \times 10^{-2}$  for  $N_U = 4$  to 30. The notch removed most of the jamming interference but increased the multiple access interference. When the spectral codes were reassigned,  $P_B$  decreased dramatically to  $4.0 \times 10^{-4}$ . The slight increase in error versus the case with no jamming and no spectral notching is due to the small amount of jamming (6%) that was not notched away.

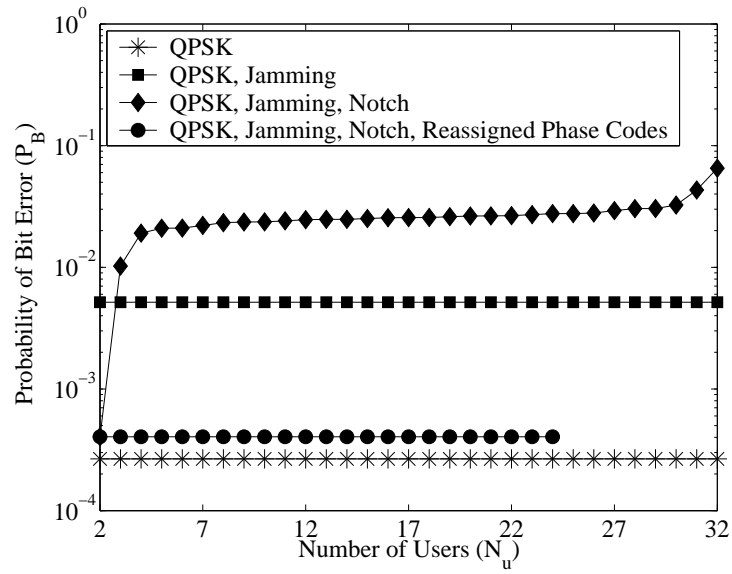


Figure 5.17 Jamming and Multiple Access Interference for  $N_U = 2$  to 32 Orthogonal Users *With and without Spectral Notching*:  $P_B$  vs  $N_U$  for TD-QPSK Signaling with  $P = 31$  Sinusoids

## 6. Conclusions and Recommendations

### 6.1 Summary

First and foremost, this thesis provides the introduction, development and characterization of a spectrally encoded transform domain,  $M$ -Ary phase shift keying (TD-MPSK) technique that provides both multiple access capability and interference suppression (avoidance). As presented, the proposed TD-MPSK system uses a form of spectral encoding, i.e., the application of independent data and multiple access phase modulations to sinusoidal spectral components, to generate multiple access communication symbols which are subsequently demodulated in the time domain using a conventional correlation receiver. The previous transform domain communication systems considered relied primarily on binary phase shift keying (BPSK) and cyclic shift keying (CSK) to provide data modulation. This thesis provides a review of conventional MPSK signaling, transform domain communications, and code division multiple access. This background is followed by a description of the TD-MPSK symbol definition and phase coding used for data modulation and multiple access implementation. Performance is characterized in terms of multiple access interference and jamming interference. The probability of error (symbol and bit) for a spectrally encoded TD-MPSK system is discussed in terms of different types of interference present. Monte Carlo simulation techniques are used to verify the analytical expressions derived explicitly for the proposed TD-MPSK system. Various modeling and simulation scenarios are considered, including, those containing jamming interference, multiple access interference, and combinations thereof, both with and without TD-MPSK spectral notching employed. This thesis concludes with a description of Monte Carlo simulations conducted to verify TD-MPSK multiple access performance with orthogonal users.

## 6.2 Conclusions

**6.2.1 Performance in the Presence of Interference.** This thesis shows that probability of symbol error ( $P_E$ ) and probability of bit error ( $P_B$ ) versus normalized signal-to-noise ratio for the proposed TD-MPSK system can be reliably estimated using conventional MPSK error equations for an orthonormal signal space, i.e., a pair of unit energy orthogonal functions that mathematically span the two-dimensional signal space. Both  $P_E$  and  $P_B$  can be reliably predicted in the presence of additional network users (multiple access interference), intentional jamming and spectral notching. The error estimates derived for different scenarios were validated using Monte Carlo simulation and analysis.

### 6.2.2 Multiple Access Performance (Randomly Coded Users).

The amount of multiple access interference induced by randomly coded network users can be estimated using equations derived as part of this research. Both  $P_E$  and  $P_B$  versus the number of users can be predicted using the derived multiple access interference expressions and previously derived conventional MPSK error equations. Interference effects on  $P_E$  and  $P_B$  can also be predicted in the presence of jamming and spectral notching. Error estimates were validated for different scenarios using Monte Carlo simulation and analysis.

### 6.2.3 Multiple Access Performance (Orthogonally Coded Users).

Multiple access interference in a synchronous network can be eliminated if users are made mutually orthogonal. For a limited number of users, the TD-MPSK multiple access phase codes and sinusoidal component amplitudes can be selected to provide this orthogonality. If the orthogonally coded users are used in an asynchronous network, error performance degrades and approaches that of randomly coded users operating in an asynchronous network.

### 6.3 Recommendations for Future Research

**6.3.1 Quadrature Amplitude Modulation.** The TD-MPSK symbols developed as part of this research are fundamentally based on two orthogonal signals defining (mathematically spanning) the two-dimensional signal space. By combining amplitude modulation of the orthogonal symbols ( $\psi_1$  and  $\psi_2$ ) with phase shift keying (PSK), a quadrature amplitude modulation (QAM) system can be developed.

**6.3.2 Synchronization.** Research has previously been conducted on synchronization of a TDCS system using BPSK and CSK modulations [2]. This research could be reviewed to see how it applies to a TD-MPSK system.

**6.3.3 Orthogonal Jammers.** One possible use of this research is the creation of a combination jammer/communication system. This combination system could generate a jammer waveform which is orthogonal (non-interfering) to friendly communication systems but disruptive to enemy communication and radar systems.

**6.3.4 Propagation Effects.** Further research can be done on propagation effects on a TDCS system. This includes the effects of multi-path, Doppler shifts, and fading. Research could be done on how these phenomena affect probability of error in the system and cross-correlation of received symbols.

**6.3.5 Optimal Multiple Access Codes.** This thesis discussed how a limited number of orthogonal users could be generated for a given magnitude spectrum. Further research could be done on extending the number of orthogonal users. Another possibility is generating additional users with symbols that have low cross correlation with symbols of the other network users; the lower the cross correlation between symbols of network users, the lower the multiple access interference.



## Appendix A. Matlab Simulation Code

### Matlab Functions

```
function [ang_vec]=randang1(points,sections)
%This function generates the random angles used by the TDCS.
%Variables
%points: the number of points in a symbol. "points" needs to be a
        %power of 2.
%sections:the number of different equally spaced angles used
%ang_vec: A vector of phases for a basis function

if round(log2(points))-log2(points)~=0
    error('Number of points needs to be a power of 2');
end

if round(log2(sections))-log2(sections)~=0
    error('Number of sections needs to be a power of 2');
end

if points<4
    error('Number of points needs to be greater >=4');
end
%random phases are generated for the first half of the frequency
%components
halfpoints=points/2-1;
A=rand(1,halfpoints);
B=A*sections;
C=floor(B);
D=C/sections*2*pi;
%second half of the frequency components generated using the fliplr
%command and the
%first half phases
ang_vec=[0,D,0,fliplr(-D)];

function [basisf]=basisgenpsk(envelope,angles,numcodes)

%This function generates the basis functions used by the TDCS.
%Basis functions are created in the frequency domain and transformed
%into the time domain.

%Variables
```

```

%envelope: Magnitude of the frequency components of the basis
            %functions
%angles: Phase of the the frequency components of the initial basis
            %function
%numcodes: Number of basis functions
%basisf: output basis functions

%Note that the magnitude of the frequency components for the "initial
%basis function" are found in the variable "envelope" and the phase
%components in the variable "angles"

```

```

[h,w]=size(envelope);

```

```

%This for loop adjusts the phase of initial basis function to
%generate the phases of the other basis functions
for m=1:numcodes
    %Magnitude of phase adjustment
    codeangles=ones(1,w/2-1)*(m-1)/numcodes*2*pi;
    %Vector of phase adjustments
    codeanglet=[0,codeangles,0,flip1r(-codeangles)];
    %Phase adjustment added to phase of initial basis function
    codeanglev=angles+codeanglet;
    %Vector is transformed to create time domain vector of basis
    %function
    basisf(m,:)=real(ifft(envelope.*exp(j*codeanglev)));
end

```

```

function [noiseenv]=env2(points,signal,noisefloor)

```

```

%This function generates a given noise floor level based
%on the number of points in a symbol. The length of the
%noise vector matches the length of the signal.

```

```

[h,w]=size(signal);
noiseenv=randn(1,w)*(noisefloor/points)^.5;

```

```

function [grayoutput]=graycoder(bits)

```

```

%This function generates a gray code of length "bits"

```

```

%variable
%bits=length of gray code word
%grayoutput=matrix where each row is a different gray code word.
%the number of rows is equal to 2^bits

A=[0;1];
%Generates the case for bits=1
if bits==1
    grayoutput=A;
%Generates the gray code for bits>1
else
    for q=1:bits-1
        [c,d]=size(A);
        E=[A;flipud(A)];
        F=[zeros(c,1);ones(c,1)];
        grayoutput=[F,E];
        A=grayoutput;
    end
end

function [databits]=datagen(numdatabits)

%Generates random vector of 1's and 0's of length "numdatabits".

databits=round(rand(1,numdatabits));

function [transmit,finalsymbols]=modulatorb(data,basis)

%This function modulates a vector of ones and zeros
%using the basis functions it is given.

%Variables
%data: The data vector of ones and zeros
%basis: A matrix where each row is a basis function
%transmit: transmitted signal with modulated symbols
%finalsymbols: Symbols for modulation

%determines the number of basis functions
[a,b]=size(basis);
%determines the number of data bits transmitted
[c,d]=size(data);
%concatenates zeros to the end of the data string

```

```

%so the system has an integer number of symbols to modulate
e=ceil(d/log2(a));
f=zeros(log2(a),e);
f(1:d)=data(1:d);
g=f';
%generates gray code
log2(a);
h=graycoder(log2(a));
%assigns a symbol to groups of databits
k=zeros(1,e);
if a~=2
    for q=1:e
        [var1,var2]=min(sum((abs(ones(a,1)*g(q,:)-h))'));
        k(q)=var2;
    end
else
    for q=1:e
        [var1,var2]=min((abs(ones(a,1)*g(q,:)-h))'));
        k(q)=var2;
    end
end
%assigns a basis function based on the symbol
%basis functions are then concatenated one after the other
final=zeros(1,b*e);
for t=1:e
    final(((t-1)*b+1):(t*b))=basis(k(t),:);
end
transmit=final;
finalsymbols=k;

```

```

function [finalbits,finalsymbols]=demodulatorb(transmit,basis)

```

```

%This function demodulates the transmitted signal using the
%basis functions it is given.

```

```

%Variables

```

```

%transmit: The input signal from the TDCS transmitter

```

```

%basis: A matrix where each row is a basis function

```

```

%finalbits: Demodulated bits

```

```

%finalsymbols: Demodulated symbols

```

```

%determines the number of basis functions
[a,b]=size(basis);
%determines the size of the transmitted signal
[c,d]=size(transmit);
%determines the number of symbols in the transmitted signal
numsyms=ceil(d/b);

QQ=zeros(b,numsyms);
QQ(1:numsyms*b)=transmit;
RR=QQ';

if a==2
    A=RR*basis(1,:)';
    F=sign(A)*-1;
    symbolx=((F+1)/2+1)';

else
    ob1=a/4+1;
    %breaks up transmitted signal into sections representing symbol
    A=RR*basis(1,:)';
    B=RR*basis(ob1,:)';

    C=ones(a+1,1)*mod(atan2(B',A'),2*pi);
    D=((2*pi*[0:a]/a)')*ones(1,numsyms);
    [E,F]=min(abs(C-D));
    F=F-1;
    F=mod(F,a);
    symbolx=F+1;
end

%generates a gray code based on the number of basis functions
h=graycoder(log2(a));

%assigns symbol to each section of the transmitted signal
% finala=zeros(numsyms,log2(a));
for q=1:numsyms
    finala(q,:)=h(symbolx(q),:);

```

```
end

finalb=finala';
final=zeros(1,numsyms*log2(a));
final(1:numsyms*log2(a))=finalb(1:numsyms*log2(a));

%demodulated bits
finalbits=final;

%demodulated symbols
finalsymbols=symbolx;
```

```

clear all
close all

iterations=1563;
numsyms=64;

tic

Bjam=[0.0000, 0.3034, 0.4142, 0.6362, 1.0888, 2.0215,...
      3.4755, 3.8799, 3.6811, 2.9683, 1.9194, 1.2279,...
      0.8696, 0.6794, 0.5667, 0.4928, 0.4406, 0.4017,...
      0.3716, 0.3477, 0.3284, 0.3125, 0.2994, 0.2884,...
      0.2793, 0.2718, 0.2656, 0.2605, 0.2566, 0.2535,...
      0.2514, 0.2502, 0.0000, 0.2502, 0.2514, 0.2535,...
      0.2566, 0.2605, 0.2656, 0.2718, 0.2793, 0.2884,...
      0.2994, 0.3125, 0.3284, 0.3477, 0.3716, 0.4017,...
      0.4406, 0.4928, 0.5667, 0.6794, 0.8696, 1.2279,...
      1.9194, 2.9683, 3.6811, 3.8799, 3.4755, 2.0215,...
      1.0888, 0.6362, 0.4142, 0.3034];

for p=1:20

    %makes the notch
    if p==3 | p==4 | p==7 | p==8 | p==11 | p==12 | p==15 | p==16 ...
        | p==19 | p==20
        B=[0,ones(1,31),0,ones(1,31)];
        B=B*(64/sum(B)).^ .5;
        varsum=sum(B.^2);
        B(5:12)=zeros(1,8);
        B(54:61)=zeros(1,8);
        varsum2=sum(B.^2);
        B=B*sqrt(varsum/varsum2);
    else
        B=[0,ones(1,31),0,ones(1,31)];
        B=B*(sum(B)/64).^ .5;
    end

    for n=1:4
        ary=2^(n)
        numdatabits2=n*numsyms;
        for m=1:23
            EbNodb(m)=m-6;

```

```

EbNo=10^(EbNodb(m)/10);
noisefloor=sum(B.^2)/2/log2(ary)/EbNo;
for k=1:iterations

    C=randang1(64,16);
    basisfunc=basisgenpsk(B,C,ary);
    Q=datagen(numdatabits2);
    [R,R2]=modulatorc(Q,basisfunc);

    if p== 2 | p==4 | p==6 | p==8 | p==10 | p==12 ...
        | p==14 | p==16 | p==18 | p==20
        Cjam=randang1(64,128);
        basisfunca=basisgenpsk(Bjam,Cjam,ary);
        Qa=zeros(1,numdatabits2);
        [Ra,R2a]=modulatorc(Qa,basisfunca);
    else
        Ra=zeros(1,64*numsyms);
    end

    if p>4
        if p>12

            D=C(2:32);
            F=zeros(1,31);
            F(1,:)=D;
            qxx=1;
            for pxx=1:31
                F(pxx)=D(pxx)+2*pi*pxx*qxx/31;
            end
            Cb=[0,F,0,fliplr(-F)];

        else
            Cb=randang1(64,16);
        end
        basisfuncb=basisgenpsk(B,Cb,ary);
        Qb=datagen(numdatabits2);
        [Rb,R2b]=modulatorc(Qb,basisfuncb);
        if p== 9 | p==10 | p==11 | p==12 | p==17 | ...
            p==18 | p==19 | p==20
            tau=ceil(rand(1)*64);
            if tau==64
                Rb=Rb;
            end
        end
    end
end

```



```

        else
            Rb=[Rb(tau+1:length(Rb)),Rb(1:tau)];
        end
    else
        Rb=Rb;
    end
else
    Rb=zeros(1,64*numsyms);
end

noisestuff=env2(64,R,noiseceil);
S=R+Ra+Rb+noisestuff;
[T,T2]=demodulator(S,basisfunc);
percenterrorsx(k)=sum(sum(abs(T(1:numdatabits2)-Q...
    )))/(numdatabits2);
percentsymbolerrorsx(k)=sum(sum(abs(sign(R2-T2...
    ))))/length(R2);

end
percenterrors(m,n,p)=mean(percenterrorsx);
percentsymbolerrors(m,n,p)=mean(percentsymbolerrorsx);
end
end
toc

save btest21 EbNodb percenterrors percentsymbolerrors iterations

```

```

%Abel Nunez
%EENG 799
%Multiple Access effects on single user by a network of
%orthogonal users

clear all
close all
EbNo=6;
kary=2
ary=2^kary;
numdatabits2=64*kary;

points=64; %length of symbol
iterations=15625; %number of iterations the program is run
tic
%%%%%%%%%%%%%%%%%%%%%%%%%%%%%%%%%%%%%%%%%%%%%%%%%%%%%%%%%%%%%%%%%%%%%%%%

pberrorfin=zeros(16,32);
pserrorfin=zeros(16,32);
counter=0;
for px=1:16
    pp=px-1;
    pberrortot=zeros(1,32);
    pserrortot=zeros(1,32);
    %jamming
    if mod(pp,2)==1
        Bjam=[0.0000, 0.3034, 0.4142, 0.6362, 1.0888, 2.0215,...
            3.4755, 3.8799, 3.6811, 2.9683, 1.9194, 1.2279,...
            0.8696, 0.6794, 0.5667, 0.4928, 0.4406, 0.4017,...
            0.3716, 0.3477, 0.3284, 0.3125, 0.2994, 0.2884,...
            0.2793, 0.2718, 0.2656, 0.2605, 0.2566, 0.2535,...
            0.2514, 0.2502, 0.0000, 0.2502, 0.2514, 0.2535,...
            0.2566, 0.2605, 0.2656, 0.2718, 0.2793, 0.2884,...
            0.2994, 0.3125, 0.3284, 0.3477, 0.3716, 0.4017,...
            0.4406, 0.4928, 0.5667, 0.6794, 0.8696, 1.2279,...
            1.9194, 2.9683, 3.6811, 3.8799, 3.4755, 2.0215,...
            1.0888, 0.6362, 0.4142, 0.3034];
    else
        Bjam=zeros(1,64);
    end
end

%notching

```

```

if mod(floor(pp/2),2)==1
    B=[0,ones(1,points/2-1),0,ones(1,points/2-1)];
    B=B*(sum(B)/64)^.5;
    varsum=sum(B.^2);
    B(5:12)=zeros(1,8);
    B(54:61)=zeros(1,8);
    varsum2=sum(B.^2);
    B=B*sqrt(varsum/varsum2);
else
    B=[0,ones(1,points/2-1),0,ones(1,points/2-1)];
    B=B*(sum(B)/64)^.5;
end

noisefloor=sum(B.^2)/2/log2(ary)/EbNo;
if px==5 | px==6
    iterations=1563*10;
else
    iterations=1563;
end
for iteration=1:iterations

    %%%%%%%%%
    %Generate Angles
    %%%%%%%%%
    if mod(floor(pp/4),2)==1
        %orthogonal angles
        Co=randang1(64,16);
        D=Co(2:32);
        F=zeros(16,31);
        F(1,:)=D;
        for q=1:30
            for p=1:31
                F(q+1,p)=D(p)+2*pi*p*q/31;
            end
        end
        G=[zeros(31,1),F,zeros(31,1),fliplr(-F)];
        G=[G;zeros(1,64)];
        for q2=32:63
            G(q2,:)=randang1(64,16);
        end
        C=G;
    else

```

```

    %regular angles
    G=zeros(32,64);
    for q2=1:32
        G(q2,:)=randang1(64,16);
    end
    C=G;
end

for kk=1:32
    basisfunc(:,:,kk)=basisgenpsk(B,C(kk,:),ary);
end

pberrorsx=zeros(1,32);
Q=datagen(numdatabits2);
[R,R2]=modulatorc(Q,basisfunc(:,:,1));

Cjam=randang1(64,128);
basisfunca=basisgenpsk(Bjam,Cjam,ary);
Qa=zeros(1,numdatabits2);
[Ra,R2a]=modulatorc(Qa,basisfunca);

Interference=env2(points,R,noiseffloor);

S=Interference+R+Ra;

for users=1:32
    [T,T2]=demodulatord(S,basisfunc(:,:,1));
    pberrorsx(users)=sum(sum(abs(T(1:numdatabits2)-Q))) ...
        /(numdatabits2);
    pserrorsx(users)=sum(sum(abs(sign(R2-T2))))/length(R2);

    if users~=32
        Qa=datagen(numdatabits2);
        [Rb,R2b]=modulatorc(Qa,basisfunc(:,:,users+1));

        if mod(floor(pp/8),2)==1
            tau=ceil(rand(1)*64);
            if tau==64
                Rb=Rb;
            else
                Rb=[Rb(tau+1:length(Rb)),Rb(1:tau)];
            end
        end
    end
end

```

```

        else
            Rb=Rb;
        end

        S=S+Rb;
    end

    end
    pberrortot=pberrortot+pberrorsx;
    pserrortot=pserrortot+pserrorsx;
    if mod(iteration,100)==0
        counter=counter+1
    end
end
pberrorfin(px,:)=pberrortot/iterations;
pserrorfin(px,:)=pserrortot/iterations;
end
toc

save bmanet21 pberrorfin pserrorfin EbNo iterations

```

```

%Abel Nunez
%EENG 799
%Multiple Access effects on single user by a network of
%orthogonal users

clear all
close all

points=64; %length of symbol
iterations=1563; %number of iterations the program is run

B=[0,ones(1,points/2-1),0,ones(1,points/2-1)];
%frequency envelope. DC and Nyquist frequency are nulled out

counter=0;

EbNo=6;
kary=2
ary=2^kary;
noisefloor=sum(B.^2)/2/log2(ary)/EbNo;
numdatabits2=64*kary;

tic

pberrortot=zeros(1,31);
pserrortot=zeros(1,31);

for iteration=1:iterations
    pberrorsx=zeros(1,31);
    pberrorsx=zeros(1,31);
    for mm=1:5
        Cx=randang1(64,16);
        basisfunc(:, :, mm)=basisgenpsk(B,Cx,ary);
        Q=datagen(numdatabits2);
        if mm==1
            Qx=Q;
            Cc=Cx;
        end
        [R(mm, :), R2(mm, :)] = modulatorc(Q, basisfunc(:, :, mm));
    end
    Rtot=sum(R);

```

```

for notcher=1:31
    BN=[0,ones(1,32-notcher),zeros(1,notcher-1),0,...
        zeros(1,notcher-1),ones(1,32-notcher)];
    BN2=BN.*B;

    basisfunc2=basisgenpsk(BN2,Cc,ary);
    noisefloor=sum(BN2.^2)/2/log2(ary)/EbNo;
    Interference=env2(points,Rtot,noisefloor);
    S=Interference+Rtot;
    [T,T2]=demodulatord(S,basisfunc2);
    pberrorsx(notcher)=sum(sum(abs(T(1:numdatabits2)-Qx)))...
        /(numdatabits2);
    pserrorsx(notcher)=sum(sum(abs(sign(R2(1,:)-T2))))...
        /length(R2(1,:));

end
pberrortot=pberrortot+pberrorsx;
pserrortot=pserrortot+pserrorsx;
end
pberrorfin=pberrortot/iterations;
pserrorfin=pserrortot/iterations;

toc

save bnotch1 pberrorfin pserrorfin EbNo iterations

```

```

%Abel Nunez
%EENG 799
%Multiple Access effects on single user by a network of
%orthogonal users

clear all
close all

points=64; %length of symbol
iterations=1563; %number of iterations the program is run

B=[0,ones(1,points/2-1),0,ones(1,points/2-1)];
%frequency envelope. DC and Nyquist frequency are nulled out

counter=0;

EbNo=6;
kary=2
ary=2^kary;
noisefloor=sum(B.^2)/2/log2(ary)/EbNo;
numdatabits2=64*kary;

tic

pberrortot=zeros(1,31);
pserrortot=zeros(1,31);

for iteration=1:iterations

    Co=randang1(64,16);
    D=Co(2:32);
    F=zeros(30,31);
    F(1,:)=D;
    for q=1:30
        for p=1:31
            F(q+1,p)=D(p)+2*pi*p*q/31;
        end
    end
    G=[zeros(31,1),F,zeros(31,1),fliplr(-F)];
    G=[G;zeros(1,64)];

```



```

for kk=1:30
    basisfunc(:, :, kk)=basisgenpsk(B, G(kk, :), ary);
end

for mm=1:5
    Q=datagen(numdatabits2);
    if mm==1
        Qx=Q;
    end
    [R(mm, :), R2(mm, :)] = modulatorc(Q, basisfunc(:, :, mm));
end
Rtot=sum(R);

pberrorsx=zeros(1, 31);
pberrorsx=zeros(1, 31);
for notcher=1:31
    BN=[0, ones(1, 32-notcher), zeros(1, notcher-1), 0, ...
        zeros(1, notcher-1), ones(1, 32-notcher)];
    BN2=BN.*B;

    basisfunc2=basisgenpsk(BN2, G(1, :), ary);
    noisefloor=sum(BN2.^2)/2/log2(ary)/EbNo;
    Interference=env2(points, Rtot, noisefloor);
    S=Interference+Rtot;
    [T, T2]=demodulatord(S, basisfunc2);
    pberrorsx(notcher)=sum(sum(abs(T(1:numdatabits2)-Qx)))/...
        /(numdatabits2);
    pserrorsx(notcher)=sum(sum(abs(sign(R2(1, :)-T2))))/...
        /length(R2(1, :));

end
pberrortot=pberrortot+pberrorsx;
pserrortot=pserrortot+pserrorsx;
end
pberrorfin=pberrortot/iterations;
pserrorfin=pserrortot/iterations;

toc

save borthonotch1 pberrorfin pserrorfin EbNo iterations

```



## Appendix B. Cross-Correlation Between PSK Symbols

n=time index

N=number of samples that make up a symbol.

P=number of sinusoids which make up a symbol.  $P < \frac{N}{2}$

$\theta_c^{(v)}$ =phase modulation of  $c^{th}$  symbol for  $v^{th}$  user.  $S_\theta = \left\{0, \frac{2\pi}{Q}, \frac{4\pi}{Q}, \dots, \frac{(Q-1)2\pi}{Q}\right\}$

$\phi_n^{(v)}$ =phase coding, superscript indicates a set of phase coding for  $v^{th}$  user

Symbol 1 is defined with the following equation. Superscript indicates user.  
Subscript indicates symbol.

$$s_c^{(v)}(n) = \frac{2}{N} \sum_{p=1}^P A_p \cos \left( 2\pi p \frac{n}{N} + \phi_p^{(v)} + \theta_c^{(v)} \right) \quad (\text{B.1})$$

Symbol 2 is defined with the following equation. Superscript indicates used.  
Subscript indicates symbol.

$$s_d^{(w)}(n) = \frac{2}{N} \sum_{p=1}^P B_p \cos \left( 2\pi p \frac{n}{N} + \phi_p^{(w)} + \theta_d^{(w)} \right) \quad (\text{B.2})$$

### B.1 Cross Correlation Between Symbol 1 and Symbol 2

$$R_{cd}^{(v,w)} = \sum_{n=0}^{N-1} S_c^{(v)}(n) S_d^{(w)}(n) \quad (\text{B.3})$$

$$= \sum_{n=0}^{N-1} \frac{2}{N} \sum_{p=1}^P A_p \cos \left( 2\pi p \frac{n}{N} + \phi_p^{(v)} + \theta_c^{(v)} \right) \frac{2}{N} \sum_{q=1}^P B_q \cos \left( 2\pi q \frac{n}{N} + \phi_q^{(w)} + \theta_d^{(w)} \right) \quad (\text{B.4})$$

$$= \frac{4}{N^2} \sum_{p=1}^P \sum_{q=1}^P \sum_{n=0}^{N-1} A_p B_q \cos \left( 2\pi p \frac{n}{N} + \phi_p^{(v)} + \theta_c^{(v)} \right) \cos \left( 2\pi q \frac{n}{N} + \phi_q^{(w)} + \theta_d^{(w)} \right) \quad (\text{B.5})$$

$$\begin{aligned} &= \frac{4}{N^2} \sum_{p=1}^P \sum_{q=1, q \neq p}^P \sum_{n=0}^{N-1} A_p B_q \cos \left( 2\pi p \frac{n}{N} + \phi_p^{(v)} + \theta_c^{(v)} \right) \cos \left( 2\pi q \frac{n}{N} + \phi_q^{(w)} + \theta_d^{(w)} \right) \\ &\quad + \frac{4}{N^2} \sum_{r=1}^P \sum_{n=0}^{N-1} A_r B_r \cos \left( 2\pi r \frac{n}{N} + \phi_r^{(v)} + \theta_c^{(v)} \right) \cos \left( 2\pi r \frac{n}{N} + \phi_r^{(w)} + \theta_d^{(w)} \right) \end{aligned} \quad (\text{B.6})$$

$$\begin{aligned} &= \frac{4}{N^2} \sum_{p=1}^P \sum_{q=1, q \neq p}^P A_p B_q \sum_{n=0}^{N-1} \frac{1}{2} \cos \left( 2\pi (p+q) \frac{n}{N} + \phi_p^{(v)} + \phi_q^{(w)} + \theta_c^{(v)} + \theta_d^{(w)} \right) \\ &\quad + \frac{4}{N^2} \sum_{p=1}^P \sum_{q=1, q \neq p}^P A_p B_q \sum_{n=0}^{N-1} \frac{1}{2} \cos \left( 2\pi (p-q) \frac{n}{N} + \phi_p^{(v)} - \phi_q^{(w)} + \theta_c^{(v)} - \theta_d^{(w)} \right) \\ &\quad + \frac{4}{N^2} \sum_{r=1}^P A_r B_r \sum_{n=0}^{N-1} \frac{1}{2} \cos \left( 4\pi r \frac{n}{N} + \phi_r^{(v)} + \phi_r^{(w)} + \theta_c^{(v)} + \theta_d^{(w)} \right) \\ &\quad + \frac{4}{N^2} \sum_{r=1}^P A_r B_r \sum_{n=0}^{N-1} \frac{1}{2} \cos \left( \phi_r^{(v)} - \phi_r^{(w)} + \theta_c^{(v)} - \theta_d^{(w)} \right) \end{aligned} \quad (\text{B.7})$$

$$= \frac{4}{N^2} \sum_{p=1}^P A_p B_p \sum_{n=0}^{N-1} \frac{1}{2} \cos \left( \phi_p^{(v)} - \phi_p^{(w)} + \theta_c^{(v)} - \theta_d^{(w)} \right) \quad (\text{B.8})$$

$$R_{cd}^{(v,w)} = \frac{2}{N} \sum_{p=1}^P A_p B_p \cos \left( \phi_p^{(v)} - \phi_p^{(w)} + \theta_c^{(v)} - \theta_d^{(w)} \right) \quad (\text{B.9})$$

## B.2 Cross Correlation Between Symbols of a Single user

$$v = w$$

$$R_{cd}^{(v,v)} = \frac{2}{N} \sum_{p=1}^P A_p A_p \cos \left( \phi_p^{(v)} - \phi_p^{(v)} + \theta_c^{(v)} - \theta_d^{(v)} \right) \quad (\text{B.10})$$

$$R_{cd}^{(v,v)} = \frac{2}{N} \sum_{p=1}^P A_p^2 \cos \left( \theta_c^{(v)} - \theta_d^{(v)} \right) \quad (\text{B.11})$$

## B.3 Autocorrelation of symbol

$$R_{cc}^{(v,v)} = \frac{2}{N} \sum_{p=1}^P A_p^2 \cos (0) \quad (\text{B.12})$$

$$R_{cc}^{(v,v)} = \frac{2}{N} \sum_{p=1}^P A_p^2 \quad (\text{B.13})$$

Mean of cross-correlation between symbols of two different users. Each symbol is assumed to be equiprobable,  $v \neq w$ , and users v and w are synchronized (symbol boundaries coincide).

$$R_{cd}^{(v,w)} = \frac{2}{N} \sum_{p=1}^P A_p B_p \cos \left( \phi_p^{(v)} - \phi_p^{(w)} + \theta_c^{(v)} - \theta_d^{(w)} \right) \quad (\text{B.14})$$

Mean

$$\mathbf{E}_\theta \left\{ R_{cd}^{(v,w)} \right\} = \mathbf{E}_\theta \left\{ \frac{2}{N} \sum_{p=1}^P A_p B_p \cos \left( \phi_p^{(v)} - \phi_p^{(w)} + \theta_c^{(v)} - \theta_d^{(w)} \right) \right\} \quad (\text{B.15})$$

$$= \frac{2}{N} \sum_{p=1}^P A_p B_p \mathbf{E}_\theta \left\{ \cos \left( \phi_p^{(v)} - \phi_p^{(w)} + \theta_c^{(v)} - \theta_d^{(w)} \right) \right\} \quad (\text{B.16})$$

$$\begin{aligned} &= \frac{2}{N} \sum_{p=1}^P A_p B_p \mathbf{E}_\theta \left\{ \cos \left( \theta_c^{(v)} - \theta_d^{(w)} \right) \cos \left( \phi_p^{(v)} - \phi_p^{(w)} \right) \right\} \\ &\quad - \frac{2}{N} \sum_{p=1}^P A_p B_p \mathbf{E}_\theta \left\{ \sin \left( \theta_c^{(v)} - \theta_d^{(w)} \right) \sin \left( \phi_p^{(v)} - \phi_p^{(w)} \right) \right\} \end{aligned} \quad (\text{B.17})$$

$$\begin{aligned} &= \frac{2}{N} \sum_{p=1}^P A_p B_p \mathbf{E}_\theta \left\{ \cos \left( \theta_c^{(v)} - \theta_d^{(w)} \right) \right\} \cos \left( \phi_p^{(v)} - \phi_p^{(w)} \right) \\ &\quad - \frac{2}{N} \sum_{p=1}^P A_p B_p \mathbf{E}_\theta \left\{ \sin \left( \theta_c^{(v)} - \theta_d^{(w)} \right) \right\} \sin \left( \phi_p^{(v)} - \phi_p^{(w)} \right) \end{aligned} \quad (\text{B.18})$$

$$\begin{aligned}
&= \frac{2}{N} \sum_{p=1}^P A_p B_p \mathbf{E}_\theta \left\{ \cos(\theta_c^{(v)}) \cos(\theta_d^{(w)}) \right\} \cos(\phi_p^{(v)} - \phi_p^{(w)}) \\
&\quad + \frac{2}{N} \sum_{p=1}^P A_p B_p \mathbf{E}_\theta \left\{ \sin(\theta_c^{(v)}) \sin(\theta_d^{(w)}) \right\} \cos(\phi_p^{(v)} - \phi_p^{(w)}) \\
&\quad - \frac{2}{N} \sum_{p=1}^P A_p B_p \mathbf{E}_\theta \left\{ \sin(\theta_c^{(v)}) \cos(\theta_d^{(w)}) \right\} \sin(\phi_p^{(v)} - \phi_p^{(w)}) \\
&\quad - \frac{2}{N} \sum_{p=1}^P A_p B_p \mathbf{E}_\theta \left\{ \cos(\theta_c^{(v)}) \sin(\theta_d^{(w)}) \right\} \sin(\phi_p^{(v)} - \phi_p^{(w)}) \quad (\text{B.19})
\end{aligned}$$

$$\begin{aligned}
&= \frac{2}{N} \sum_{p=1}^P A_p B_p \mathbf{E}_\theta \left\{ \cos(\theta_c^{(v)}) \right\} \mathbf{E}_\theta \left\{ \cos(\theta_d^{(w)}) \right\} \cos(\phi_p^{(v)} - \phi_p^{(w)}) \\
&\quad + \frac{2}{N} \sum_{p=1}^P A_p B_p \mathbf{E}_\theta \left\{ \sin(\theta_c^{(v)}) \right\} \mathbf{E}_\theta \left\{ \sin(\theta_d^{(w)}) \right\} \cos(\phi_p^{(v)} - \phi_p^{(w)}) \\
&\quad - \frac{2}{N} \sum_{p=1}^P A_p B_p \mathbf{E}_\theta \left\{ \sin(\theta_c^{(v)}) \right\} \mathbf{E}_\theta \left\{ \cos(\theta_d^{(w)}) \right\} \sin(\phi_p^{(v)} - \phi_p^{(w)}) \\
&\quad - \frac{2}{N} \sum_{p=1}^P A_p B_p \mathbf{E}_\theta \left\{ \cos(\theta_c^{(v)}) \right\} \mathbf{E}_\theta \left\{ \sin(\theta_d^{(w)}) \right\} \sin(\phi_p^{(v)} - \phi_p^{(w)}) \quad (\text{B.20})
\end{aligned}$$

$$\mathbf{E}_\theta \left\{ R_{cd}^{(v,w)} \right\} = 0 \quad (\text{B.21})$$

Variance of  $R_{cd}^{(v,w)}$

$$\text{var} \left\{ R_{cd}^{(v,w)} \right\} = \mathbf{E}_\theta \left\{ \left[ \frac{2}{N} \sum_{p=1}^P A_p B_p \cos \left( \phi_p^{(v)} - \phi_p^{(w)} + \theta_c^{(v)} - \theta_d^{(w)} \right) \right]^2 \right\} \quad (\text{B.22})$$

$$\begin{aligned} &= \mathbf{E}_\theta \left\{ \frac{4}{N^2} \sum_{p=1}^P A_p B_p \cos \left( \phi_p^{(v)} - \phi_p^{(w)} + \theta_c^{(v)} - \theta_d^{(w)} \right) \right. \\ &\quad \left. \times \sum_{q=1}^P A_q B_q \cos \left( \phi_q^{(v)} - \phi_q^{(w)} + \theta_c^{(v)} - \theta_d^{(w)} \right) \right\} \quad (\text{B.23}) \end{aligned}$$

$$\begin{aligned} &= \mathbf{E}_\theta \left\{ \frac{4}{N^2} \sum_{p=1}^P \sum_{q=1}^P A_p B_p A_q B_q \cos \left( \phi_p^{(v)} - \phi_p^{(w)} + \theta_c^{(v)} - \theta_d^{(w)} \right) \right. \\ &\quad \left. \times \cos \left( \phi_q^{(v)} - \phi_q^{(w)} + \theta_c^{(v)} - \theta_d^{(w)} \right) \right\} \quad (\text{B.24}) \end{aligned}$$

$$\begin{aligned} &= \frac{4}{N^2} \sum_{p=1}^P \sum_{q=1}^P A_p B_p A_q B_q \mathbf{E}_\theta \left\{ \cos \left( \phi_p^{(v)} - \phi_p^{(w)} + \theta_c^{(v)} - \theta_d^{(w)} \right) \right. \\ &\quad \left. \times \cos \left( \phi_q^{(v)} - \phi_q^{(w)} + \theta_c^{(v)} - \theta_d^{(w)} \right) \right\} \quad (\text{B.25}) \end{aligned}$$



$$\begin{aligned}
&= \frac{2}{N^2} \sum_{p=1}^P \sum_{q=1}^P A_p B_p A_q B_q \\
&\quad \times \mathbf{E}_\theta \left\{ \cos \left( \phi_p^{(v)} - \phi_p^{(w)} + \theta_c^{(v)} - \theta_d^{(w)} + \phi_q^{(v)} - \phi_q^{(w)} + \theta_c^{(v)} - \theta_d^{(w)} \right) \right\} \\
&\quad + \frac{2}{N^2} \sum_{p=1}^P \sum_{q=1}^P A_p B_p A_q B_q \\
&\quad \times \mathbf{E}_\theta \left\{ \cos \left( \phi_p^{(v)} - \phi_p^{(w)} + \theta_c^{(v)} - \theta_d^{(w)} - \phi_q^{(v)} + \phi_q^{(w)} - \theta_c^{(v)} + \theta_d^{(w)} \right) \right\} \quad (\text{B.26})
\end{aligned}$$

$$\begin{aligned}
&= \frac{2}{N^2} \sum_{p=1}^P \sum_{q=1}^P A_p B_p A_q B_q \\
&\quad \times \mathbf{E}_\theta \left\{ \cos \left( \phi_p^{(v)} - \phi_p^{(w)} + \phi_q^{(v)} - \phi_q^{(w)} + \theta_c^{(v)} - \theta_d^{(w)} + \theta_c^{(v)} - \theta_d^{(w)} \right) \right\} \\
&\quad + \frac{2}{N^2} \sum_{p=1}^P \sum_{q=1}^P A_p B_p A_q B_q \\
&\quad \times \mathbf{E}_\theta \left\{ \cos \left( \phi_p^{(v)} - \phi_p^{(w)} - \phi_q^{(v)} + \phi_q^{(w)} + \theta_c^{(v)} - \theta_d^{(w)} - \theta_c^{(v)} + \theta_d^{(w)} \right) \right\} \quad (\text{B.27})
\end{aligned}$$

$$\begin{aligned}
&= \frac{2}{N^2} \sum_{p=1}^P \sum_{q=1}^P A_p B_p A_q B_q \\
&\quad \times \mathbf{E}_\theta \left\{ \cos \left( \phi_p^{(v)} - \phi_p^{(w)} + \phi_q^{(v)} - \phi_q^{(w)} \right) \cos \left( \theta_c^{(v)} - \theta_d^{(w)} + \theta_c^{(v)} - \theta_d^{(w)} \right) \right\} \\
&\quad - \frac{2}{N^2} \sum_{p=1}^P \sum_{q=1}^P A_p B_p A_q B_q \\
&\quad \times \mathbf{E}_\theta \left\{ \sin \left( \phi_p^{(v)} - \phi_p^{(w)} + \phi_q^{(v)} - \phi_q^{(w)} \right) \sin \left( \theta_c^{(v)} - \theta_d^{(w)} + \theta_c^{(v)} - \theta_d^{(w)} \right) \right\} \\
&\quad + \frac{2}{N^2} \sum_{p=1}^P \sum_{q=1}^P A_p B_p A_q B_q \\
&\quad \times \mathbf{E}_\theta \left\{ \cos \left( \phi_p^{(v)} - \phi_p^{(w)} - \phi_q^{(v)} + \phi_q^{(w)} \right) \cos \left( \theta_c^{(v)} - \theta_d^{(w)} - \theta_c^{(v)} + \theta_d^{(w)} \right) \right\} \\
&\quad - \frac{2}{N^2} \sum_{p=1}^P \sum_{q=1}^P A_p B_p A_q B_q \\
&\quad \times \mathbf{E}_\theta \left\{ \sin \left( \phi_p^{(v)} - \phi_p^{(w)} - \phi_q^{(v)} + \phi_q^{(w)} \right) \sin \left( \theta_c^{(v)} - \theta_d^{(w)} - \theta_c^{(v)} + \theta_d^{(w)} \right) \right\} \quad (\text{B.28})
\end{aligned}$$

$$\begin{aligned}
&= \frac{2}{N^2} \sum_{p=1}^P \sum_{q=1}^P A_p B_p A_q B_q \cos(\phi_p^{(v)} - \phi_p^{(w)} + \phi_q^{(v)} - \phi_q^{(w)}) \\
&\quad \times \mathbf{E}_\theta \left\{ \cos(\theta_c^{(v)} - \theta_d^{(w)} + \theta_c^{(v)} - \theta_d^{(w)}) \right\} \\
&\quad - \frac{2}{N^2} \sum_{p=1}^P \sum_{q=1}^P A_p B_p A_q B_q \sin(\phi_p^{(v)} - \phi_p^{(w)} + \phi_q^{(v)} - \phi_q^{(w)}) \\
&\quad \times \mathbf{E}_\theta \left\{ \sin(\theta_c^{(v)} - \theta_d^{(w)} + \theta_c^{(v)} - \theta_d^{(w)}) \right\} \\
&\quad + \frac{2}{N^2} \sum_{p=1}^P \sum_{q=1}^P A_p B_p A_q B_q \cos(\phi_p^{(v)} - \phi_p^{(w)} - \phi_q^{(v)} + \phi_q^{(w)}) \\
&\quad \times \mathbf{E}_\theta \left\{ \cos(\theta_c^{(v)} - \theta_d^{(w)} - \theta_c^{(v)} + \theta_d^{(w)}) \right\} \\
&\quad - \frac{2}{N^2} \sum_{p=1}^P \sum_{q=1}^P A_p B_p A_q B_q \sin(\phi_p^{(v)} - \phi_p^{(w)} - \phi_q^{(v)} + \phi_q^{(w)}) \\
&\quad \times \mathbf{E}_\theta \left\{ \sin(\theta_c^{(v)} - \theta_d^{(w)} - \theta_c^{(v)} + \theta_d^{(w)}) \right\} \tag{B.29}
\end{aligned}$$

$$\begin{aligned}
&= \frac{2}{N^2} \sum_{p=1}^P \sum_{q=1}^P A_p B_p A_q B_q \cos(\phi_p^{(v)} - \phi_p^{(w)} + \phi_q^{(v)} - \phi_q^{(w)}) \mathbf{E}_\theta \left\{ \cos(2\theta_c^{(v)} - 2\theta_d^{(w)}) \right\} \\
&\quad - \frac{2}{N^2} \sum_{p=1}^P \sum_{q=1}^P A_p B_p A_q B_q \sin(\phi_p^{(v)} - \phi_p^{(w)} + \phi_q^{(v)} - \phi_q^{(w)}) \mathbf{E}_\theta \left\{ \sin(2\theta_c^{(v)} - 2\theta_d^{(w)}) \right\} \\
&\quad + \frac{2}{N^2} \sum_{p=1}^P \sum_{q=1}^P A_p B_p A_q B_q \cos(\phi_p^{(v)} - \phi_p^{(w)} - \phi_q^{(v)} + \phi_q^{(w)}) \mathbf{E}_\theta \{ \cos(0) \} \\
&\quad - \frac{2}{N^2} \sum_{p=1}^P \sum_{q=1}^P A_p B_p A_q B_q \sin(\phi_p^{(v)} - \phi_p^{(w)} - \phi_q^{(v)} + \phi_q^{(w)}) \mathbf{E}_\theta \{ \sin(0) \} \tag{B.30}
\end{aligned}$$

$$\begin{aligned}
&= \frac{2}{N^2} \sum_{p=1}^P \sum_{q=1}^P A_p B_p A_q B_q \cos(\phi_p^{(v)} - \phi_p^{(w)} + \phi_q^{(v)} - \phi_q^{(w)}) \mathbf{E}_\theta \left\{ \cos(2\theta_c^{(v)} - 2\theta_d^{(w)}) \right\} \\
&\quad - \frac{2}{N^2} \sum_{p=1}^P \sum_{q=1}^P A_p B_p A_q B_q \sin(\phi_p^{(v)} - \phi_p^{(w)} + \phi_q^{(v)} - \phi_q^{(w)}) \mathbf{E}_\theta \left\{ \sin(2\theta_c^{(v)} - 2\theta_d^{(w)}) \right\} \\
&\quad + \frac{2}{N^2} \sum_{p=1}^P \sum_{q=1}^P A_p B_p A_q B_q \cos(\phi_p^{(v)} - \phi_p^{(w)} - \phi_q^{(v)} + \phi_q^{(w)}) \tag{B.31}
\end{aligned}$$

$$\begin{aligned}
&= \frac{2}{N^2} \sum_{p=1}^P \sum_{q=1}^P A_p B_p A_q B_q \cos(\phi_p^{(v)} - \phi_p^{(w)} + \phi_q^{(v)} - \phi_q^{(w)}) \\
&\quad \times \mathbf{E}_\theta \left\{ \cos(2\theta_c^{(v)}) \cos(2\theta_d^{(w)}) + \sin(2\theta_c^{(v)}) \sin(2\theta_d^{(w)}) \right\} \\
&\quad - \frac{2}{N^2} \sum_{p=1}^P \sum_{q=1}^P A_p B_p A_q B_q \sin(\phi_p^{(v)} - \phi_p^{(w)} + \phi_q^{(v)} - \phi_q^{(w)}) \\
&\quad \times \mathbf{E}_\theta \left\{ \sin(2\theta_c^{(v)}) \cos(2\theta_d^{(w)}) - \cos(2\theta_c^{(v)}) \sin(2\theta_d^{(w)}) \right\} \\
&\quad + \frac{2}{N^2} \sum_{p=1}^P \sum_{q=1}^P A_p B_p A_q B_q \cos(\phi_p^{(v)} - \phi_p^{(w)} - \phi_q^{(v)} + \phi_q^{(w)}) \tag{B.32}
\end{aligned}$$

$$\begin{aligned}
&= \frac{2}{N^2} \sum_{p=1}^P \sum_{q=1}^P A_p B_p A_q B_q \cos(\phi_p^{(v)} - \phi_p^{(w)} + \phi_q^{(v)} - \phi_q^{(w)}) \\
&\quad \times \mathbf{E}_\theta \left\{ \cos(2\theta_c^{(v)}) \right\} \mathbf{E}_\theta \left\{ \cos(2\theta_d^{(w)}) \right\} \\
&\quad + \frac{2}{N^2} \sum_{p=1}^P \sum_{q=1}^P A_p B_p A_q B_q \cos(\phi_p^{(v)} - \phi_p^{(w)} + \phi_q^{(v)} - \phi_q^{(w)}) \\
&\quad \times \mathbf{E}_\theta \left\{ \sin(2\theta_c^{(v)}) \right\} \mathbf{E}_\theta \left\{ \sin(2\theta_d^{(w)}) \right\} \\
&\quad - \frac{2}{N^2} \sum_{p=1}^P \sum_{q=1}^P A_p B_p A_q B_q \sin(\phi_p^{(v)} - \phi_p^{(w)} + \phi_q^{(v)} - \phi_q^{(w)}) \\
&\quad \times \mathbf{E}_\theta \left\{ \sin(2\theta_c^{(v)}) \right\} \mathbf{E}_\theta \left\{ \cos(2\theta_d^{(w)}) \right\} \\
&\quad + \frac{2}{N^2} \sum_{p=1}^P \sum_{q=1}^P A_p B_p A_q B_q \sin(\phi_p^{(v)} - \phi_p^{(w)} + \phi_q^{(v)} - \phi_q^{(w)}) \\
&\quad \times \mathbf{E}_\theta \left\{ \cos(2\theta_c^{(v)}) \right\} \mathbf{E}_\theta \left\{ \sin(2\theta_d^{(w)}) \right\} \\
&\quad + \frac{2}{N^2} \sum_{p=1}^P \sum_{q=1}^P A_p B_p A_q B_q \cos(\phi_p^{(v)} - \phi_p^{(w)} - \phi_q^{(v)} + \phi_q^{(w)}) \quad (\text{B.33})
\end{aligned}$$

$$\begin{aligned}
\text{var} \left\{ R_{cd}^{(v,w)} \right\} &= \frac{2}{N^2} \sum_{p=1}^P \sum_{q=1}^P A_p B_p A_q B_q \cos(\phi_p^{(v)} - \phi_p^{(w)} + \phi_q^{(v)} - \phi_q^{(w)}) \\
&\quad \times \mathbf{E}_\theta \left\{ \cos(2\theta_c^{(v)}) \right\} \mathbf{E}_\theta \left\{ \cos(2\theta_d^{(w)}) \right\} \\
&\quad + \frac{2}{N^2} \sum_{p=1}^P \sum_{q=1}^P A_p B_p A_q B_q \cos(\phi_p^{(v)} - \phi_p^{(w)} - \phi_q^{(v)} + \phi_q^{(w)}) \quad (\text{B.34})
\end{aligned}$$

Variance of  $R_{cd}^{(v,w)}$  in terms of  $\phi$  for BPSK. This equation describes the variance with no restrictions on  $\phi$ .

$$\begin{aligned} \text{var} \left\{ R_{cd}^{(v,w)} \right\} &= \frac{2}{N^2} \sum_{p=1}^P \sum_{q=1}^P A_p B_p A_q B_q \cos \left( \phi_p^{(v)} - \phi_p^{(w)} + \phi_q^{(v)} - \phi_q^{(w)} \right) \\ &+ \frac{2}{N^2} \sum_{p=1}^P \sum_{q=1}^P A_p B_p A_q B_q \cos \left( \phi_p^{(v)} - \phi_p^{(w)} - \phi_q^{(v)} + \phi_q^{(w)} \right) \end{aligned} \quad (\text{B.35})$$

$$\text{var} \left\{ R_{cd}^{(v,w)} \right\} = \frac{4}{N^2} \sum_{p=1}^P \sum_{q=1}^P A_p B_p A_q B_q \cos(\phi_p^{(v)} - \phi_p^{(w)}) \cos(\phi_q^{(v)} - \phi_q^{(w)}) \quad (\text{B.36})$$

Variance of  $R_{cd}^{(v,w)}$  in terms of  $\phi$  for  $M = 2^k$  PSK where  $k > 1$ . This equation describes the variance with no restrictions on  $\phi$ .

$$\text{var} \left\{ R_{cd}^{(v,w)} \right\} = \frac{2}{N^2} \sum_{p=1}^P \sum_{q=1}^P A_p B_p A_q B_q \cos \left( \phi_p^{(v)} - \phi_p^{(w)} - \phi_q^{(v)} + \phi_q^{(w)} \right) \quad (\text{B.37})$$

The reason (B.36) and (B.37) differ is the expected value of  $\cos(2\theta)$  is 1 for BPSK and 0 for MPSK, where  $M = 2^k$ ,  $k > 1$ .

#### B.4 Expected Value of the Variance for the BPSK Case with Random Data Phase Modulation

Assuming  $\phi$  is uniformly distributed,  $U[0, 2\pi)$ , the expected value for the BPSK case,  $\mathbf{E}_\phi \left\{ (B.36) \right\}$ , becomes

$$\mathbf{E}_\phi \left\{ (B.36) \right\} = \mathbf{E}_\phi \left\{ \frac{4}{N^2} \sum_{p=1}^P \sum_{q=1}^P A_p B_p A_q B_q \cos(\phi_p^{(v)} - \phi_p^{(w)}) \cos(\phi_q^{(v)} - \phi_q^{(w)}) \right\} \quad (B.38)$$

$$\begin{aligned} &= \mathbf{E}_\phi \left\{ \frac{4}{N^2} \sum_{p=1}^P \sum_{q=1, q \neq p}^P A_p B_p A_q B_q \cos(\phi_p^{(v)} - \phi_p^{(w)}) \cos(\phi_q^{(v)} - \phi_q^{(w)}) \right\} \\ &\quad + \mathbf{E}_\phi \left\{ \frac{4}{N^2} \sum_{p=1}^P A_p^2 B_p^2 \cos^2(\phi_p^{(v)} - \phi_p^{(w)}) \right\} \end{aligned} \quad (B.39)$$

$$\begin{aligned} &= \mathbf{E}_\phi \left\{ \frac{4}{N^2} \sum_{p=1}^P \sum_{q=1}^P A_p B_p A_q B_q \cos(\phi_p^{(v)}) \cos(\phi_p^{(w)}) \cos(\phi_q^{(v)} - \phi_q^{(w)}) \right\} \\ &\quad - \mathbf{E}_\phi \left\{ \frac{4}{N^2} \sum_{p=1}^P \sum_{q=1}^P A_p B_p A_q B_q \sin(\phi_p^{(v)}) \sin(\phi_p^{(w)}) \cos(\phi_q^{(v)} - \phi_q^{(w)}) \right\} \\ &\quad + \mathbf{E}_\phi \left\{ \frac{4}{N^2} \sum_{p=1}^P A_p^2 B_p^2 \cos^2(\phi_p^{(v)} - \phi_p^{(w)}) \right\} \end{aligned} \quad (B.40)$$

$$\begin{aligned}
&= \frac{4}{N^2} \sum_{p=1}^P \sum_{q=1}^P A_p B_p A_q B_q \mathbf{E}_\phi \left\{ \cos(\phi_p^{(v)}) \right\} \cos(\phi_p^{(w)}) \cos(\phi_q^{(v)} - \phi_q^{(w)}) \\
&\quad - \frac{4}{N^2} \sum_{p=1}^P \sum_{q=1}^P A_p B_p A_q B_q \mathbf{E}_\phi \left\{ \sin(\phi_p^{(v)}) \right\} \sin(\phi_p^{(w)}) \cos(\phi_q^{(v)} - \phi_q^{(w)}) \\
&\quad + \frac{4}{N^2} \sum_{p=1}^P A_p^2 B_p^2 \left( \frac{1}{2} + \frac{1}{2} \mathbf{E}_\phi \left\{ \cos(2\phi_p^{(v)} - 2\phi_p^{(w)}) \right\} \right)
\end{aligned} \tag{B.41}$$

$$= \frac{4}{N^2} \sum_{p=1}^P A_p^2 B_p^2 \left( \frac{1}{2} + \frac{1}{2} \mathbf{E}_\phi \left\{ \cos(2\phi_p^{(v)} - 2\phi_p^{(w)}) \right\} \right)$$

$$= \frac{4}{N^2} \sum_{p=1}^P A_p^2 B_p^2 \left( \frac{1}{2} \right)$$

$$\mathbf{E}_\phi \left\{ (B.36) \right\} = \frac{2}{N^2} \sum_{p=1}^P A_p^2 B_p^2 \tag{B.42}$$



## B.5 Expected Value of the Variance for the MPSK Case with Random Data Phase Modulation

Assuming  $\phi$  is uniformly distributed,  $U[0, 2\pi)$ , the expected value for the MPSK case,  $\mathbf{E}_\phi \left\{ (B.37) \right\}$ , becomes

$$\begin{aligned} \mathbf{E}_\phi \left\{ (B.37) \right\} &= \mathbf{E}_\phi \left\{ \frac{2}{N^2} \sum_{p=1}^P \sum_{q=1, q \neq p}^P A_p B_p A_q B_q \cos(\phi_p^{(v)}) \cos(-\phi_p^{(w)} - \phi_q^{(v)} + \phi_q^{(w)}) \right. \\ &\quad - \frac{2}{N^2} \sum_{p=1}^P \sum_{q=1, q \neq p}^P A_p B_p A_q B_q \sin(\phi_p^{(v)}) \sin(-\phi_p^{(w)} - \phi_q^{(v)} + \phi_q^{(w)}) \\ &\quad \left. + \frac{2}{N^2} \sum_{r=1}^P A_r^2 B_r^2 \right\} \end{aligned} \quad (B.43)$$

$$\begin{aligned} &= \frac{2}{N^2} \sum_{p=1}^P \sum_{q=1, q \neq p}^P A_p B_p A_q B_q \mathbf{E}_\phi \left\{ \cos(\phi_p^{(v)}) \cos(-\phi_p^{(w)} - \phi_q^{(v)} + \phi_q^{(w)}) \right\} \\ &\quad - \frac{2}{N^2} \sum_{p=1}^P \sum_{q=1, q \neq p}^P A_p B_p A_q B_q \mathbf{E}_\phi \left\{ \sin(\phi_p^{(v)}) \sin(-\phi_p^{(w)} - \phi_q^{(v)} + \phi_q^{(w)}) \right\} \\ &\quad + \frac{2}{N^2} \sum_{r=1}^P A_r^2 B_r^2 \end{aligned} \quad (B.44)$$

$$\begin{aligned} &= \frac{2}{N^2} \sum_{p=1}^P \sum_{q=1, q \neq p}^P A_p B_p A_q B_q \mathbf{E}_\phi \left\{ \cos(\phi_p^{(v)}) \right\} \mathbf{E}_\phi \left\{ \cos(-\phi_p^{(w)} - \phi_q^{(v)} + \phi_q^{(w)}) \right\} \\ &\quad - \frac{2}{N^2} \sum_{p=1}^P \sum_{q=1, q \neq p}^P A_p B_p A_q B_q \mathbf{E}_\phi \left\{ \sin(\phi_p^{(v)}) \right\} \mathbf{E}_\phi \left\{ \sin(-\phi_p^{(w)} - \phi_q^{(v)} + \phi_q^{(w)}) \right\} \\ &\quad + \frac{2}{N^2} \sum_{r=1}^P A_r^2 B_r^2 \end{aligned} \quad (B.45)$$

$$\mathbf{E}_\phi \left\{ (B.37) \right\} = \frac{2}{N^2} \sum_{r=1}^P A_r^2 B_r^2 \quad (\text{B.46})$$

## **B.6 Expected Value of the Variance for the BPSK and MPSK Case with Random Multiple Access Phase Coding**

if  $\phi$  is uniformly distributed,  $\mathbf{U}[0, 2\pi)$ , the expected value for the BPSK case is the same as the MPSK case

$$= \frac{2}{N^2} \sum_{r=1}^P A_r^2 B_r^2 \quad (\text{B.47})$$

## B.7 Orthogonal Users for PSK Symbols

Symbol  $c$  is defined with the following equation. Superscript indicates user. Subscript indicates symbol.

$$s_k^{(v)}(n) = \frac{2}{N} \sum_{p=1}^P A_p \cos \left( 2\pi p \frac{n}{N} + \phi_p^{(v)} + \theta_k^{(v)} \right) \quad v = 0, \dots, G-1 \quad (\text{B.48})$$

$$\phi_p^{(v)} = \phi_p + \sum_{q=1}^p \text{sgn}(A_q) \frac{q2\pi v}{G}$$

$$G = \sum_{r=1}^P \text{sgn}(A_r)$$

$$\text{sgn}(t) = \begin{cases} 1 & t > 0 \\ 0 & t = 0 \\ -1 & t < 0 \end{cases}$$

$G$ =number of users.  $\frac{P}{G}$  is a positive integer.

Symbol  $d$  is defined with the following equation. Superscript indicates user. Subscript indicates symbol.

$$s_l^{(w)}(n) = \frac{2}{N} \sum_{p=1}^P A_p \cos \left( 2\pi p \frac{n}{N} + \phi_p^{(w)} + \theta_l^{(w)} \right) \quad w = 0, \dots, G-1 \quad (\text{B.49})$$

$$\phi_p^{(w)} = \phi_p + \sum_{q=1}^p \text{sgn}(A_q) \frac{q2\pi w}{\sum_{r=1}^P \text{sgn}(A_r)}$$

Cross correlation between Symbol c and Symbol d

$$R_{cd}^{(v,w)} = \sum_{n=0}^{N-1} S_c^{(v)} \left( \frac{n}{N} \right) S_d^{(w)} \left( \frac{n}{N} \right) \quad (\text{B.50})$$

$$R_{cd}^{(v,w)} = \frac{2}{N} \sum_{p=1}^P A_p^2 \cos \left( \phi_p^{(v)} - \phi_p^{(w)} + \theta_c^{(v)} - \theta_d^{(w)} \right) \quad (\text{B.51})$$

$$= \frac{2}{N} \sum_{p=1}^P A_p^2 \cos \left[ \left( \sum_{q=1}^p \text{sgn}(A_q) \frac{q2\pi(v-w)}{G} \right) + \theta_c^{(v)} - \theta_d^{(w)} \right] \quad (\text{B.52})$$

A) If  $v=w$

$$R_{cd}^{(v,v)} = \frac{2}{N} \sum_{p=1}^P A_p^2 \cos \left( \theta_c^{(v)} - \theta_d^{(w)} \right) \quad (\text{B.53})$$

B) If  $v \neq w$  and  $A_p$  can only take on values of  $A$  or  $0$

$$R_{cd}^{(v,w)} = \frac{2}{N} \sum_{r=1}^P A_r^2 \cos \left( \theta_c^{(v)} - \theta_d^{(w)} + \left( \sum_{q=1}^p \text{sgn}(A_q) \frac{q2\pi(v-w)}{G} \right) \right) \quad (\text{B.54})$$

$$\begin{aligned} &= \frac{2}{N} \sum_{r=1}^P A_r^2 \cos \left( \theta_c^{(v)} - \theta_d^{(w)} \right) \cos \left( \sum_{q=1}^p \text{sgn}(A_q) \frac{q2\pi(v-w)}{G} \right) \\ &\quad - \frac{2}{N} \sum_{r=1}^P A_r^2 \sin \left( \theta_c^{(v)} - \theta_d^{(w)} \right) \sin \left( \sum_{q=1}^p \text{sgn}(A_q) \frac{q2\pi(v-w)}{G} \right) \end{aligned} \quad (\text{B.55})$$

$$\begin{aligned}
&= \frac{2}{N} \cos \left( \theta_c^{(v)} - \theta_d^{(w)} \right) \sum_{r=1}^P A_r^2 \cos \left( \sum_{q=1}^p \text{sgn}(A_q) \frac{q2\pi(v-w)}{G} \right) \\
&\quad - \frac{2}{N} \sin \left( \theta_c^{(v)} - \theta_d^{(w)} \right) \sum_{r=1}^P A_r^2 \sin \left( \sum_{q=1}^p \text{sgn}(A_q) \frac{q2\pi(v-w)}{G} \right) \quad (\text{B.56})
\end{aligned}$$

$$\begin{aligned}
R_{cd}^{(v,w)} &= \frac{2}{N} \cos \left( \theta_c^{(v)} - \theta_d^{(w)} \right) (0) \\
&\quad - \frac{2}{N} \sin \left( \theta_c^{(v)} - \theta_d^{(w)} \right) (0) = 0 \quad (\text{B.57})
\end{aligned}$$

## Bibliography

- [1] L. Couch, *Digital and Analog Communication Systems*. New York, New York: Macmillan Publishing Company, 1993.
- [2] M. Roberts, "Synchronization of a transform domain communication system," Master's thesis, Air Force Institute of Technology, 2000.
- [3] B. Sklar, *Digital Communications, Fundamentals and Applications*. Saddle River, New Jersey: Prentice Hall, 2001.
- [4] R. Peterson, R. Ziemer, and D. Borth, *Introduction to Spread-Spectrum Communications*. Englewood Cliffs, New Jersey: Prentice-Hall, 1995.
- [5] R. Radcliffe, "Design and simulation of a transform domain communication system," Master's thesis, Air Force Institute of Technology, 1996.
- [6] P. Swackhammer, "Design and simulation of a multiple access transform domain communication system," Master's thesis, Air Force Institute of Technology, 1999.
- [7] M. Jeruchim, *Simulation of Communication Systems*. New York, New York: Plenum Press, 1992.
- [8] *Learning Matlab*. Natick, Massachusetts: MathWorks Inc., 2002.
- [9] L. Scharf, *Statistical Signal Processing: Detection, Estimation, and Time Series Analysis*. Reading, Massachusetts: Addison-Wesley Publishing Company, 1990.
- [10] P. J. Lee, "Computation of the bit error rate of coherent m-ary psk with gray code bit mapping," *IEEE Transactions on Communications*, pp. 488–491, 1986.
- [11] J. Proakis and D. Manolakis, *Digital Signal Processing, Principles, Algorithms, and Applications*. Saddle River, New Jersey: Prentice-Hall, 1996.
- [12] M. Roberts, "Initial acquisition performance of a transform domain communication system: Modeling and simulation results," *MILCOM 2000 Proceedings. 21st Century Military Communications. Architectures and Technologies for Information Superiority*, vol. 2, pp. 1119–1123, 2000.
- [13] K. Gilhousen, I. Jacobs, R. Padovani, A. Viterbi, L. Weaver, and C. Wheatley, "On the capacity of a cellular cdma system," *IEEE Transactions on Vehicular Technology*, vol. 40, pp. 303–312, 1991.
- [14] R. Van Nee and R. Prasad, *OFDM for Wireless Multimedia Communications*. Boston, Massachusetts: Artech House Publishers, 2000.

REPORT DOCUMENTATION PAGE				Form Approved OMB No. 074-0188	
<p>The public reporting burden for this collection of information is estimated to average 1 hour per response, including the time for reviewing instructions, searching existing data sources, gathering and maintaining the data needed, and completing and reviewing the collection of information. Send comments regarding this burden estimate or any other aspect of the collection of information, including suggestions for reducing this burden to Department of Defense, Washington Headquarters Services, Directorate for Information Operations and Reports (0704-0188), 1215 Jefferson Davis Highway, Suite 1204, Arlington, VA 22202-4302. Respondents should be aware that notwithstanding any other provision of law, no person shall be subject to a penalty for failing to comply with a collection of information if it does not display a currently valid OMB control number.</p> <p><b>PLEASE DO NOT RETURN YOUR FORM TO THE ABOVE ADDRESS.</b></p>					
1. REPORT DATE (DD-MM-YYYY) 23-03-2004		2. REPORT TYPE Master's Thesis		3. DATES COVERED (From - To) Jun 2003 - Mar 2004	
4. TITLE AND SUBTITLE  INTERFERENCE SUPPRESSION IN MULTIPLE ACCESS COMMUNICATIONS USING M-ARY PHASE SHIFT KEYING GENERATED VIA SPECTRAL ENCODING				5a. CONTRACT NUMBER	
				5b. GRANT NUMBER	
				5c. PROGRAM ELEMENT NUMBER	
6. AUTHOR(S)  Nunez, Abel S., Captain, USAF				5d. PROJECT NUMBER	
				5e. TASK NUMBER	
				5f. WORK UNIT NUMBER	
7. PERFORMING ORGANIZATION NAMES(S) AND ADDRESS(S) Air Force Institute of Technology Graduate School of Engineering and Management (AFIT/EN) 2950 P Street, Building 640 WPAFB OH 45433-7765				8. PERFORMING ORGANIZATION REPORT NUMBER  AFIT/GE/ENG/04-20	
9. SPONSORING/MONITORING AGENCY NAME(S) AND ADDRESS(ES) James P. Stephens, Sr. AFRL/SNRW Bldg 620 2241 Avionics Circle Room N3-F10 Wright-Patterson AFB, OH 45433-7333      Comm (937)255-5579      DSN 785-5579				10. SPONSOR/MONITOR'S ACRONYM(S)	
				11. SPONSOR/MONITOR'S REPORT NUMBER(S)	
12. DISTRIBUTION/AVAILABILITY STATEMENT  APPROVED FOR PUBLIC RELEASE; DISTRIBUTION UNLIMITED.					
13. SUPPLEMENTARY NOTES					
14. ABSTRACT <p>A conceptual transform domain communication system (TDCS) is shown capable of operating successfully using M-Ary phase shift keying (MPSK) data modulation in a multiple access environment. Using spectral encoding, the conceptual TDCS provides an effective means for mitigating interference affects while achieving multiple access communications. The use of transform domain processing with MPSK data modulation (TD-MPSK) provides higher spectral efficiency relative to other modulation techniques (antipodal signaling and cyclic shift keying) considered previously for TDCS applications. The proposed TD-MPSK technique uses spectral encoding for both data and multiple access phase modulations. Demodulation of the spectrally encoded TD-MPSK communication symbols is accomplished using conventional, multi-channel time domain correlation techniques.</p> <p>Analytic expressions for TD-MPSK probability of symbol error (<math>P_E</math>) and probability of bit error (<math>P_B</math>) are derived and validated using simulated results over the range of signal-to-noise ratios typically considered for communications. This validation includes scenarios with: 1) multiple access interference, 2) spectral notching, 3) jamming present and 4) combinations of all three. For a J/S of 3.14 dB and a <math>E_b/N_0</math> of 6 dB, <math>P_B</math> dropped by up to a factor of 3 for TD-QPSK in a MA environment for the case when spectral notching was present versus the case when spectral notching wasn't present. The cross-correlation between communication symbols of different synchronous users can be made identically zero through proper selection of multiple access phase codes (orthogonal signaling). For a synchronous network containing orthogonal users, <math>P_E</math> and <math>P_B</math> are unaffected as the number of orthogonal network users increases. For a J/S of 3.14 dB and a <math>E_b/N_0</math> of 6 dB, <math>P_B</math> dropped by a factor of 12 for TD-QPSK in a MA environment for the case when spectral notching was present versus the case when spectral notching wasn't present.</p>					
15. SUBJECT TERMS Transform Domain, Spread Spectrum, Spectral Shaping, Jamming Suppression, Low Probability of Intercept, Multiple Access, Code Division Multiple Access, Multiple Phase-Shift Keying					
16. SECURITY CLASSIFICATION OF:			17. LIMITATION OF ABSTRACT	18. NUMBER OF PAGES	19a. NAME OF RESPONSIBLE PERSON
a. REPORT	b. ABSTRACT	c. THIS PAGE			Michael Temple, PhD,
U	U	U	UU	127	19b. TELEPHONE NUMBER (Include area code) (937)255-6565 x4279; e-mail: michael.temple@afit.edu